Selectivity and efficiency of receptor mediated G protein activation

Dissertation

zur

Erlangung des Doktorgrades

der Naturwissenschaften

(Dr. rer. nat.)

dem

Fachbereich Pharmazie der

Philipps-Universität Marburg

vorgelegt von

Olga S. Ilyaskina

aus **Noginsk-9 (Russische Föderation)**

Marburg/Lahn **2020**

Erstgutachter: **Prof. Dr. Moritz Bünemann**

Zweitgutachter: **Prof. Dr. Carsten Culmsee**

Eingereicht am **09.05.2020**

Tag der mündlichen Prüfung am **07.07.2020**

Hochschulkennziffer: 1180

Посвящается моему отцу

капитану второго ранга Прокопцу Сергею Николаевичу

Table of Contents

Abbreviations

[^{3}H] Sc tritium labelled scopolamine (antagonist of mAChRs)

μOR μ-opioid receptor

ACh acetylcholine (agonist for muscarinic acetylcholine receptors)

Are arecoline (agonist for muscarinic acetylcholine receptors)

BCh Bethanechol (partial agonist for muscarinic acetylcholine receptors)

BQCA Benzyl quinolone carboxylic acid (positive allosteric modulator for muscarinic acetylcholine receptors)

cAMP cyclic adenosine monophosphate

CCh carbachol (synthetic agonist for mAChRs)

Cer Cerulean (a variant of eCFP)

CFP cyan fluorescent protein (eCFP: enhanced CFP)

DAMGO [D-Ala2, N-Me-Phe4, Gly5-ol]-Enkephalin acetate salt (μOR peptide agonist)

DMEM Dulbecco's Modified Eagle's Medium

EC_{50} half-maximal effective concentration (concentration-response curves)

ETbR Endothelin b receptor

FCS fetal calf serum

FRET Förster/Fluorescence Resonance Energy Transfer

FSK forskolin

Gal Gallamine (negative allosteric modulator for muscarinic acetylcholine receptors)

GDP guanosine 5′-diphosphate sodium salt

GFP green fluorescent protein

GPCR G-protein-coupled receptor

G-protein guanine nucleotide binding protein

GTP guanosine 5′-triphosphate sodium salt

GTPγS guanosine 5′-[γ-thio]triphosphate tetralithium salt

HEK human embryonic kidney (cell line; used in this study: HEK293T)

HRP horseradish peroxidase

Ipx Iperoxo

Iso isoprenaline (agonist for β-AR)

kDa kilodalton

k_{off} constant of dissociation

M_1-R type 1 muscarinic acetylcholine receptor

M_2-R type 2 muscarinic acetylcholine receptor

M_3-R type 3 muscarinic acetylcholine receptor

M_4-R type 4 muscarinic acetylcholine receptor

M_5-R type 5 muscarinic acetylcholine receptor

mAChRs muscarinic acetylcholine receptors

MCh methacholine

NA noradrenaline (agonist for α_{2A}-AR and β-AR)

NAM negative allosteric modulator

PAGE polyacrylamide gel electrophoresis

PAM positive allosteric modulator

PBS phosphate buffered sodium (buffer)

Pilo Pilocarpine

PKA protein kinase A

PLC phospholipase C

RAMP Receptor activity-modifying protein

RT room temperature (25℃)

S.E.M. standard error of the mean

SDS Na^+ dodecyl sulphate

TP-R thromboxane A_2 receptor

U46619 9,11-Dideoxy-11α,9α-epoxymethanoprostaglandin F2α (synthetic agonist for TP-R)

wt wild-type

YFP yellow fluorescent protein

α_{2A}-AR α_{2A}-adrenoreceptor

β_1-AR β_1-adrenergic receptor

β_2-AR β_2-adrenergic receptor

1 Introduction

1.1 G-protein-coupled receptors (GPCRs)

G protein coupled receptors are transmembrane proteins consisting of external N-terminus, 7 transmembrane helices, 3 extra- and 3 intracellular loops, and internal C-terminus. When activated by specific ligand they couple to heterotrimeric G proteins which transduce the conformational change of the receptor to the further signalling pathways. GPCRs represent the largest receptor family accounting for more than eight hundred members (Fredriksson et al. 2003) and, thus, are involved in many physiological functions. Since more than 30% of approved drugs on the market target GPCRs (Insel et al. 2018), the molecular mechanisms of G protein mediated signaling are of great interest.

Apart from binding and activating G proteins, GPCRs can undergo phosphorylation by recruiting G protein coupled receptor kinases (GRKs) in an agonist dependent manner. Furthermore, phosphorylated and agonist activated receptors are recognized by arrestins, which induce receptor desensitization, internalization and potentially activate non-canonical signalling pathways including, MAP kinase and RhoA activation (X. Zhang and Eggert 2013). Moreover, GPCR can be modulated by RAMPs. These proteins can modify not only the specificity of the receptor-G protein interaction but also receptor trafficking (Booe et al. 2015).

1.1.1 Investigated GPCRs

1.1.1.1 Muscarinic acetylcholine receptors (mAChRs)

Historically, muscarinic acetylcholine receptors were named after alkaloid muscarine isolated from *Amanita muscaria*, the application of which led to selective mAChRs activation. The inhibitors of muscarinic receptors derived from belladonna alkaloids, such as scopolamine and atropine have been broadly used in medicine since medieval ages (Aronstam and Patil 2009).

Muscarinic acetylcholine receptors belong to class A (rhodopsin-like) GPCRs and constitute a family with 5 subtypes (Gudermann et al., 1996). Stimulation of M_5-R, M_3-R and M_1-R activate G_q protein leads to an increase of IP_3 production and Ca^{2+} concentration within a cell (Caulfield 1993). M_3 receptors are mostly expressed in smooth muscles, particularly in trachea, urinary bladder, and iris, as well as in glands, such as salivary glands (Gautam 2004) and pancreatic ß-cells (Gautam et al. 2007)(Eglen and Watson 1996), whereas M_1-Rs and M_5-Rs are mostly involved in the transduction of cholinergic signals in the central nervous system and autonomic ganglia. They are present in several brain regions and big blood vessels.

Activation of M_1-R or M_5-Rs might lead to increased gastric acid secretion (via *V. nerve*) and vein contraction (Jürgen Wess 2004).

In contrast to odd-numbered receptors, M_2-R and M_4-R members of the muscarinic receptor family couple to G_i proteins, which results in the inhibition of adenylyl cyclase and a drop in cytosolic cAMP levels (Caulfield 1993). M_4-R is present in lungs and responsible for NO-dependent smooth muscle relaxation. M_2-muscarinic receptors are expressed in heart tissues and autonomic nerve endings. Activation of these receptors lead to a negative inotropic and chronotropic effect, as well as reduced noradrenaline release (Brodde and Michel 1999).

Due to such expression diversity in a variety of different tissues, mAChRs regulate many important physiological processes, which has allowed these receptors to stay in the focus of pharmacological interest for years. Although, muscarinic receptor ligands are broadly represented on the pharmaceutical market, even recently launched drugs still expose adverse reactions and have a narrow treatment window. Therefore, an improvement in the chemical and pharmacological properties of cholinergic drugs is necessary.

In this study, we initially decided to focus on muscarinic receptors as a well-established and broadly investigated GPCR model due to the high homology of this receptor family. As has been mentioned above, M_1-and M_3-Rs are classic G_q coupling GPCRs (Dippel et al. 1996; Berstein et al. 1992; K. Leach et al. 2012; Smrcka et al. 1991). However, changes in the concentration of second messengers after treatment with Pertussis and Cholera toxins (Dippel et al., 1996; Zang, et al., 2011; Burford, et al., 1995; Wess,1993; Burford et al., 1996; Ramachandran et al., 1989) suggest a possible coupling to G_i and G_s proteins. In contrast, M_2-R is a classic G_i family coupled receptor (Leach, et al., 2012; Wess, 1993; Dell'Acqua, et al., 1993). Despite the fact that mAChRs couple to different G protein classes, the comparison of crystal structures of these GPCRs revealed only small differences in transmembrane helices (Thal, et al., 2016; Haga, et al., 2012; Albert et al., 2002) meaning that the current knowledge of receptor structures does not allow for a prediction of the coupling to a particular G protein class or subtype (Wess, 1998; Wong, , 2003). However, recent cryo-EM structures of M_1-R and M_2-R with G proteins resolve conserved motifs and residues to be important for GPCR-G protein specific interaction. In particular, receptor C-terminal polybasic cluster and extended TM5 helix, as well as several residues of G protein α5 helix are shown to play a significant role in M_1-R-$G_{q/11}$ selectivity (Maeda *et al.*, 2019).

1.1.1.2 Adrenergic receptors

Adrenoceptors are the most thoroughly studied GPCRs. Being broadly expressed in cardiovascular and both central and peripheral nervous systems, adrenergic receptors are involved in the whole body homeostasis (Ahles and Engelhardt 2014). They are subdivided into three groups: α_1-ARs, α_2-ARs and β-ARs (Bylund et al. 1994).

The β_1-AR functionally dominates over other adrenergic receptors expressed in a heart, regulating excitation-contraction of the myocardium (Dorn 2010). The β_2 adrenergic receptor was the first specifically characterized GPCR from the group of adrenergic receptors, and known to play an important role in the cardiovascular and respiratory system (Reihsaus et al. 1993). Its ligands are broadly used in clinics to treat pathological conditions associated with hypertension, asthma and chronic obstructive pulmonary conditions. Since approximately 30% of the total adrenergic receptors expressed in the myocardium are β_2-AR, the question of β_2- and β_1-ARs drug selectivity is quite acute for the pharmaceutical modulation of cardiac function and failure (Baker 2010; Lymperopoulos, Rengo, and Koch 2013)**.** Both β_1- and β_2-ARs bind to stimulatory G proteins and modulate intracellular Ca^{2+} via an increase in cAMP levels (R. A. Cerione et al. 1985).

In contrast to β_1-and β_2-ARs, β_3-adrenoceptor was the last to be cloned and is less studied. It is expressed in several parts of the gastrointestinal system, adipose tissue and kidney (Krief et al. 1993). Therapeutic agents targeting β_3-adrenoceptor have only recently been launched on the pharmaceutical market (Ahles and Engelhardt 2014).

All three isoforms of α_2-ARs: α_{2A}-, α_{2B}-and α_{2C}- ARs bind to G_i family proteins (Ahles and Engelhardt 2014). This subtype of the adrenergic receptors contributes to insulin secretion, effects blood pressure, lipolysis, and is involved in neurotransmitter release (Knaus et al. 2007)**.**

Being associated with G_q proteins, activation of α_1-ARs induces smooth muscle cell contractions and regulates blood pressure. Furthermore, α_1-ARs are expressed in central and peripheral nervous systems where they control the neurotransmitter release (Piascik and Perez 2001)**.**

In this study α_{2A}-AR, β_1-AR and β_2-AR were investigated in terms of G protein selectivity.

1.1.1.3 Thromboxane A_2 receptors

The thromboxane A_2 receptor was the first GPCR cloned from the family of prostanoid (TP) receptors. Historically, the role of TP-R was associated with blood cell function. Nowadays, its expression was identified in a variety of tissues such as vascular smooth

muscle cells (Halushka 2000), platelets, airways and cardiomyocytes (Coleman, Smith, and Narumiya 1994). The physiological role of TP receptors is rather broad: platelet aggregation, closure of umbilical vessels at birth, wound healing and scar formation, modulation of the filtration rate in kidney and gastric secretion (Remuzzi, Fitzgerald, and Patrono 1992). Moreover, TP-receptor ligands have been found to be experimentally effective in the study of different myocardial perfusion disorders, hypertension, and the pathophysiology of cardiopulmonary and circulatory diseases (Halushka 2000).

Activation of TP-Rs leads to intracellular Ca^{2+} mobilization via G_q protein (Shenker et al. 1991). However, IP_3-independent signalling and the absence of PTX or CTX treatment effect indicates the interaction of these GPCRs with $G_{12/13}$ family proteins (Knezevic, Borg, and Le Breton 1993). It has been shown that stimulation of TP-R with thromboxane synthetic analogue U46619 induces platelet aggregation through G_{13} protein-dependent signalling pathways (Moers et al. 2003), whereas receptor interaction with G_{12} protein has been reported to play an important role in vasoconstriction (Offermanns et al. 1994; L. Zhang, Brass, and Manning 2009). The G_{12}/G_{13} proteins-induced Rho/Rho kinase is a potential pharmacological target due to its involvement in various pathological processes such as malignant cell proliferation and metastasis (Worzfeld, Wettschureck, and Offermanns 2008; Kelly et al. 2006). Due to the adverse reactions caused by wide expression and involvement in cardiovascular homeostasis the TP-R ligands are rather unpopular on the pharmaceutical market. Although only one drug was approved for asthma and severe allergy treatment (Horiguchi et al. 2002), the interest of TP-R antagonists as an alternative to NSAIDs is very high.

1.1.1.4 Endothelin receptors

Endothelin receptors are important in vascular resistance, cardiac output, and renal vasoconstriction (Leung et al. 2002). Therefore, these receptors are of great interest for hospital medicine being targets for the treatment of acute pulmonary states (Filep et al. 1994) and anaphylaxis reactions (Richter, Cloutier, and Sirois 2007). Endothelin receptors are subdivided into two types: ET_AR and ET_BR. In this research project we focused on ETR_B as a GPCR which can bind to two G protein classes: G_i and G_q family (S. Liu et al. 2003), being a suitable agent to expand the mAChR-G protein binding model, described previously. In comparison to M_1- and M_3-Rs, ET_BR has been shown to exhibit less potent G_q coupling when compared to G_o (Doi et al. 1999). However, the experiments on the co-expression of different G proteins with ETR_B and measurements of second messenger concentrations also suggest G_s and G_{13} binding (Takigawa et al. 1995; B. Liu and Wu 2003). Interestingly, several studies

suggest agonist-dependent selectivity of G protein coupling to ET_BR as well as ET_ARs (Shraga-Levine and Sokolovsky 2000).

1.1.1.5 Opioid receptors

Opioid receptors (ORs) are expressed in nociceptive neural circuit and also in regions of the central nervous system related to reward and emotion systems (Al-hasani and Bruchas 2011). There are four classes of opioid receptors reported so far: mu (μ), delta (δ) and kappa (κ) and opioid receptor like-1 (ORL1). Only a single gene was identified for each of the classes (Pasternak and Snyder 1975). Opioid receptors can form homo- or heterodimers and activate different G-protein dependent pathways. Binding of the agonist to the opioid receptor triggers G_i family protein activation leading to the inhibition of adenylyl cyclase and following a decrease in cAMP. Moreover, βγ-subunits derived from $G\alpha_i$-protein directly enhance the activity of the inward rectifying potassium channel Kir3, which causes hyperpolarization of the neuronal cell and induces inhibition of action potential formation. Another important effect of the opioid-receptors is the inhibition of transmitter release by Gβγ-mediated inhibition of presynaptic NPQ-type Ca_V-channels (Al-hasani and Bruchas 2011).

Opioids, such as morphine or codeine, are natural and synthetic opioid receptors ligands. They differ by chemical structure which influences their efficiency and affinity to the receptor. Some of the opioids have a high selectivity level and bind strongly only to one of the receptor class, whereas others have a low affinity to all of the opioid receptor types. Moreover, endogenous opioids have been discovered. Already in 1975 researchers sequenced the first endogenous opioid, enkephaline (Hughes 1975), followed by the discovery of two more opioid peptides, dynorphin A and β-endorphine. Enkephalines have been associated with the δ-opioid receptors, whereas dynorphine A shows a high affinity to κ-opioid receptors and β-endorphine to μ- and δ-opioid receptors. A synthetic peptide DAMGO (D-Ala^2,$MePhe^4$,$Gly(ol)^5$enkephaline) is known as a full μ-OR agonist and commonly used in pharmacological experiments (Pasternak and Pan 2013).

Although opiates are used to treat pain and pain associated disorders (Pasternak and Pan 2013), such as post-operative pain and cancer, in all cases the induction of addiction when used frequently is a major problem. Therefore, opioids have been listed on various „Substance-Control Schedules“ and can only be used under supervision of medical specialists. Additionally, regular usage of opiate may cause analgesia - an insensibility to feel pain (Pasternak and Pan 2013).

1.2 Heterotrimeric G proteins

G proteins or GTP-binding proteins represent the most common signalling system in human cells. They transduce the change in the GPCR conformation across the membrane into intracellular responses and are involved in many different signalling cascades, such as regulation of ion-channel open probability, kinase mediated protein phosphorylation and alteration of protein expression levels. Thus, G protein signalling pathways modulate many cellular functions including cellular excitability, cell contractions, chemotaxis, cell migration and cytoskeletal changes (Goh and Pennefather 1989).

G proteins are heterotrimeric and consist of three functional subunits: Gα (39-52 kDa), Gβ (35-36 kDa), and Gγ (7-10 kDa). Both Gα and Gβγ-subunits have a lipophilic membrane anchor. Independent of the heterotrimeric isoform composition, the Gα subunit carries the nucleotide-binding site. The GDP-bound form of Gα is inactive and associated with Gβγ subunits. GPCRs triggers the activation of G proteins by increasing the probability of the nucleotide-binding site to be in the "open" conformation (T. Flock et al. 2015). Exchange of GDP to GTP leads to G protein activation due to a reduced affinity of Gα towards Gβγ (Mixon et al. 1995; Lambright et al. 1996; Van Eps et al. 2011), resulting in subunit dissociation or rearrangement (Bünemann, Frank, and Lohse 2003). Both activated Gα and Gβγ subunits independently interact with their downstream effectors (Gilman 1987; Iniguez-Lluhi, Kleuss, and Gilman 1993). The G protein cycle is completed when GTP is hydrolysed to GDP (Goricanec et al. 2016).

The variety of different techniques such as cloning or genome sequencing, led to the discovery of genes encoding α, β and ɣ subunits of heterotrimeric G proteins. Whereas the GPCRs family is extremely large, only 16 genes encoding 21 Gα subunits, 5 genes encoding 5 Gβ (Hurowitz et al. 2000) and 12 genes encoding Gγ are known (Downes et al. 1999). However, the variety of feasible heterotrimeric combinations is quite broad and possibly important for the specificity of signal transduction across the membrane (Hildebrandt 1997). G protein isoforms are grouped into 4 major G protein classes (Table 1), defined by the type of Gα subunits: G_s, $G\alpha_i$, $G\alpha_{q/11}$ and $G\alpha_{12/13}$ (Hamm 1998). Different Gα subunits regulate various target proteins (Table 1).

Table 1. G protein classes and homology of Gα subunits

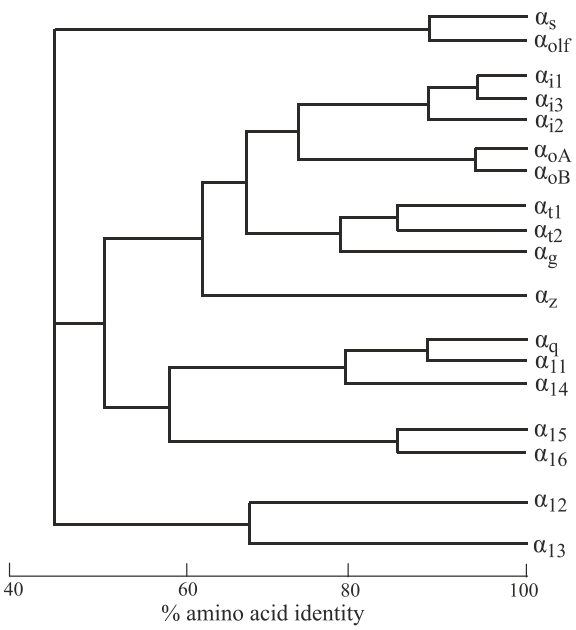

Gα class	Associated effector	2nd messenger	Receptor examples
$G\alpha_s$	Adenylyl cyclase	cAMP (increased)	$\beta_{1,2}$-adrenergic receptors, glucagon receptors
$G\alpha_i$	Adenylyl cyclase	cAMP (decreased)	μ-opioid receptors, even numbers of mAChRs, α_{2A}-adrenergic receptors
$G\alpha_q$	Phospholipase C	IP_3, DAG increased	H_1-Histamine receptors,odd numbers of mAChRs thromboxane receptors
$G\alpha_{12/13}$	RhoGEF	ROCK, SRF-dependent gene transcription	purinergic receptors, thrombin und thromboxane receptors

Table 1: Diversity of Gα subunits, modified from Simon et al. 1991; Syrovatkina et al. 2016. Homology of Gα proteins is shown as a diagram on the left of the table. The scale below the diagram depicts the percentage of similarity in amino acid sequence between different mammalian Gα subunits. No splice variants of G_s proteins are shown. The respective G protein classes defined by the type of the Gα subunit are given in the table on the right. Each of the four G protein classes is characterized by the effector, 2nd messenger, and the GPCR it couples to.

1.2.1 Gα subunit

The Gα subunits share between 70 and 80% sequence identity and almost 100% structural similarity (Table 1) for all G protein classes as well as among mammalian species (Kaziro et al. 1991). This subunit consists of a helical domain and a nucleotide-binding domain. The latter one is highly conserved for all G protein superfamily and contains the nucleotide-binding site, which is important for the nucleotide exchange and functional role of the G protein. The nucleotide binding domain also mediates the association of Gα subunit with Gβ. These contacts are formed between β2, β3 strands of Gβ and α2 helix of Gα, and between the N-terminus helix of Gα and β-propeller structure (Wall et al. 1995). Due to the myristoylated N-terminal of Gα (Maurine E Linder et al. 1991) nucleotide-binding domain carries the “anchor” which tags Gα subunit to the membrane.

The second domain of the Gα subunit, helical domain, is linked to the nucleotide-binding domain by means of flexible loops: switch I, switch II and switch III which form a hydrophobic core for nucleotide binding and undergo structural changes upon Gα activation. By binding to the receptor of the C-terminus, Gα undergoes a disorder-to-order

conformational change and therefore allosterically transduces the active receptor conformation into the rearrangement of the nucleotide-binding domain of the Gα subunit. Receptor-induced movement of the α5 helix leads to its dislocation from the β6 strand and the GDP release (Oldham et al. 2006; Van Eps et al. 2011). The mutations of the TCAT motif at the β6 strand of the Gα subunit, which is responsible for the Gα interaction with the guanine ring, enhance GDP release leading to constitutive G protein signalling (Thomas, Schmidt, and Neer 1993). The "empty" Gα subunit exists mostly in the "opened" conformation and has a distinct distance between helical and nucleotide binding domains (DeVree et al. 2016). Thus, G protein forms a very stable ternary complex (De Lean, Stadel, and Lefkowitz 1980) with the active receptor in absence of nucleotides bound to the Gα subunit. The stability of this complex is even more enhanced due to the ability of the G protein to allosterically increase the time of the agonist being bound to the ligand binding pocket of the receptors, for instance by a lid closure above the agonist molecule (DeVree et al. 2016).

1.2.2 Gβγ subunits

Gβ and Gγ subunits undergo specific assembly right after translation (Mende et al. 1995) and are delivered to the plasma membrane already in a complex (Mervine et al. 2006). They stay tightly bound to each other and function as a dimer (Dupré et al. 2008).

Most combinations of the 5 Gβ- and 12 Gγ-subunits are functional. Some combinations seem to preferentially bind certain receptors or activate specific signalling pathways (McCudden et al. 2005). However, there is currently no evidence showing the preference of individual Gβγ-combinations towards certain Gα-subunits. In this work, only $G\beta_1\gamma_2$-subunits were investigated as the most characterized Gβγ combination (Dingus and Hildebrandt 2012). The Gβ subunit consists of seven β-blade motifs which form a narrow channel structure. At the bottom of this channel the Gα subunit binding site is positioned. Gγ subunits are rather small (7-10 kDa) and consist of two helices. The N-terminus of Gγ is tightly bound to the N-terminus of the Gβ subunit forming a coiled-coil domain (Wall et al. 1995; Lambright et al. 1996). Although, both Gα and Gγ subunits bind Gβ, no direct contacts between their helices were found. Recently resolved cryo-EM structures of M_1-R-G_{11} and PTH_1-R-G_s complexes suggest the possible interaction of Gβ residues and helix 8 of the receptor, but whether these contacts play a role in receptor or G protein functionality is not clear (Maeda et al. 2019b; Zhao et al. 2019).

1.2.3 Selectivity of G proteins

As previously mentioned, in comparison to GPCRs, G proteins have a lower variability, but the amount of combinations from different isoforms of 16 α, 5 β and 12 γ subunits is quite

large (Hillenbrand et al. 2015). In addition, activated Gα as well as Gβγ alone can interact with more than 25 different effectors (Siderovski and Willard 2005; Patel et al. 2014) (Table 1), further enhancing the complexity of GPCR-induced signalling pathways. Although GPCRs exhibit a high degree of selectivity to a particular G protein class, it is a well-known phenomenon, that many GPCRs can activate several isoforms of G proteins from different families (Allgeier et al. 1994; Eason et al. 1992; Kilts et al. 2000; Hermans 2003; Herrlich et al. 1996). The number of potential combinations could be even more increased by the existence of different biased GPCR-agonists, which could preferentially activate certain G proteins better than others. Taken together, the complexity of GPCR-G protein coupling mechanisms gives rise to the question of how the receptor actually finds the right G protein.

The specific receptor function to induce a particular cellular response is known to be determined by the type of the Gα subunit of the G protein (Kleuss et al. 1993; Kisselev and Gautamsb 1993; Strathmann and Gautam 1991; Yan, Kalyanaraman, and Gautam 1996; McIntire, MacCleery, and Garrison 2001). Due to direct interaction with the Gβ subunit which has been shown in G protein crystals (Wall et al. 1995; Lambright et al. 1996), Gα subunit determines the specificity of the downstream effectors of activated Gβγ.

Experiments with mutated Gα and chimeras between different Gα subunits have shown the importance of the C-termini of Gα subunits for G-protein-receptor specificity (Conklin et al. 1993; Hamm et al. 1988). Also, based on sequencing results of different Gα subunits and computational evolutionary analysis, α5 of Gα was shown to play an important role in receptor- G protein coupling selectivity (Oldham and Hamm 2008; Slessareva et al. 2003) (T. Flock et al. 2015). Due to the high sequence homology and different G protein coupling specificity among family members, the mAChRs model is well suited to investigate receptor-G protein selectivity. Recently resolved cryo-EM structures of M_1-R- and M_2-R-G protein complexes has also revealed the TM5 and TM6 as determinants of G protein selectivity of the muscarinic receptor family (Maeda et al. 2019b). Although, the structural data indicate the importance of different residue clusters for receptor-G protein specific interactions, the dynamics of GPCR-G protein is still not covered. In this work, I focus on the determinants of receptor-G protein selectivity.

The results section include figures, text and calculated kinetic values from the publication of the thesis author (Ilyaskina, Lemoine, and Bünemann 2018) and should not be accounted as plagiarized material**.**

1.3 Real-time measurements using Förster Resonance Energy Transfer (FRET)

Förster resonance energy transfer microscopy is based on the physical phenomenon of radiationless energy transmission from donor to acceptor light-sensitive molecules. Due to its sensitivity to distance below the optical diffraction limited resolution (<10 nm), FRET has been broadly used in biochemistry and molecular biology to study the conformational changes of the protein or protein-protein interaction dynamics (Figure 1). Intramolecular FRET is measured when both donor and acceptor fluorophores are incorporated in the same protein and the simultaneous alteration of acceptor over donor intensities reflect the conformational change of the protein (Figure 1B) (Stumpf and Hoffmann 2016). In my research project I mainly used intermolecular FRET which allows to determine the interaction of the protein labelled with donor and the protein labelled with acceptor fluorophore (Figure 1A).

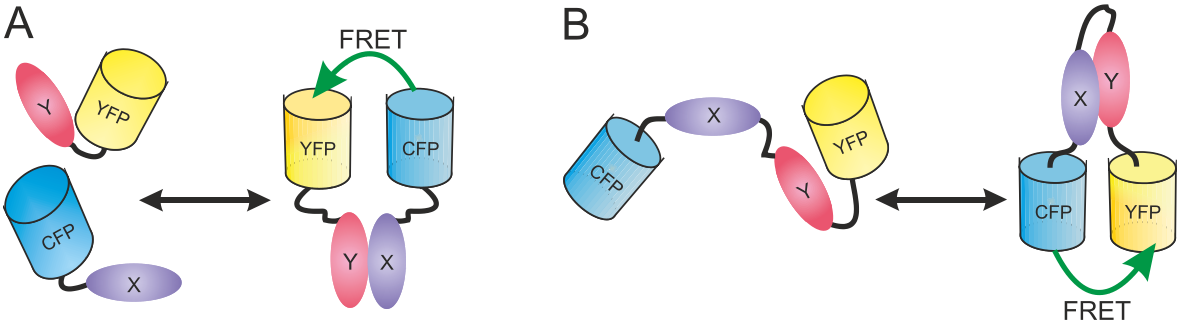

Figure 1. Inter- and intramolecular FRET scheme
Intermolecular Förster resonance energy transfer **(A)** takes place when the binding of two labeled proteis donors (CFP) and acceptor (YFP) fluorophores come into close proximity (<10 nm) and therefore the FRET efficiency increases. Intramolecular FRET **(B)** allows the detection of conformational alterations of the protein by measuring the change in the distances between the CFP and YFP fluorophores inserted into one molecule. Modified from Zhang et al. 2002.

There are three most critical factors necessary in order for FRET to occur (Broussard et al. 2013b). As previously mentioned, FRET is a distance sensitive method. Resonance energy transfer between two fluorophores is observed when the donor and acceptor molecules come into proximity of 1 to 10 nm. The German physicist Theodor Förster developed FRET theoretical analysis and described the dependence of energy transfer efficiency (E1.1) on the inverse sixth-distance between donor and acceptor (Forster 1948).

$$E = \frac{1}{1+\left(\frac{r}{R_0}\right)^6} \qquad \text{(E1.1)}$$

Apart from the distance, a FRET pair of fluorophores should fulfil the requirement that the emission spectrum of the donor fluorophore must overlap with the excitation spectrum of the acceptor fluorophore (Figure 2A,B).

Since the resonance energy transfer is based on dipole-dipole interactions between fluorophores the donor and acceptor must be orientated parallel to achieve the optimal orientation factor (κ), ranging from 0 to 4. Even when the distance between FRET-pair fluorophores is less than 10 nm, the perpendicular position of the donor emission vector to the acceptor reduces FRET efficiency to zero. However, the degree of structural flexibility of fluorescent proteins used as FRET pairs in biological experiments allows the variety of orientations with averaged κ from 2 to 3 (Shrestha et al. 2015).

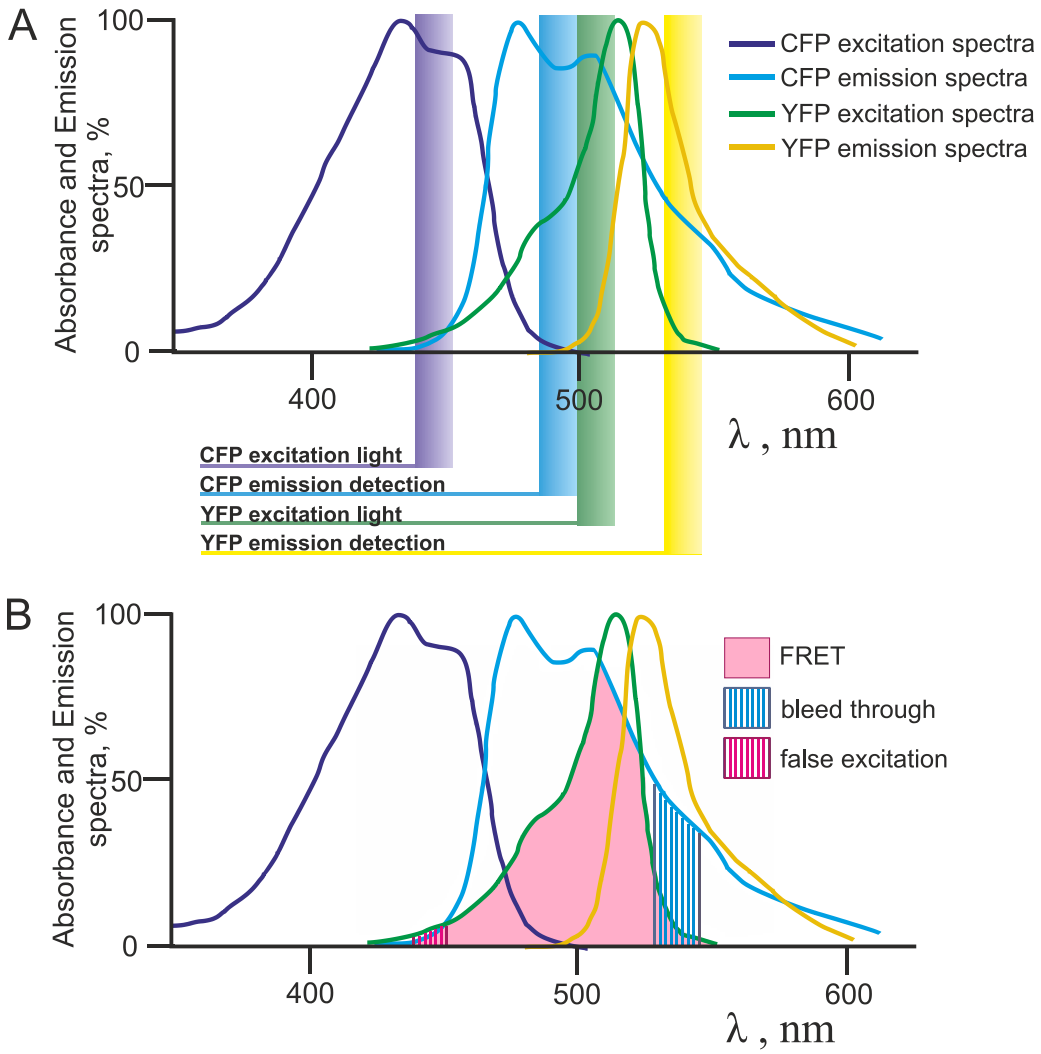

Figure 2. Excitation and emission spectra of CFP and YFP as a FRET pair
Normalized excitation and emission spectra of CFP and YFP are depicted. **(A)** The fields of CFP and YFP excitation as well as recorded emission ranges are depicted in accordance to the filters and detectors incorporated into the Nikon microscope (section 2.2.4.1). **(B)** The light magenta under the curve area represents the overlap of donor (CFP) emission spectra with acceptor (YFP) excitation spectra due to which resonance energy transfer between this pair of fluorophores can occur. The blue and pink striped areas depict the bleed through and false excitation regions (section 2.2.4.6) according to the used equipment (section 2.2.4.1). Modified from Broussard et al. 2013.

1.3.1 Real-time detection of G-protein binding in permeabilized cells

The stability of ternary complex (Agonist-Receptor-G protein) as well as the rate of G protein activation were determined by means of different biochemical approaches *in vitro* (De Lean, Stadel, and Lefkowitz 1980; Higashijima et al. 1987). In order to follow the minor changes in GPCR-G protein interaction dynamics in regular membrane environment, the ternary complex life-time was prolonged by cell permeabilization and depleting the nucleotides out of cell plasma membrane (Hommers et al. 2010). As development and validation of this method is part of my research project, the detailed description is given in section 3.1.

1.3.2 Real-time measurement of G-protein activity in intact cells

The detection of G protein activation by means of FRET has been observed either as an increase or decrease of YFP/CFP intensity ratio, depending on the G protein subtype and insertion site of the fluorophores. The drop of FRET signal suggests the dissociation of Gα and Gβγ subunits (Hein and Bünemann 2009) or a conformational change of the G protein (Figure 3). However, the low initial YFP/CFP emission ratio and increase of the FRET signal upon agonist application can also indicate G protein activation due to the G protein subunits rearrangement without their complete dissociation form each other (Bünemann, Frank, and Lohse 2003). Usually, the direction of change in YFP/CFP emission ratio depends on Gα type and can vary within one G protein family: G_s and G_q activation reflects in FRET-signal decrease; G_{i1} activation leads to increase in signal, whereas the drop in YFP/CFP emission ratio indicates Go protein activation.

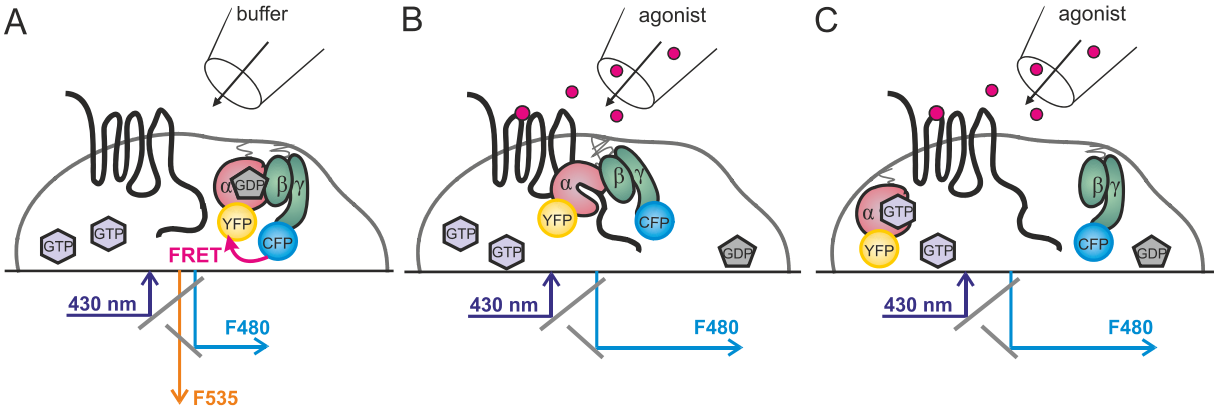

Figure 3. G-protein activation FRET assay scheme
HEK293T cells are transfected as described in Table 2, placed on coverslips and constantly perfused with external buffer. **(A)** A close proximity of YFP and CFP tagged to Gα and Gβγ subunits of inactive G protein suggests a high initial FRET signal. Upon stimulation of GPCR with agonist G proteins are activated leading to the rearrangement of Gα and Gβγ subunits **(B)** and/or their subsequent dissociation from each other **(C)**. In case of high initial FRET signal both (A) and (B) reflect in a decrease in YFP/CFP intensity ratio.

1.4 Aim of the study

Recently, there were several research projects driven by the idea to investigate the mechanism of GPCR-G protein selectivity. The family of G protein coupled receptors (GPCRs) is the largest receptor family and each member detects specific ligands, which in turn activate selected members of one or more G protein families. Breakthroughs in GPCR crystallization gave detailed insight into the GPCR structures (Thal et al. 2016; Haga et al. 2012), and GPCRs activation and interaction with downstream partners. However, the selectivity of receptor-G protein coupling and its underlying mechanisms remain unclear (Li et al. 2012; T. Flock et al. 2015).

In accordance with the ternary complex model agonist, receptor and G protein remain stably coupled till GTP binds to the Gα subunit and immediately triggers G protein activation and its dissociation from the receptor (Dohlman 1991; De Lean, Stadel, and Lefkowitz 1980). We hypothesized that the mechanism underlying the coupling selectivity must be encoded in the receptor-G protein interaction. Therefore, I set out to measure the kinetics and affinity of the GPCR-G protein interaction in the absence of nucleotides in order to determine the affinity of the G proteins for the receptors in a quantitative manner. Due to the high concentration of nucleotides in the cytosol, the ternary complex has a very short lifetime (Oldham and Hamm 2008), therefore, previous methods to measure the GPCR-G protein affinity were mostly based on biochemical assays and required complicated protein purification steps (R. a Cerione et al. 1984; Eason et al. 1992; R. A. Cerione et al. 1985; Rubenstein, Linder, and Ross 1991). Thus, the advantage of a FRET-based approach is to quantify G protein affinity to the receptor in a regular plasma membrane environment. The aim of this research project was to assess the kinetics of the agonist driven interaction of GPCRs with representative G proteins from all 4 classes by means of FRET.

2 Materials and Methods

2.1 Materials

2.1.1 Antibodies

Anti-$G\alpha_q$ rabbit polyclonal (Santa Cruz Biotechnology, INC, $G\alpha_q$(E-17):sc-393, dilution 1:200 in 5% milk blocking buffer), anti-$G\alpha_o$ mouse monoclonal (Santa Cruz Biotechnology, INC, $G\alpha_o$(E-1):sc-393874, dilution 1:200 in 5% milk blocking buffer) antibodies were used to detect the expression of respective Gα subunits of G proteins. Anti-Gβ polyclonal rabbit antibody (Santa Cruz Biotechnology, INC, Gβ(T-20):sc-378, dilution 1:500 in 5% milk blocking buffer) was applied for the detection of $G\beta_1\gamma_2$ expression. Anti-actin monoclonal

mouse antibody (MP Biomedicals, actin G9100, dilution 1:100000 in 5% milk blocking buffer) was used as a loading control after membrane stripping.

2.1.2 Plasmids

The plasmids used during my PhD project (Table 2) were already published and available in the lab.

Table 2. Plasmids used in the study

Plasmid	Species	Reference	Vector
α_{2A}-AR (HA-tagged)	mouse	Bünemann et al., *Proc.Natl.Acad.Sci.USA, 2003*	pcDNA3
α_{2A}-YFP	mouse	Krasel et al., *J.Biol.Chem.2005*	pcDNA3
β_2-AR	human	Krasel et al., *J.Biol.Chem.2005*	pcDNA3
$G\alpha_q$-wt	mouse	Hughes et al., *J.Biol.Chem.2001*	pcDNA3
$G\alpha_o$-wt	rat	Frank et al., *J.Biol.Chem,2005*	pcDNA3
$G\alpha_{i1}$-wt	rat	*Wise et al., 1997*	pcDNA3
$G\alpha_{i2}$-wt	rat	Frank et al., *J.Biol.Chem,2005*	pcDNA3
$G\alpha_{i3}$-wt	rat	Frank et al., *J.Biol.Chem,2005*	pcDNA3
$G\alpha_s$-wt	rat	Hein et al., *J.Biol.Chem.2006*	pcDNA3
$G\alpha_q$-YFP	mouse	Hughes et al., *J.Biol.Chem.2001*	pcDNA3
$G\alpha_o$- YFP	rat	Hommers et al., *J.Biol.Chem.2005*	pcDNA3
$G\alpha_s$-YFP	human	*Hein et al., J. Biol. Chem. 2006*	pcDNA3
$G\alpha_{13}$-YFP	mouse	*Bodmann et al., FASEB J, 2017*	pcDNA3
$G\alpha_q$-CFP	human	Hughes et al., *J.Biol.Chem.2001*	pcDNA3
$G\alpha_o$-CFP	rat	Frank et al., *J.Biol.Chem,2005*	pcDNA3
$G\beta_1$-wt	human	Bünemann et al., *Proc.Natl.Acad.Sci.USA, 2003*	pcDNA3
$G\gamma_2$-wt	bovine	Bünemann et al., *Proc.Natl.Acad.Sci.USA, 2003*	pcDNA3
$G\beta_1$-Cer	human	Frank et al., *J.Biol.Chem,2005*	pcDNA3
CFP-$G\gamma_2$	bovine	Bünemann et al., *Proc.Natl.Acad.Sci.USA, 2003*	N1-eCFP (Clontech)
M_1-R	human		pcDNA3
M_2-R	human	Roseberry et al., *Mol.Pharmacol.2001*	pGES
M_3-R	human	Missouri S&T cDNA Resource Center (www.cdna.org), #MAR030TN00	pcDNA3

TP-wt	human	*Bodmann et al., FASEB J, 2017*	pcDNA3
TP-YFP	human	*Bodmann et al., FASEB J, 2017*	pcDNA3
M_3-R-YFP	human	*Hoffmann et al., 2012*	pcDNA3
YFP-β_2-AR-CFP	human	Dorsch et al., *Nat.Methods 2009*	pcDNA3
mYFP (membrane associated)		Hein et al., EMBO J. 2005	pcDNA3
mCFP (membrane associated)		Cloned in AG Bünemann from mYFP construct	pcDNA3
pcDNA3		Invitrogen	pcDNA3

2.1.3 Chemicals

If not indicated in the table, the substance was purchased from Sigma-Aldrich (Steinheim, Germany).

Table 3. Chemicals, used in the research project

Reagent	Supplier
Dulbecco's modified Eagle's medium (DMEM) high glucose	Biochrom
Fetal calf serum (FCS)	Biochrom
Phosphate-buffered saline (PBS)	Biochrom
Penicillin/streptomycin	Biochrom
L-glutamine	Biochrom
trypsin-EDTA	Biochrom
Saponin	AppliChem
Acetic acid	Carl Roth
Acrylamide/Bisacrylamide	Carl Roth
Agar	AppliChem
Ampicillin	AppliChem
APS	Sigma Aldrich
ß-merapthoethanol	Sigma Aldrich
BSA (delipidated)	Sigma Aldrich
Bradford reagent	Sigma Aldrich
Dimethyl sulfoxide	Sigma Aldrich

EDTA	Sigma Aldrich
Ethanol	Carl Roth
G-418	Capricorn
HEPES	Sigma Aldrich
Immersion Oil Immersol	Zeiss
Isopropanol	Carl Roth
LB-broth	AppliChem
L-Glutamine	AppliChem
Milk powder	Carl Roth
Poly-L-lysine Hydrobromide (PLL)	Sigma Aldrich
PAGE-size standards	Thermo Scientific
Tris	Sigma Aldrich
TEMED	Carl Roth
Tween (20)	Sigma-Aldrich
U-46619	Cayman Chemical
Acethylcholine	Sigma Aldrich
Carbachol	Sigma Aldrich
Petussis toxin	Sigma-Aldrich
BQCA	Cayman Chemical
Bethanechol chloride	Alfa Aesar
Iperoxo	Sigma-Aldrich
GTPγS	Sigma-Aldrich
Scopolamine methylchloride [N-methyl-^{3}H]	American Radiolabeled Chemicals
Choline Chloride	Santa Cruz Biotech
Pilocarpine	TCI
Arecoline	TCI
Gallamine	Sigma-Aldrich
Daltroban	Sigma-Aldrich

2.1.4 Buffers

All the buffers were prepared in the lab apart from PBS (purchased from Capricorn Scientific GmbH, Ebsdorfergrund, Germany). High glucose DMEM (purchased from Biochem) was only supplied with additional substances depending on cell line. Ultra-filtered water (Ultra Clear UV plus, Reinstwassersystem; SG Wasseraufbereitung, Barsbüttel, Germany) was used for all water-based buffers.

Unless indicated differently, the working solutions for the assays were used in a single-strength concentration.

Dulbecco's Modified Eagle Medium (DMEM) supplements list

Compund	**Concentration**
Fetal calf serum (FCS)	10,00%
L-Glutamine	2 mM
Penicillin	100 U/ml
Streptomycin	100 µg/ml

-store at 4 ℃ up to 5 weeks

External buffer

Compound	**Concentration**
NaCl	137 mM
KCl	5.4 mM
HEPES (4-(2-hydroxyethyl)-1-piperazineethanesulfonic acid)	10 mM
$CaCl_2$	2 mM
$MgCl_2$	1 mM
pH	7.4

-filter sterile

Internal buffer

Compound	**Concentration**
K^+-aspartate	100 mM

KCl	30 mM
HEPES	10 mM
EGTA (ethylene glycol-bis(β-aminoethyl ether)-N,N,N',N'-tetraacetic acid)	5 mM
$MgCl_2$	1 mM
NaCl	10 mM
pH	7.35

-filter sterile
-store at 4℃

LB-broth (bacterial medium)

Compound	**Concentration**
Peptone	1.0 %
Yeast extract	0.5 %
NaCl	1 %
Water	

-autoclave
-store at RT

LB-agar

Compound	**Concentration**
Agar	1.5 %
LB-broth	

-autoclave
-store at RT

TSB (transformation and storage buffer for chemical competent *E.coli*)

Compound	**Concentration**
PEG 3000	10 %
DMSO	5 %
$MgSO_4$ or $MgCl_2$	20 mM
LB-broth	

-filter sterile
-store at -20℃

5 x KCM buffer

Compound	Concentration
KCl	500 mM
$CaCl_2$	150 mM
$MgCl_2$	250 mM
Sterile water	

-store at 4℃

Homogenation buffer

Compound	Concentration
HEPES	10 mM
EDTA	0.05 %
NaCl	0.9 %
Water	pH 7.4

-store at 4℃

Assay buffer

Compound	Concentration
HEPES	20 mM
$MgCl_2$	1 mM
Water	pH 7.4

-store at 4℃

Lysis buffer (Western-Blot)

Compound	Concentration
Tris	20 mM
EDTA	2 mM
Proteinase inhibitors mix (Complete ULTRA tablets mini, EDTA free, Roche)	1 tablet / 10 ml buffer
Water	

- store aliquoted at -20℃

5 x Sample buffer (Western-Blot)

Compound	Concentration
Glycerine	50 % (m/v)
Tris	312.5 mM
SDS	10 % (m/v)
β-mercaptoethanol	25 % (m/v)
Bromephenol blue	0.1 % (m/v)
Water	

- store aliquoted at 4℃

10 x Running buffer for SDS-PAGE (Western-Blot)

Compound	Concentration
Glycerine	14,4 % (m/v)
Tris (base)	2.5 M
SDS	10 % (m/v)
Water	

- store at RT

10 x TBS

Compound	Concentration
NaCl	5 M
Tris (base)	2 mM
Water	
pH	7.5

- store at RT

1 x TBST

Compound	Concentration
Tween 20	0.05 % (v/v)
TBS	

- store at RT

1 x Transfer buffer (Western Blot)

Compound	Concentration
Tris (base)	25 mM
Glycerine	1.4 %
Methanol	20 %
Water	
pH	8.3

- store at RT

Blocking milk (Western Blot)

Compound	Concentration
Milk powder skim	5 % (m/v)
TBST	

- to be fresh prepared

Stripping buffer (Western Blot)

Compound	Concentration
Glycerine	1.5 (m/v)
SDS	0.1 % (m/v)
Tween 20	1 % (v/v)
Water	

-store at RT

PFA (Paraformaldehyde, Immunofluorescence)

Compound	Concentration
PFA	4 %
PBS	

- PFA is soluble in PBS at 70℃
- store filtered at 4℃

Blocking solution (Immunofluorescence)

Compound	Concentration
FCS	5 % (v/v)
Triton X	0.2 % (v/v)
SDS	

- to be fresh prepared

2.1.5 Software

-Plasmid sequences, alignments:

ApE- A plasmid Editor

-Data analysis and statistics:

Microsoft Excel 2013 (Microsoft, Redmond, WA)

GraphPad Prism 5 (San Diego, CA, USA)

OriginLabs OriginPro 8.5(Northampton, MA, USA)

OriginPro 9.1 (Northampton, MA, USA)

Nest-o-patch (Friedrich-Alexander-Universität, Erlangen-Nürnberg, Germany)

-Image analysis and its modification:

ImageJ 1.46r (National Institutes of Health, Maryland, USA)

LAS AF light (Leica Microsystems, Germany)

-Figures modifications and vector graphics:

CorelDraw X4

2.1.6 Bacteria strains and cell lines

HEK293T (Human Embryonic Kidney 293T) used for all FRET-experiments, radioligand binding and biochemical assays was a kind gift from Martin Lohse. HEK293 cell line was used in order to create stable Flag-M3-R expression clones.

2.1.7 Consumable material

Table 4. Materials used in the studies

Consumables Supplier	Supplier
Centrifuge tubes (15 ml, 50 ml)	Greiner Bio-One
Cover slips, 25 mm	VWR
Cryogenic vessels	Hartenstein
Dishes for cell culture(150 mm, 100 mm,60 mm, 96-well plates, 6-well)	Sarstedt
Pasteur pipettes	Hartenstein
Petri dishes	Hartenstein

Pipette tips 2µl, 20µl-200µl, 1000 µl	Sarstedt
PVDF membrane	Roche
Reaction vessels (1.5 ml)	Sarstedt
Syringes for single use	Neolab
Stripps, 12-well	Greiner Bio-One
Whatman® paper	VWR

2.2 Methods

The recipes of the buffers, used in the following protocols, are given in the section 2.1.4.

2.2.1 Molecular biology

2.2.1.1 Generation of chemical competent *E.coli*

Competent *E.coli* were prepared according to a modified protocol by Chung et al. (Chung, Niemela, and Miller 1989). The *E.coli* DH5α strain was plated on an LB-agar plate and incubated overnight at 37 °C. A single colony was picked and precultured overnight in 10 ml LB-broth on the shaker at 37 °C. Five to 10 ml of bacteria preculture was added to the 250 LB-broth final volume and shaken at 37℃ until OD600=0.4-0.6. The bacteria were harvested by 10 minutes centrifugation at 5000 rpm 4℃. The pellet was resuspended in 25 ml of ice-cold TSB buffer. The suspension was incubated on ice for 2 hours, aliquoted and frozen in liquid nitrogen. Aliquots stored at -80 °C.

2.2.1.2 Transformation of chemical competent *E.coli*

Bacteria (chemical competent *E.coli*) should be thawed on ice.

Compound	**Concentration**
5x KCM-buffer	20 µL
Autoclaved water	80 µL
DNA	0.5 µg
Competent bacteria	100 µL

The mixture was incubated on ice for 10 minutes, then 20 minutes at RT. One ml LB-broth (autoclaved) was added to the mixture and bacteria were incubated for 50 minutes at 37°C at 850 rpm (ThermoMix). Sixty-80 µl of the final mixture was plated on agar (with the antibiotic respective to the resistant factor encoded in the plasmid) and incubated overnight at 37°C.

2.2.1.3 Plasmid preparation

Plasmids were purified from 100 mL bacteria suspension grown overnight with an appropriate amount of antibiotic using Qiagen Plasmid Midi Kit according to the manufacturer's protocol.

2.2.2 Biochemical approaches

2.2.2.1 Western-Blotting

Western blots were done on transiently transfected HEK293T cells. Cells were split on 10 cm dishes and transfected with double amount of Plasmid mixture "G protein binding experiments" (Table 6 section 1) by Effectene Reagent Kit (QUAGEN) as described in section cell culture and transfection and depicted in Figure 11. The transfection was stopped after 18 hours by changing medium. Twenty-four hours later, transfected cells were washed once with PBS buffer, resuspended in 1 ml Lysis buffer, scratched from the plate and transferred into a 1.5 ml tube. The cell suspension was briefly dipped in liquid nitrogen and stored at -80°C. The whole-cell lysates were thawed on ice homogenised by 30 second pulse by Ultra-Turrax (Model IKA T10 basic). The protein amount was determined by with BCA Reagent kit.

The 10% SDS 1.5 mm thick PAGE gel was poured according to the following protocol:

Separating Gel (1 Gel-10 ml)	
H_2O	4 ml
30% Acrylamid	3.3 ml
1.5 M Tris (pH=8.8)	2.5 ml
10% SDS	0.1 ml
10% APS	0.1 ml
TEMED	4 µl

The edge of separating gel was smoothed with Isopropanol, which was depleted right after polymerisation and before pouring the concentration gel on top.

Concentrating Gel (1 Gel-5 ml)	
H_2O	3.4 ml
30% Acrylamide	0.83 ml
0.5 M Tris (pH=6.8)	0.63 ml
10% SDS	0.05 ml
10% APS	0.05 ml
TEMED	5 µl

Each probe was diluted until 100 µg of protein in 40 µl of Lysis buffer with addition of 5 µl 5x sample buffer. Samples were vortexed, shortly centrifuged and denaturized by heating up to 95 °C for 15 minutes at 650 rpm (Thermomix). The samples were centrifuged again and loaded into SDS-Page pockets. In at least 1 pocket pro gel, 10 µl of Page Ruler was added. Electrophoresis was performed for 25 min at 60 V in concentrating gel and for 1-2 hours at 100-120 V in separating gel. The PVDF membrane (Roche) was activated in MetOH and stored in transfer buffer till the "sandwich" of membrane, gel, and sponges was built. The protein transfer to the PVDF membrane was performed by means of wet blotting 2 hours at 200 mA and overnight (about 18 hours) at 20 mA at 4 °C with a constant mix. The membrane was blocked by 1-hour incubation with 5% milk in TBST (further "milk") at RT. The primary antibody was diluted in "milk" and incubated with the membrane overnight at 4 °C following 1-hour incubation at RT. The membrane was washed three times each 15 minutes with TBST buffer (Table 5). The secondary HRP-labelled antibody diluted in "milk" was applied on the membrane for 1-hour at RT with no light access (Table 5). The membrane was again washed three times 15 minutes each with TBST buffer. In order to detect bioluminescence with Chemidoc (BioRad, LiveAcquire: 300 sec, 10 images), the membrane was incubated with ECL Kits HRP detecting solution (3 ml of each solution per 1 membrane) for 10 minutes on the shaker with no light access. TIFF-images were quantified by means of ImageJ (1.46r; http://imagej.nih.gov/ij/).

The following steps were only performed if another antibody was used on the same membrane (e.g. protein loading or expression control). The membrane was stripped, washed with water (5 minutes on the shaker) and incubated with stripping buffer for 15 minutes. The stripping buffer was further depleted by washing twice for 5 minutes with PBS followed by the same process this time with TBST. The membrane was blocked by "milk" and primary and secondary antibodies were applied as described previously for the first run of protein detection.

Table 5. Antibodies used in the study

Target	Application	Clonality	Item	Dilution	Species	Supplier
$G\alpha_q$	primary	polyclonal	E-17:sc-393	1:200	rabbit	Santa Cruz Biotech.
$G\alpha_o$	primary	monoclonal	E-1:sc-393874	1:200	mouse	Santa Cruz Biotech.
Gβ	primary	polyclonal	T-20:sc-378	1:500 in	rabbit	Santa Cruz Biotech.

Actin	primary	monoclonal	G9100	1:100000	mouse	MP Biomedicals
Mouse	secondary		7076	1:3500	horse	Cell Signalling
Rabbit	secondary		7074/P2	1:3500	goat	Cell Signalling

2.2.2.2 Immunofluorescence

The immunofluorescence analysis was performed for the control of M_3-R expression by the stable HEK293 cell line. The plasmid encoding M_3-R with Flag tag at the N-terminus was transfected in HEK293 cells by Effectene Quagen Kit according to the manufacturer's protocol. The first generation clone selection was performed after 2 weeks of culturing transfected cells in DMEM 10% FCS supplied with 1.0 μg/ml G418. Second generation clone selection was done after 2 weeks culturing of the clone 1 in DMEM 10 % FCS supplied with 0.5 μg/ml G418. For the Flag-tag immunostaining, the depicted clone was cultured on glass coverslips coated with Poly-L-lysine. Cells were washed once with PBS and if needed followed by 4% PFA (paraformaldehyde) incubation (to control the amount of unfolded or degraded M_3-R-Flag in the cytosol) at RT for 15 minutes. PFA was properly washed with PBS and cells were incubated for 1 hour with blocking solution. First antibody (Harpine Anti-Flag goat, 1:200 in blocking solution) was applied on the cells for 2 hours. Second antibody (anti-goat 1:2000, blocking solution) was applied for 1 hour and protected from light. After washing steps with PBS, cells were fixed on coverslips by Vectraschield mounting medium at the RT with no light access for 1 hour. The fixed immunostained cells were stored in a light-protective case at 4°C or directly analysed under epifluorescence Leica microscope (Leica DMI 6000B with a Leica DFC360 FX camera). Confocal pictures were acquired with an excitation wavelength of 405 nm (laser diode) and 514 nm (Ar-laser).

2.2.2.3 Radioligand binding assay

The expression levels of wild type M_3-Rs were determined in the membranes as described in Cembala et al. (Cembala et al. 1998). HEK293T cells were transiently transfected with M_3-wt, YFP labelled Gα of interest, $G\beta_1$-wt, and CFP labelled $G\gamma_2$ subunit. Cells were harvested 2 days after transfection into homogenization buffer and homogenized using Ultra-Turrax. In order to isolate membranes, the homogenized cells were centrifuged for 15 min at 10 000 g at 4°C and resuspended in assay buffer (20 mM HEPES, 1 mM $MgCl_2$ at pH 7.4). Protein concentration was determined by Pierce BCA protein kit (Thermo Scientific, IL, USA) according to the manufacturer's instructions. The incubation of membranes with [^{3}H]-scopolamine methyl chloride (specific activity: 80 Ci/mmol, American

Radiolabeled Chemicals, MO, USA) in a total volume of 1 ml assay buffer was performed at 37 °C for 1 h. The separation of free and bound radioligand was done by filtration through glass fibre filters (Whatman®, 25 mm). The counting procedure was done after extraction of radioactivity from the glass fibre filters at least 12 h in 4 ml scintillation fluid (Ultima Gold, Perkin Elmer, USA) using Liquid scintillation analyser (1600-TR, Tri-Carb, Pakard, Canberra Company). Non-specific binding was determined in presence of 10 μM atropine.

2.2.3 Cell culture and transfection

Experiments were performed in HEK (human embryonic kidney) 293T cells (a kind gift from M. Lohse, Würzburg, Germany). Cells were maintained in high glucose culturing medium (4.5 g/L) Dulbecco's Modified Eagle Medium (DMEM) supplemented with 10 % FCS, 2 mM L-glutamine, 100 U/mL penicillin and 0.1 mg/mL streptomycin at 37°C, 5% CO_2. Cells were passaged every 2-3 days in 10 cm Petri dishes. Cell culturing in 6 cm dishes was performed for further transfection with DNA of interest. When cell density in the plate was estimated from 30-70%, cells were transfected with a mixture of plasmids not exceeding 3.2 μg of total DNA per 3.5 ml medium (Table 6. Plasmid mixtures for HEK293T cells transfection) using Effectene Transfection Reagent according to the manufacturer's instructions (Qiagen, Hilden, Germany). Transfection procedure lasted normally 16-20 hours and was stopped by changing medium on 6 cm plates. Eighteen hours before FRET-experiments, transfected cells were transferred from 6 cm plates to 6-well plates 25 mm coverslips (cover glasses were preincubated 40 min with poly-L-lysine for a better cell adhesion). Fluorescent microscopy experiments were performed at room temperature.

Table 6. Plasmid mixtures for HEK293T cells transfection

1. G-protein binding experiments (permeabilized cells)	
Plasmid	**μg**
Receptor-YFP	0.5
Gα-wt / pcDNA3 (no Gα)	1.5
$G\beta_1$-wt	0.5
CFP-$G\gamma_2$	0.25
2. Gα-subunit direct binding to the receptor experiments (intact cells)	
Plasmid	**μg**
Receptor-YFP	0.5
Gα-CFP	1.5
$G\beta_1$-wt	0.5

$G\gamma_2$-wt	0.25
3. Gα-subunit direct binding to the receptor experiments (permeabilized cells)	
Plasmid	**µg**
Receptor-wt	0.5
Gα-YFP	0.8
$G\beta_1$-wt	0.5
CFP-$G\gamma_2$	0.25

2.2.4 Fluorescence microscopy

2.2.4.1 FRET-microscopy equipment

The FRET measurements were performed on single cells selected for membrane staining of YFP and CFP fluorescence. The round shape of cells was taken as an indicator of proper permeabilization (Figure 6B vs Figure 6E). Dual-emission imaging of YFP and CFP of a single cell (or its membrane) was performed by inverted fluorescence microscope (Eclipse Ti; Nikon, Düsseldorf, Germany) supplemented with a light-emitting diode (LED) excitation system (pE-2; CoolLED, Andover, UK) containing LEDs emitting light at 425 nm for CFP and 500 nm for YFP excitation. The filters ET 430/24x (CFP excitation), ET 500/20x (YFP excitation), T455LP (combined fluorescence of CFP and YFP) or CFP/YFP-beam splitter supplied with CFP/YFP emission filter (Cat.No. 59017bs and 59017m) purchased in Chroma were introduced into the Nikon microscope. In order to simultaneously record CFP and YFP fluorescence using a fast CCD camera (Evolve512, Roper Scientific), z488/800-1064rpc (separating emission of CFP and YFP), ET 480/40 (CFP emission only) and HC 534/20 (YFP emission only) were set in an Optosplit II (Cairn Research). Microscope, camera and DG-4 were controlled using NIS-Elements AR (Laboratory Imaging). Synchronization of camera and lamp was driven by a Nikon software implicated triggering-box. During FRET measurements cells were excited with 430 nm light (CFP excitation wave length) and the CFP and YFP emissions were recorded simultaneously. Depending on the fluorescence intensity, the illumination time was set to 30-90 ms at an interval of 500 ms. The intensity of both LEDs was set to 2%. Image recording frequency was set to 2 Hz in correlation to the exposure time (60-100 ms). Fluorescence intensities were acquired using imaging software NIS-Elements advanced research (Nikon Corporation, Melville, NY, USA). FRET was followed over time by plotting the ratio of YFP intensity divided by CFP intensity upon excitation of CFP at 425 nm LED. All fluorescence data were corrected for background fluorescence, false YFP excitation, CFP spillover and photobleaching.

2.2.4.2 FRET-microscopy in single living intact or permeabilized cells

The single cell FRET measurements were done at RT 48 hours after transfection. Coverslips with transiently transfected HEK293T cells were set in a microscope chamber and washed once with External buffer to reduce the amount of auto fluorescent proteins coming from FCS supplemented DMEM. FRET measurements of G protein activation were performed in external buffer. During the experiment intact cells were continuously superfused with external buffer or buffer containing ligands in different concentrations using a fast-switching 8 channel valve-controlled pressurised perfusion system with solenoid valves (Ala-VC^3-8SP, Ala Scientific Instruments). FRET measurements on G protein-receptor binding under nucleotide-depleted conditions were performed in internal buffer (high potassium buffer) on single permeabilized cells. The cell permeabilization procedure was done directly on a coverslip directly before the measurement by brief (2 minutes) cell exposure to 0.05 % Saponin. The nucleotides and the rest of Saponin were depleted by washing 5 times with internal buffer (Hommers et al. 2010).

2.2.4.3 Multiple-Cell FRET imaging

The efficiency of G protein activation by the receptor of interest was determined by means of multiple-cell FRET assay in intact cells transiently transfected as previously described in Frank et al., 2005. Fluorescence was excited with violet light of 435 nm with short light pulses of 10-40 ms followed by darkness for the same time interval (10–40 ms) to minimize photobleaching. Each of the 12 channels was equipped with an independent excitation/detection unit. Excitation light passed band-pass filters of 435 ± 20 nm. After passage using a dichroic mirror (511 nm), the fluorescent light passed band-pass filters of 483 ± 16 nm and 540 ± 25 nm for the detection of blue (CFP) and yellow light (YFP), respectively. Emitted light was detected by low noise silicone photodiodes (OSD15-5T, Centronic, Croydon, UK). After a >100000-fold amplification of the photocurrent with a two-stage amplifier (operational amplifiers OPA111 and OPA121, Texas Instruments, USA) fluorescent signals were digitized and sent (FTDI-USB, 921600 baud) to a personal computer (core2duo, 3 GHz or faster). Computer software was programmed to allow the continuous recording of fluorescence data, for instantaneous display on a conventional screen, and to file data for subsequent data analysis. As all electronic components were chosen to be smaller than 9 mm (i.e. 96-well format), each of the 12 channels could be equipped with independent excitation/detection units, so that fluorescence data could be continuously monitored at a high data sampling rate (~100 Hz).Transfected HEK293T cells were cultivated in 12-well strips (TC, 96-well format, Greiner Bio-One) were washed with and maintained in external buffer A

(137 mM NaCl, 5.4 mM KCl, 1.0 mM $MgCl_2$, 2.0 mM $CaCl_2$, 10 mM HEPES, 2% Brilliant Black) at 32.5 °C. The final volume was 275 µl per well. Injections of test compounds (agonists and antagonists) were made with a volume of 22 µl added gradually with gentle up and down movements of the 12-channel injecting unit equipped with 50 mm needles (1.2 mm diameter), resulting in a 13.5-fold dilution of stock solutions. Alternatively, cells were stimulated with an overflow apparatus allowing fast (< 3 sec) change of the standard buffer to induce receptor stimulation.

2.2.4.4 Quantification of absolute and relative expression levels by means of fluorescence.

The stoichiometry of the relative expression level of YFP and CFP was calibrated to the reference construct. HEK293T cells transiently transfected with YFP-β_2-AR-CFP plasmid (Dorsch et al., 2009), where fluorophore fused to tags ß$_2$-R with 1:1 ratio. YFP and CFP selective intensities were measured individually and corrected for the background. F_{CFP} was divided by F_{YFP} to calculate the calibration factor. To calculate the individual expression ratio, the F_{CFP}/F_{YFP}-ratio of the Gγ/M_3-R-FRET cells was measured similarly and was divided by the calibration factor to estimate the amount of CFP-Gγ_2 overexpression over M_3-R-YFP.

2.2.4.5 Confocal microscopy

Confocal microscope Leica DMI 6000B supplied with Leica DFC360 FX camera was used to acquire images of immunofluorescent labelled cells stably expressing Flag-tagged M_3-R as well as for high quality imaging of localization of fluorescent receptors and G proteins in transiently transfected permeabilized cells.

2.2.4.6 Correction factors

As mentioned in the methods, apart from the background fluorescence raw FRET data were corrected for several factors caused by crosstalk between chosen FRET-pair fluorophores as well as settled filters and lenses.

Due to the overlap of donor emission and acceptor excitation, there is a varied degree of contamination of acceptor emission channel with donor emission fluorescence, called “bleed through” or “spillover” (Figure 2B) (Ishikawa-Ankerhold, Ankerhold, and Drummen 2012). The contribution of CFP in the YFP detected emission (F_{534} channel) was calculated as “bleed through” correction factor by dividing emission from F_{534} by F_{488} derived from HEK293T cells expressing only membrane associated CFP. The “bleed through” correction factor is assumed to be a systematic error which depends on the filters and detection elements used and, therefore, has a constant value which can only differ over a long period of time due to the amortisation of the filters. At the time of the experiments performed in this research project,

the contribution of CFP fluorescence into YFP detected emission accounted for was 0.3886 (~ 40%).

Furthermore, the crosstalk of fluorophores also includes the direct excitation of the acceptor at the donor absorption wavelength (Shrestha et al. 2015), called "false excitation". In order to measure the correction factor for false YFP excitation, HEK293T cells were transfected with YFP-containing plasmid alone and the emission in the F_{534} channel was recorded for excitation at 430 nm. As in the case of "bleed through" correction factor, the "false excitation" value is constant and was compiled as 0.0452 (~ 4%).

Since the recording of both donor and acceptor fluorescent intensities was performed under consecutive excitation of the donor only, the total YFP expression in the cell was calculated as YFP emission under 500 nm excitation wavelength derived from the additional 20 seconds measurement, which took part after the main experiment.

Thus, the final sensitized YFP emission (F_{YFP}^{C}) can be calculated (Youvan et al. 1997) by following equation:

$$F_{YFP}^{C} = F_{YFP}^{d} - 0.4 * F_{CFP} - 0.04 * F_{YFP}^{t} \qquad \text{(E2.1)}$$

where F_{YFP}^{d} and F_{CFP} are YFP and CFP emission intensities respectively measured during actual experiment, F_{YFP}^{t} is the intensity of YFP measured in F_{534} channel under direct acceptor excitation, 0.4 and 0.04 are "spillover" and "false excitation" correction factors calculated for Nikon setup respectively.

The final corrected FRET signal was calculated as a ratio of corrected YFP (F_{YFP}^{C}) over measured CFP F_{CFP} intensities.

One more parameter which has been corrected for most of the experiments described in this work is photobleaching. Due to continuous or frequent illumination the fluorophore is caged in a dark triple excited state and therefore unable to repetitively enter excitation/emission cycles (Ishikawa-Ankerhold, Ankerhold, and Drummen 2012). Thus the emitted light fades over time which lead to the drift in FRET signal. The photobleaching correction was performed by fitting the exponential function to the base line of each individual FRET experiment recording in Origin 8.5.

2.2.5 Data analysis and statistics

In this section I would like to briefly discuss the basic concepts of chemical reaction kinetics. The rate of chemical reaction (w) is one of the most important quantitative kinetic parameters of biochemical process and is defined as the alteration of the amount of substance

that reacts (n) or the amount of reaction product (n) at a particular time point at a particular volume:

$$\omega = \pm\frac{1}{V}\frac{dn}{dt} \quad \text{(E3.1)}$$

If we assume my experiments are constricted to a single living cell, the volume of the system where the reaction takes place is constant:

$$\omega = \pm\frac{d}{dt}\left(\frac{n}{V}\right) = \pm\frac{dc}{dt} \quad \text{(E3.2)}$$

The dependence of the chemical process rate (w) from the concentration of different components of the reacting system (C) is described by the following equation:

$$\omega = f(c_1, c_2, \ldots c_m) \quad \text{(E3.3)}$$

Depending on the reaction, function f can be more complex. Empirically, it has been shown that the rate of chemical reaction is proportional to the reagent concentration (C) raised to the nth power:

$$\omega = -\frac{1}{v_i}\frac{dc_i}{dt} = kc_1^{n_1}c_2^{n_2}. \ldots (i = 1, 2, \ldots m) \quad \text{(E3.4)}$$

where *vi* is the stoichiometry coefficient of the reagent, *t* is a time point, k is a rate constant.

Since in my research project I focus on the interaction of two proteins which under the application of the ligand form a stable complex, the general equation for this biochemical process looks like:

$$L + R + G \leftrightarrow Z \quad \text{(E3.5)}$$

Where L is ligand, R-receptor, G - G protein and Z is a ternary complex. Under nucleotide-depleted conditions the GPCR-G protein binding is a limiting factor for the rate of the reaction, the influence of agonist association and dissociation rate in the E3.5 is further neglected. All experiments were done at RT, therefore, no extra calculations were required for comparison of different kinetics parameters.

If we define z as total amount of ternary complexes Z which can be formed according to the amount of the receptors expressed (R), and b is a number of receptors bound to G proteins by the time point t, E3.4 can be presented as:

$$\omega = k\,(z - b) = \frac{db}{dt} \quad \text{(E3.6)}$$

$$k\,dt = \frac{db}{z-b} \quad \text{(E3.7)}$$

Where (z-b) is the amount of the receptors not bound to G proteins at the time t.

By integrating from 0 to b and 0 to t, the equation E3.7 is transformed to:

$$\int_0^b \frac{d\varepsilon}{z-\varepsilon} = k\int_0^t d\tau \quad \text{(E3.8)}$$

$$ln\frac{z}{z-b} = kt \quad \text{(E3.9)}$$

$$k = \frac{1}{t}\, ln\frac{z}{z-b} \quad \text{(E3.10)}$$

The time point when the particular concentration of the ternary complexes is achieved:

$$t = \frac{ln\frac{z}{z-b}}{k} \quad \text{(E3.11)}$$

The time when half of the receptors are occupied by the G proteins is defined as half-time of the reaction ($\tau_{1/2}$). It means, that the number of ternary complexes formed by the half-time of the GPCR-G protein binding reaction is defined as Z/2. Therefore:

$$\tau_{1/2} = \frac{ln2}{k} \approx \frac{0.693}{k} \quad \text{(E3.12)}$$

Since this relation is simple and can be depicted as in Figure 4, we can conclude that the half-life of a first-order reaction is a constant.

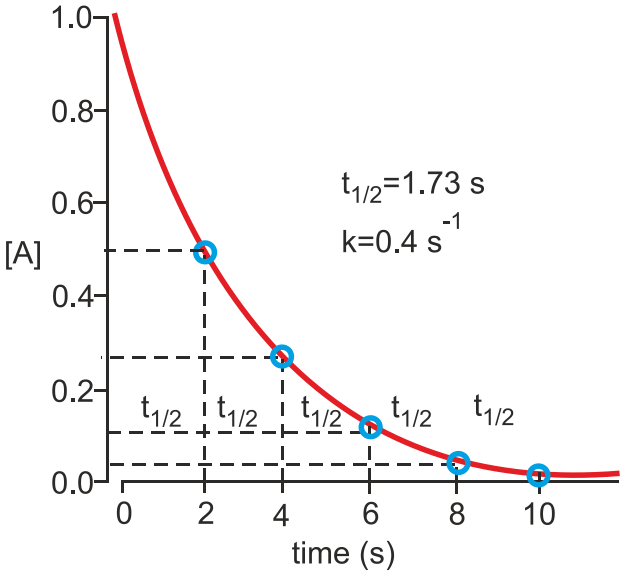

Figure 4. Half times for the example of the first-order reaction

Since $\tau_{1/2}$ depends on the initial concentrations of the interacting partners and their individual properties (E3.6, E3.7), the given numbers are not the case for all biochemical reactions.

The potentiation of E3.12 leads to the exponential dependence of the amount of free and G-protein occupied receptors on time of the reaction:

$$(z - b) = ze^{-kt} \quad \text{(E3.13)}$$

The reactions which kinetics can be described by equations E3.12 and E3.13 are defined as first-order reactions and if plotted as logarithmic concentration over time represent a straight line (Figure 5).

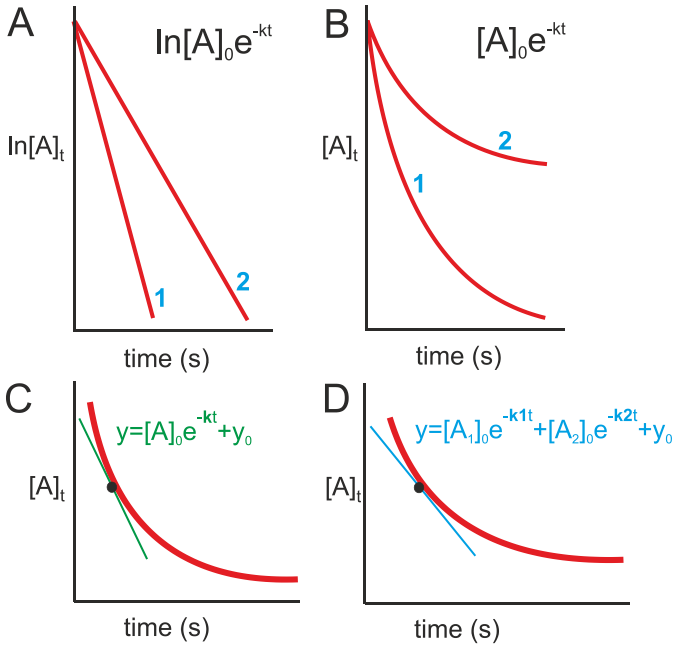

Figure 5. Comparison of the decay of first-order reactions
The schemes depict the logarithmic **(A)** and linear **(B)** dependence of biochemical agent concentration over time. The presented tangents to mono-**(C)** and two-exponential **(D)** curves are supplied with the equations used to calculate rate constants.

The rates of association and dissociation of GPCR and G protein were calculated by fitting the mono- (Figure 5C) or two-phase (Figure 5D) exponential functions to the curves derived from FRET experiments as depicted in Figure 19C.

Individual traces are shown as either absolute or relative YFP/CFP emission ratio changes. Absolute changes in YFP/CFP emission ratio were calculated as a difference in average values of the last 10 seconds before or after an event. The relative change of FYFP/FCFP was calculated by normalization to the maximum peak after application of saturating agonist concentration relative to the G protein-free state, determined by application of GTPγS. As a measure of the affinity of G protein-receptor complex, dissociation kinetics of the complex were measured under nucleotide-free conditions in response to agonist withdrawal. Resulting data of the offset kinetics (decrease in FRET) were fitted by a monoexponential function.

3. Results

3.1 Imaging ternary complex by means of FRET

In order to investigate the affinity of the receptor-G protein interaction, the dynamics of G proteins binding to activated GPCRs and their subsequent dissociation was analysed by FRET microscopy under conditions of GTP-depletion. HEK293T (Human Embryonic Kidney) cells expressing M_3-R-YFP, $G\alpha_q$, $G\beta_1$ subunits, and CFP-$G\gamma_2$ were subjected to

single cell FRET imaging (Figure 6A,B) similar to the process described previously (Milde, et al., 2013). In intact non-GTP-depleted cells, we observed a small and rapidly reversible increase in FRET as also shown previously for other receptors (Figure 6C) (Hein, Bünemann, 2005). We then permeabilized cells by a 2 minute exposure to 0.05% saponin (Figure 6D,E,F) in order to deplete membranes from nucleotides, thus allowing the development of relatively stable agonist-receptor-G protein complexes (Hommers et al. 2010). The amplitude of the FRET signals in permeabilized cells was substantially higher, indicating a largely increased occupancy of receptors with G proteins (Figure 6F). Most importantly, after withdrawal of the agonist we observed much slower dissociation kinetics of G_q from M_3-R in absence of nucleotides (Figure 6C vs. F) which reflects the high intrinsic affinity of G proteins to active receptors under conditions of nucleotide-depletion. The rapid drop of the FRET signal in response to GTPγS indicates nucleotide-dependent fast dissociation of the remaining receptor-G protein complexes (Figure 6F).

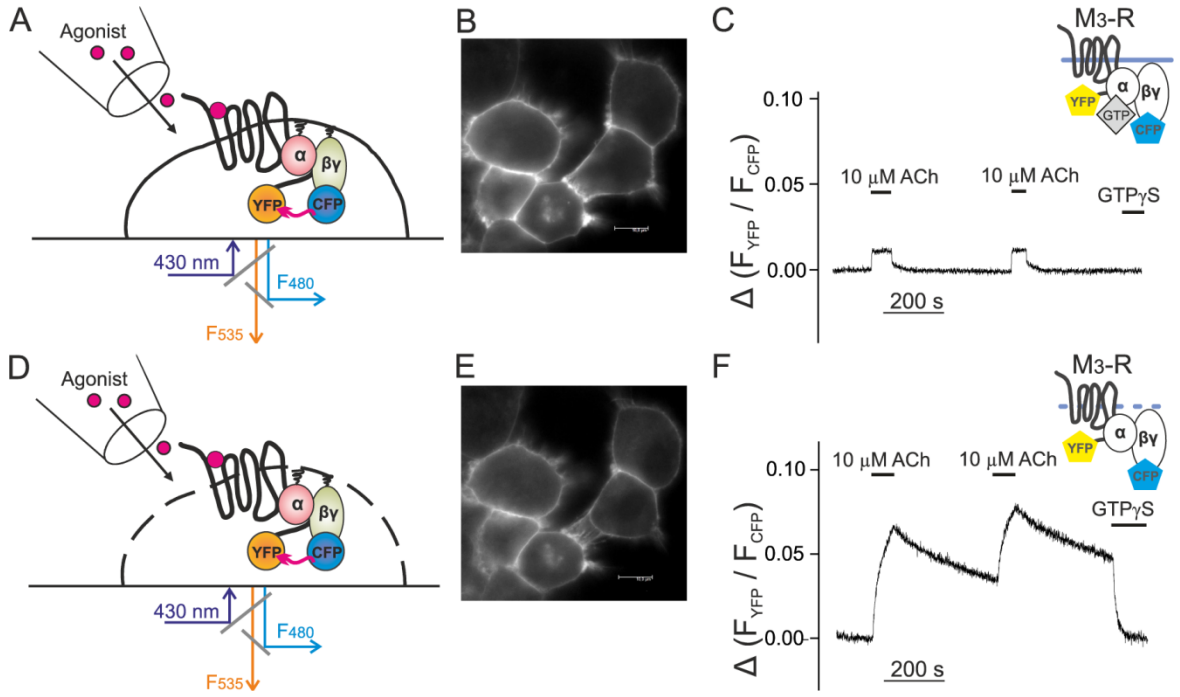

Figure 6. Dynamics of G protein-M3-R interaction in absence of nucleotides
CFP-labelled G_q protein binding to the YFP-labelled M_3-R was measured by means of FRET in intact **(A, B, C)** and in permeabilized **(D, E, F)** cells as schematically illustrated in (**A, D)**. Confocal microscopy images of CFP fluorescence in HEK293T cells transfected with M_3-R C-terminally labelled with YFP, $G\alpha_q$-wt, $G\beta_1$-wt, and $G\gamma_2$ N-terminally labelled with CFP were derived prior **(B)** and after membrane permeabilization by brief incubation with Saponin **(E)**. FRET measurements were performed on single intact and permeabilized cells excited at 435 nm and exposed to agonist or GTPγS as indicated **(C** and **F** respectively**)**. The YFP/CFP emission ratio derived from a single cell was calculated and plotted over time **(E, F).** Upon receptor stimulation a stable receptor - G protein complex was formed only in absence of nucleotides **(F)**.

3.2 Selectivity of G protein binding to mAChRs

3.2.1 Quantification of G protein intrinsic affinity to M_3-R

Based on reports that M3-Rs may also couple to $G_{i/o}$ and even G_s proteins (Jones, et al., 1991), we wanted to quantify the selectivity of M_3-Rs binding to 4 different classes of G proteins under conditions of nucleotide depletion. Therefore, we compared the agonist (10 µM acetylcholine (ACh)) evoked FRET signal between fluorescent M_3-R and fluorescent Gβγ subunits proteins when $G\alpha_q$, $G\alpha_o$, $G\alpha_s$, $G\alpha_{13}$ or pcDNA3 instead of Gα was transfected (Figure 7A). As depicted in Figure 7A, there were no significant differences in the small agonist-evoked FRET signals in cells transfected with $G\alpha_s$ or $G\alpha_{13}$ compared with those that were transfected with empty vector instead of cDNA encoding for Gα subunits, indicating no detectable interactions.

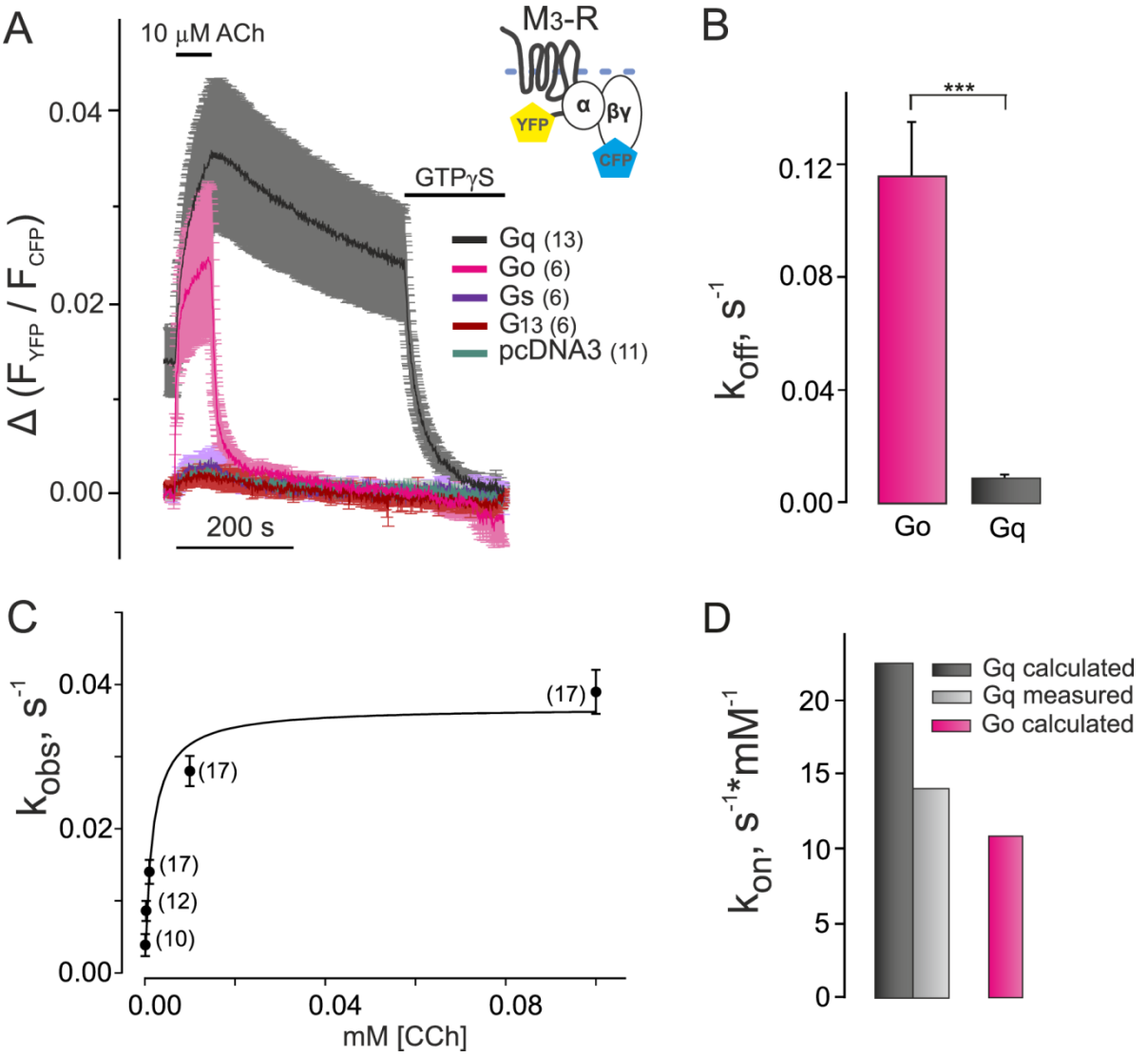

Figure 7. Quantification of G protein-receptor selectivity
Interaction of G_o, G_q, G_s or G_{13} proteins with M_3-R induced by agonist application was measured by means of FRET in permeabilized cells similar as described in Figure 6F. **(A)** The graph depicts average FRET signals derived from cells, transiently transfected with YFP

labeled M_3-R, CFP-labeled $G\gamma_2$ subunit and indicated in the legend Gα subunit. YFP/CFP emission ratios were normalized to minimum receptor occupancy state induced by GTPγS application. Compared to the increase in FRET signal under ACh application when no Gα but the empty vector pcDNA3 was transfected no specific binding of either G_s or G_{13} protein binding to M_3-R was observed. **(B)** Quantification of dissociation constants (k_{off}, s^{-1}) for G_o and G_q proteins from M_3-R (n=14; n=30 respectively) are illustrated. **(C)** Hyperbolic function was fitted to the measured values of on-rate kinetics (k_{obs}, s^{-1}) of G_q protein binding to M_3-R induced by different CCh concentrations under GTP-depleted conditions **(D)** Comparison of k_{on} values of M_3-R-G_q association kinetics (light grey) obtained from fitted hyperbolic function using equation E4.2 and steady-state experiments (k_{on}^{C} of G_q (black)) and G_o data (magenta), calculated using equation E4.3. All data are plotted as mean ± SEM for each condition. N of each experiment is shown in brackets if not indicated in the legend.

The comparison of G_q and G_o dissociation rate from M_3-R during the withdrawal of agonist in absence of nucleotides revealed a significant 13-fold difference: 0.009 ± 0.002 s^{-1} and 0.116 ± 0.019 s^{-1} respectively (Figure 7B, Figure 19C exponential - fit example), which indicates a lower affinity of the M_3-R-G_o complex. Moreover, since we actually measured the interaction of fluorescent Gβγ with fluorescent receptors using overexpressed native Gα subunits for a more accurate comparison between receptor-G protein coupling, we also performed experiments with fluorescently labelled versions of both $G\alpha_q$ and $G\alpha_o$ as a control. No labelling associated differences in the dissociation kinetics for both G proteins were detected (Figure 8).

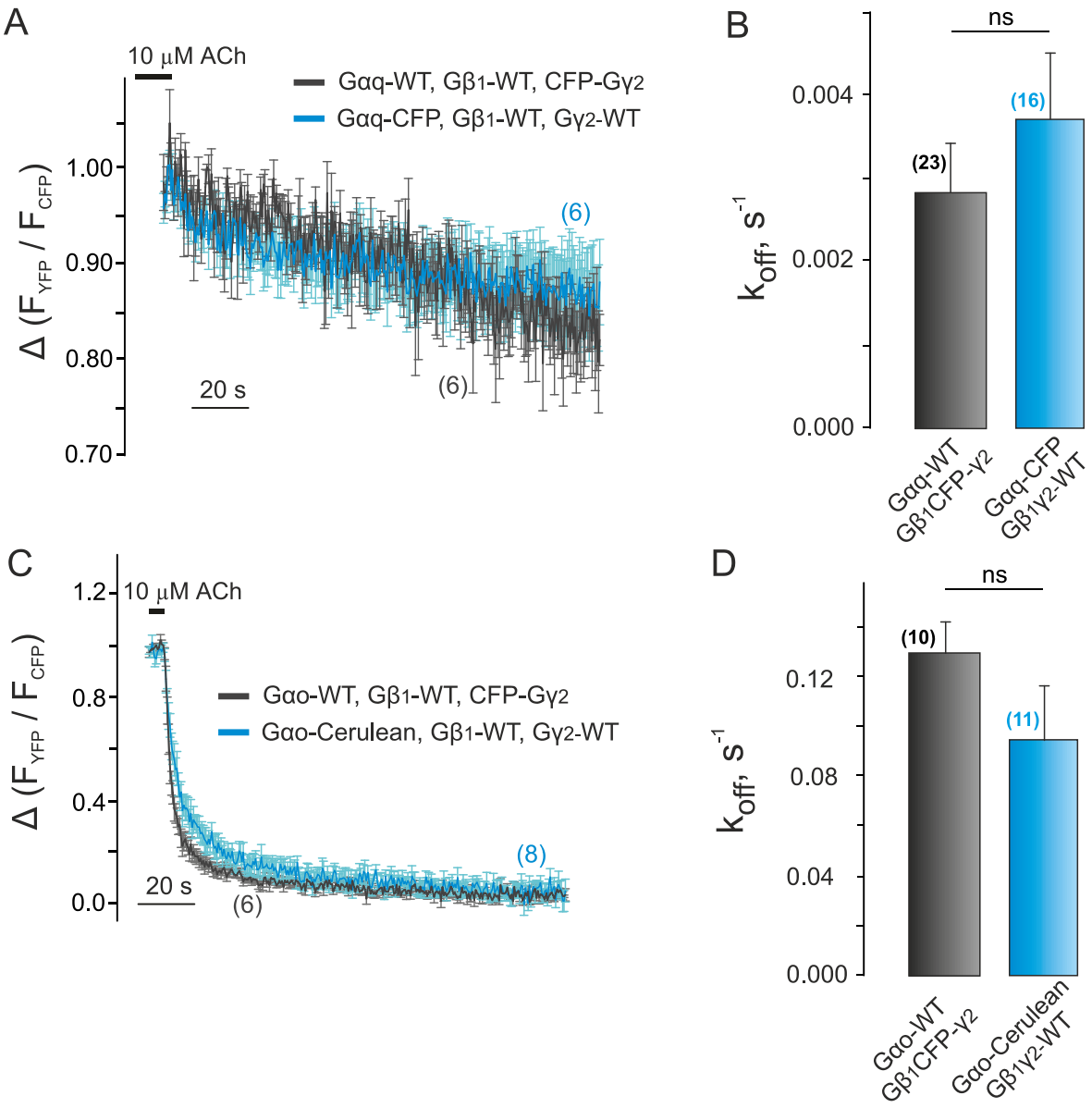

Figure 8. The stability of M_3-R-G protein ternary complexes was independent of the labelling site on the G protein

The decay kinetics of G_q-M_3-R complex dissociation upon agonist withdrawal under nucleotide-free conditions **(A)** were compared when the G protein was (CFP)-labelled on N-terminus of Gγ or Cerulean-labelled in the helical domain of the $G\alpha_q$ subunit. **(B)** Dissociation kinetics were calculated as described in section 2.2.5. Similar to G_q, the stability of M_3-R-G_o complex was measured by means of FRET **(C,D).** No significant difference between conditions of Gα-labelled and Gγ-labelled G proteins was observed in respect to calculated k_{off} values. Statistical analysis was performed by one-way ANOVA with Bonferroni post-hoc test (*P < 0.05).

Similarly, long lifetimes of receptor-G protein complexes were observed for other receptors such as β_1-, β_2-, and α_{2A}-ARs as well as TP-R only for G protein subtypes which are known to be activated by the respective receptor (Figure 29, Figure 30, Figure 32). Although, the binding of $G\alpha_s$ and $G\alpha_{13}$ to M_3-R was not detected, these G proteins did bind with high

affinity to receptors such as β_1-, β_2-andrenergic receptors (β-AR) and thromboxane TxA_2 receptor (TP-R) in accordance with the literature data. Correspondingly, we could not detect G_{13} or G_s activation via stimulation of M_3-R (Figure 9).

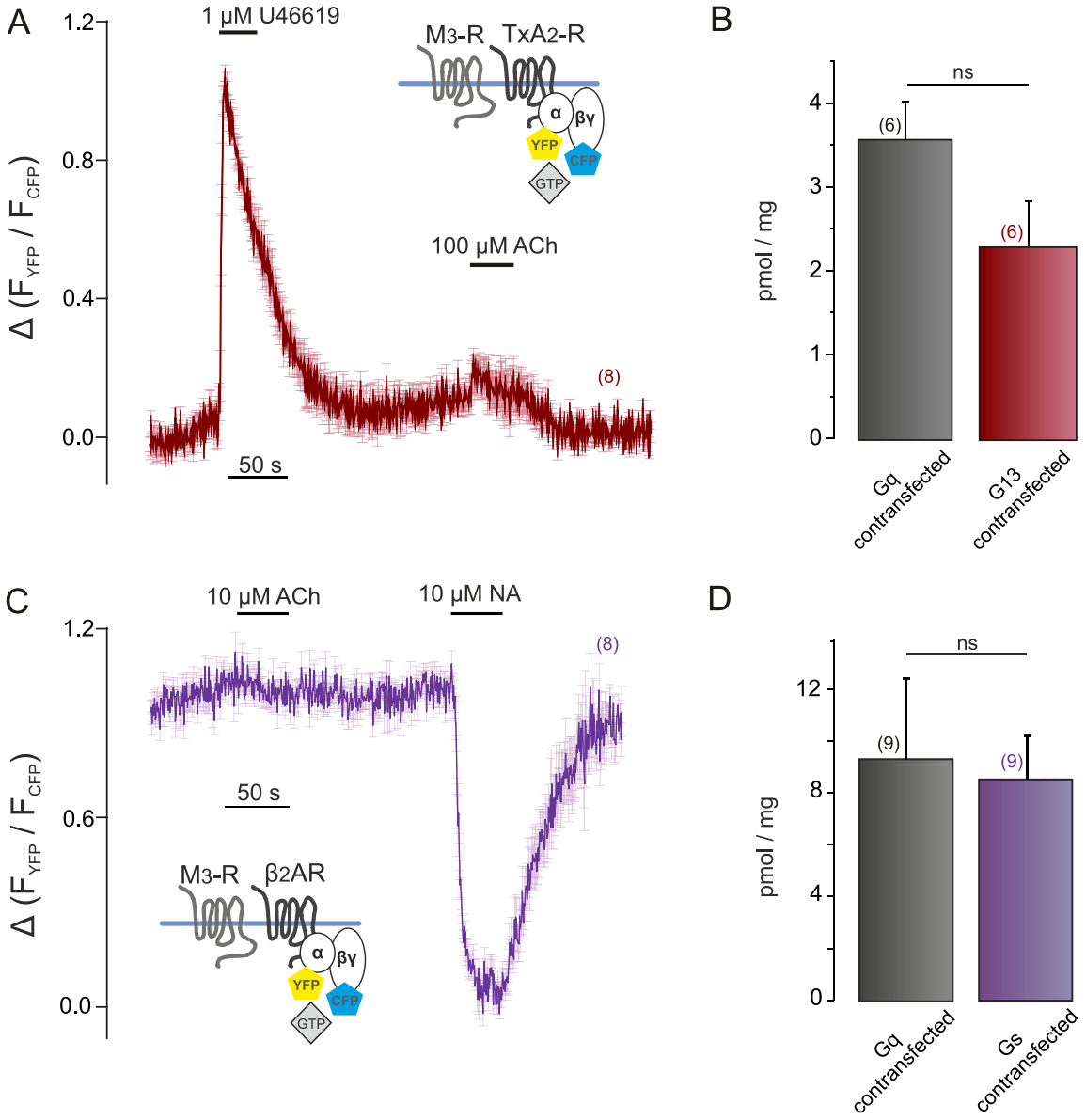

Figure 9. Stimulation of M_3-R did not result in G_{13} and G_s activation
Depicted is the average trace of G_{13} activation measured by means of FRET **(A)** in intact cells by selective stimulation of either TP-R with U46619 or cotransfected M_3-R with ACh. G_{13} activation is reflected in a robust increase in YFP/CFP emission ratio under U46619 whereas the perfusion of the same cell with ACh led to only a slight change in FRET signal, indicating the absence of G13 activation via M_3-R. **(C)** Average FRET signal trace of G_s activation by stimulation of β_2AR or cotransfected M_3-R. No activation of G_s was observed upon M_3-R-agonist application. The absence of difference in M_3-R expression levels transfected with G_q versus G_{13} proteins **(B)** or G_q versus G_s protein **(D)** were confirmed by [^{3}H]-scopolamine radioligand binding (section 2.2.2.5). HEK293T cells were transiently transfected as described in Table 6 section 2. Data are shown as mean ± SEM, n of each experiment is given in brackets. Statistical analysis was performed by one-way ANOVA with Bonferroni post-hoc test (*P < 0.05).

However, we observed a robust agonist-induced FRET signal in cells transfected with $G\alpha_o$, which was comparable in amplitude with signals obtained in $G\alpha_q$ expressing cells (Figure 7A, Figure 18A pink vs. black).

Under these conditions we determined the G protein/receptor expression ratio to be 2- to 6-fold (Figure 10) and also detected no major alterations of $G\beta\gamma$ expression in dependence of the co-expressed $G\alpha$ subtype (Figure 11). Based on the broad expression profiles of β and γ subunits of G proteins in different tissues, we have chosen $G\beta_1$ and $G\gamma_{12}$ subunits for our experiments as a prototypical $\beta\gamma$ dimer (Dingus and Hildebrandt 2012; McIntire 2009).

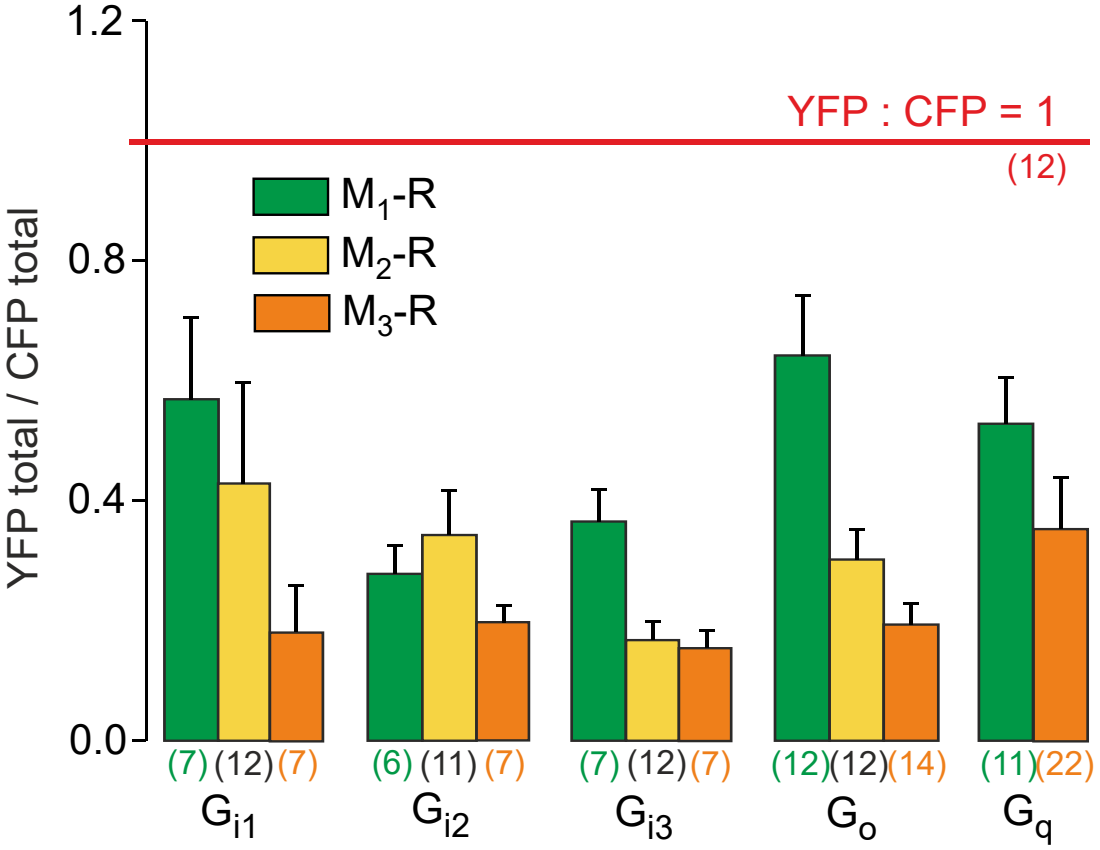

Figure 10. Quantification of donor vs. acceptor fluorophores stoichiometry
The individually measured CFP and YFP intensities were calculated as described in section 2.2.4.4. HEK293T cells were transiently transfected with M_1-, M_2-, or M_3-R and respective G proteins (see Table 6, section 1). The red line depicts the YFP/CFP fluorophores intensities ratio equal to 1. The ratio was derived from the cells transfected with YFP-β_2-AR-CFP (Dorsch et al. 2009) as a reference construct, bearing both fluorophores in one molecule without exhibiting detectable FRET, which were permeabilized as indicated in Figure 6 . The data are represented as mean ± SEM, n of each experiment is shown in brackets. No significant differences in stoichiometry within G_q and G_i family proteins were observed when the same mAChR was transfected. Statistical analysis was performed by one-way ANOVA with Bonferroni post-hoc test (*$P < 0.05$).

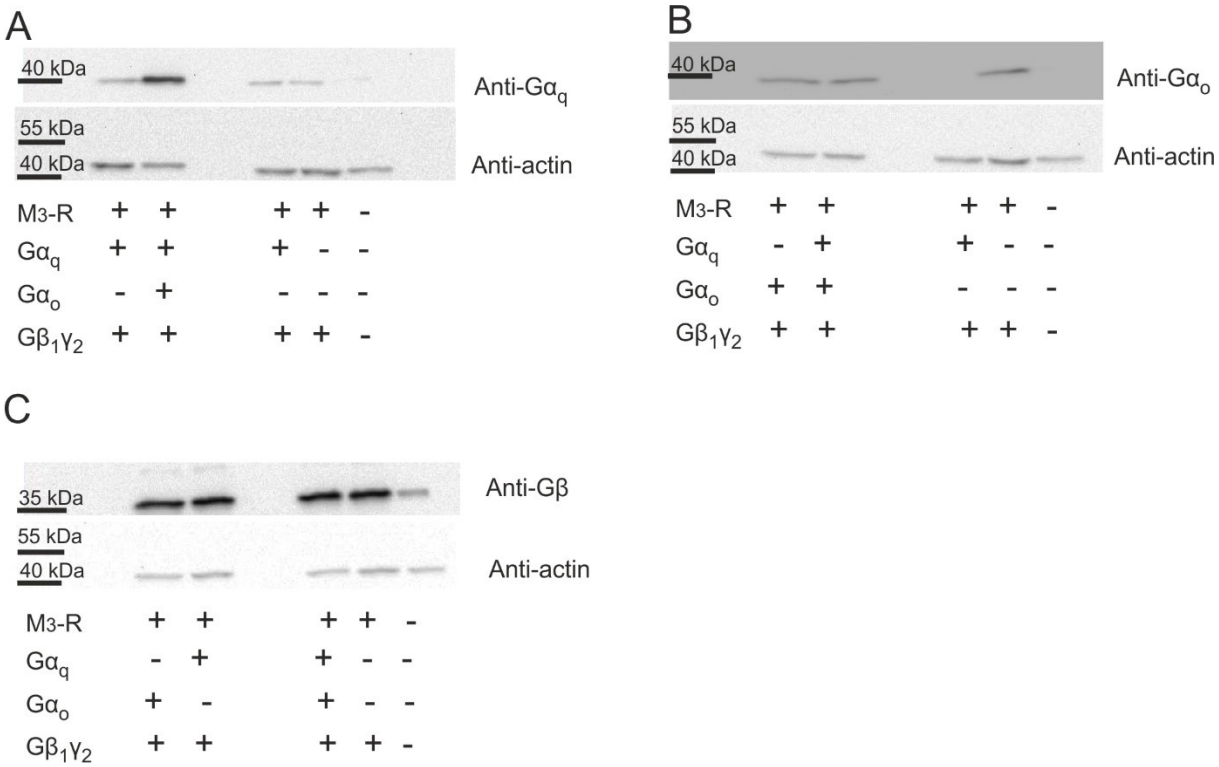

Figure 11. $G\alpha_q$, $G\alpha_o$ and $G\beta_1\gamma_2$ G protein subunit expression in transiently transfected HEK293T cells

Western-blot was performed on the cellular membranes derived from HEK293T cells transiently transfected as depicted in the Figures. Gβγ expression **(C)** levels were compared in the absence or presence of coexpression of $G\alpha_q$ **(A)** or $G\alpha_o$ **(B)** subunits. The amount of the transfected plasmids and detailed antibody list are given in Table 2 and Table 5 respectively. Anti-actin monoclonal mouse antibody was used as a loading control after membrane stripping.

3.2.2 Verification of effective nucleotide-removal in permeabilized cells

In experiments studying M_3-R interaction with either G_q or G_o proteins in the presence of high or low concentrations of GDP or GTP we verified accurate control of nucleotides in permeabilized cells (Figure 12). Whereas 100 nM concentration of nucleotides led to a descending of FRET signal amplitude in response to perfusion with ACh, 100 μM GTP/GDP concentration caused the dramatically reduced G_q or almost fully diminished G_o protein binding to M_3-R.

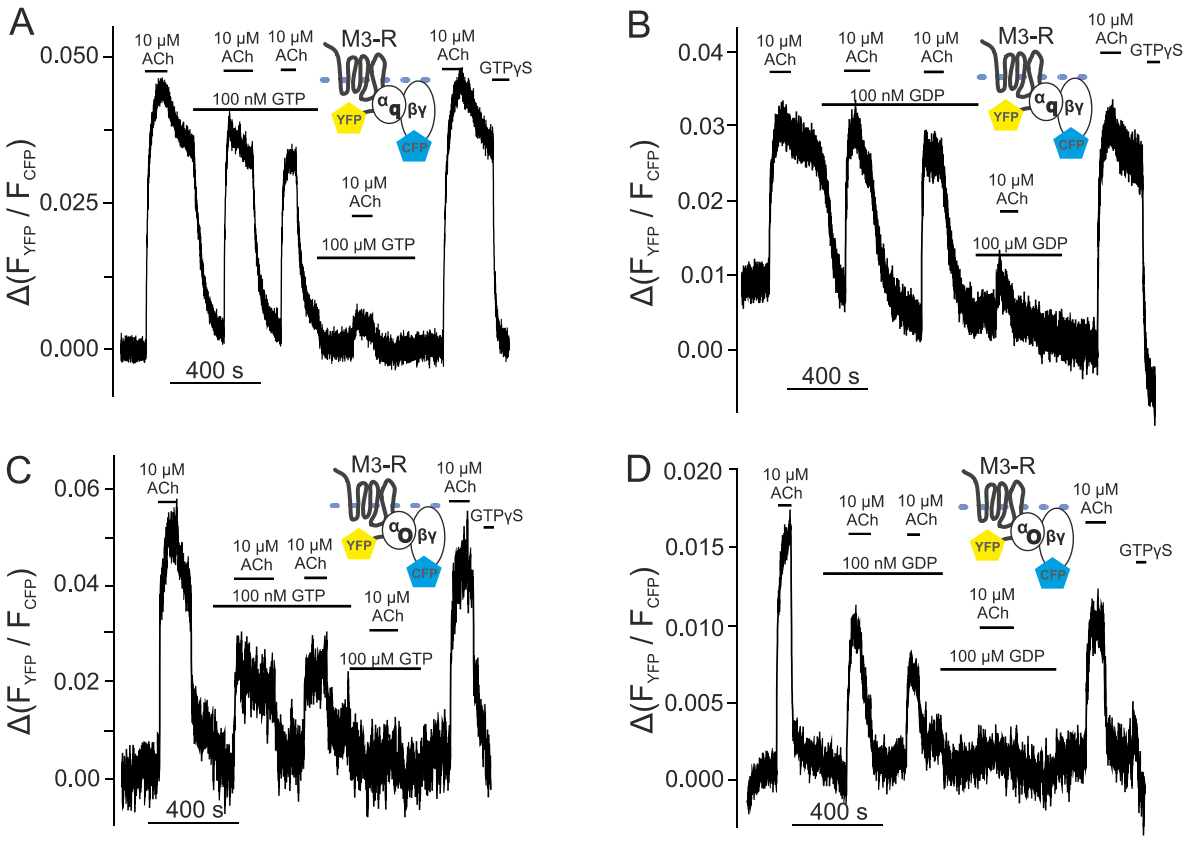

Figure 12. Ternary complex formation and dissociation in presence of low and high nucleotides concentration

Representative traces depict binding of G_q **(A,B)** and G_o **(C,D)** proteins to M_3-R (n=6-10 similar experiments) measured by means of FRET in single permeabilized HEK293T cells. The first stimulation with ACh and the ensuing agonist withdrawal of up to 3 minutes was done in absence of nucleotides. The drop in YFP/CFP intensity ratio under the application of buffer supplied with low (100 nM) GTP **(A,C)** or GDP **(B,D)** concentration reflect the dissociation of respective G protein from the receptor. Cells were transfected as indicated in Table 6 section 2.

In both G_o and G_q transfected cells the response to stimulation of the M_3-R with ACh in the presence of 100 nM nucleotides was reduced and decreased over time when the agonist was still present. The second application of the agonist in presence of low GTP or GDP concentrations reached the previous steady-state much faster without a clear decline, which is in line with nucleotide binding as a rate limiting state for reaching a fast equilibrium at the previous application of agonist. GTP or GDP at a concentration of 100 µM led to a faster off-rate of the G_q protein from the M_3-R. G_q binding to M_3-R under stimulation with 10 µM ACh in the presence of 100 µM GDP/GTP was much reduced and mimicked the conditions of G_q binding to M_3-R in intact non-permeabilized HEK293T cells depicted in Figure 6C. After wash out of the nucleotides by the rapid buffer exchange perfusion system and following stimulation with 10 µM ACh the YFP/CFP emission ratio increased to similar values as in response to the initial agonist application for both G_q and G_o proteins (Figure 12 A-D).

Cells, transiently expressing YFP-tagged M_3-R, $G\alpha_q$-wt or $G\alpha_o$-wt, $G\beta_1$-wt, and $G\gamma_2$–CFP were permeabilized by 2 minutes incubation with 0.05% Saponin and released from GTP and GDP via several washing steps with internal buffer. Single cells were washed 2 minutes with internal buffer via rapid superfusion (< 10 ms) to get the stable baseline. The increase of FRET signal was induced by stimulation with 10 µM ACh. The withdrawal of agonist was performed by depletion of ACh with a constant superfusion of the cell with internal buffer. The overlay of G_q and G_o dissociation from M_3-R is shown in Figure 13A,C dependent on the presence of nucleotides. The dissociation kinetics of G_q but not G_o from M_3-R were significantly accelerated by GTP (Figure 13B,D). The non-significantly different k_{off} values for G_o-M_3-R dissociation kinetics can be explained by low affinity of G_i family proteins to M_3-R (Figure 18).

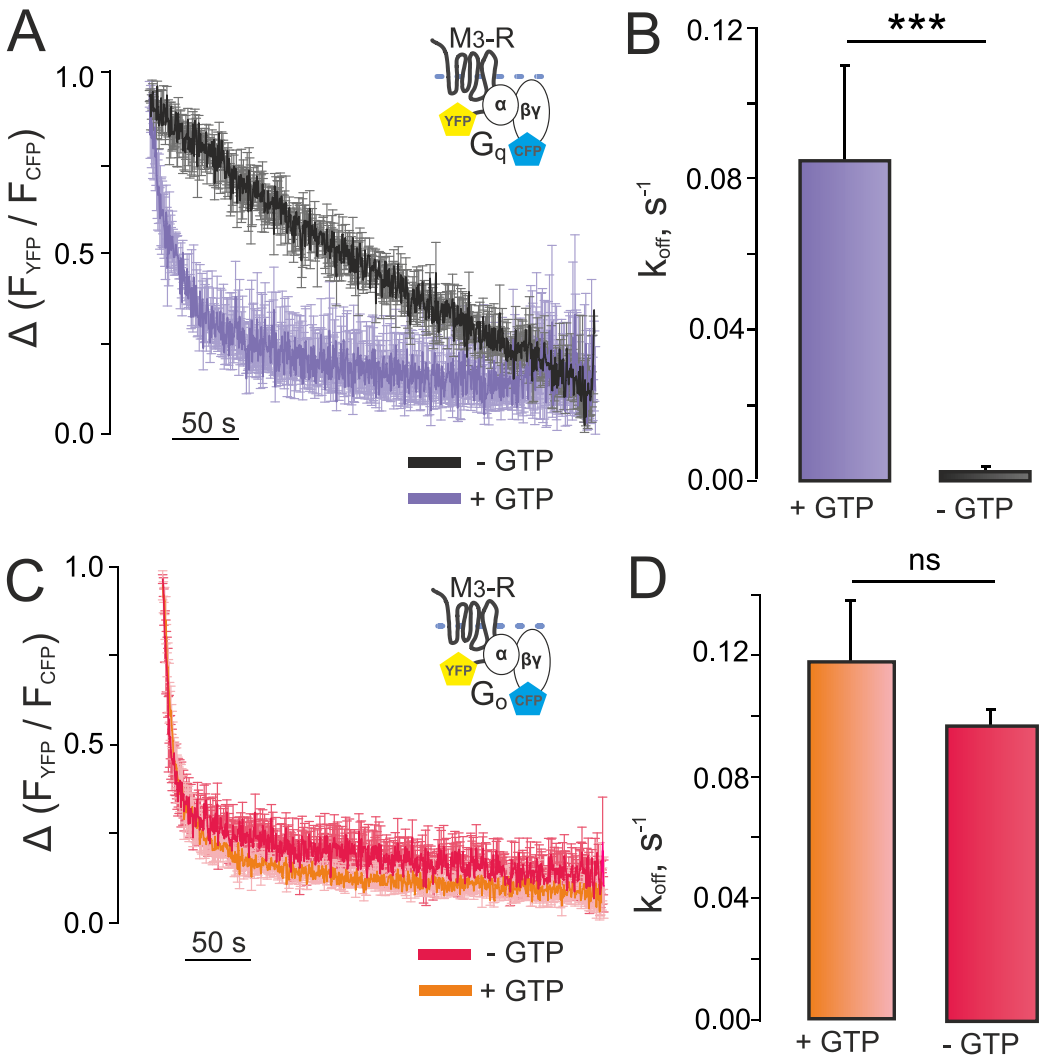

Figure 13. M_3-R-G protein ternary complex stability upon the reintroduction of GTP into permeabilized cells

Illustrated are averaged traces of F_{YFP}/F_{CFP} alterations induced by agonist withdrawal from permeabilized cells expressing G_q-CFP **(A)** or G_o-CFP **(C)** and M_3-R-YFP in the presence or

absence of 100 nM GTP. HEK293T cells were transfected with M_3-R-YFP and G_q or G_o protein as described in Methods (Plasmid mix. G protein binding). K_{off} values of the M_3-R G_q- (**B**) or G_o-protein (**D**) interaction were determined by fitting an monoexponential decay function to individual FRET-decays shown in **A** and **C** for both conditions (with or without GTP) and were plotted as averaged data. All data are presented as mean ± SEM. Statistical analysis was performed by one-way ANOVA with Bonferroni post-hoc test (*P < 0.05).

3.2.3 Preassembly of M_3-Rs and G_q, G_o proteins under nucleotide-free conditions

The question whether GPCRs and G proteins preassemble in intact cells is a matter of debate (Kuravi et al. 2010). It has been reported in several studies that a precoupling of G_q proteins to inactive receptors may exist. The crucial role of M_3-R receptor C-terminus in G protein-receptor preassembly as well as polybasic region in helix 8 has been revealed (Qin et al. 2012). Although, the M_3 muscarinic receptor used in previously described assays is labelled with the fluorescent protein on the C-terminus which might impair inactive receptor-G protein precoupling (Qin et al. 2012), I decided to test for the presence of nucleotide-sensitive pre-association of receptors and G proteins in permeabilized cells. The application of GTPγS prior to the agonist did not lead to remarkable decrease in YFP/CFP emission ratio, indicating no detectable association either G_q or G_o proteins with unstimulated M_3-R in the developed nucleotide-free FRET-based assay (Figure 14).

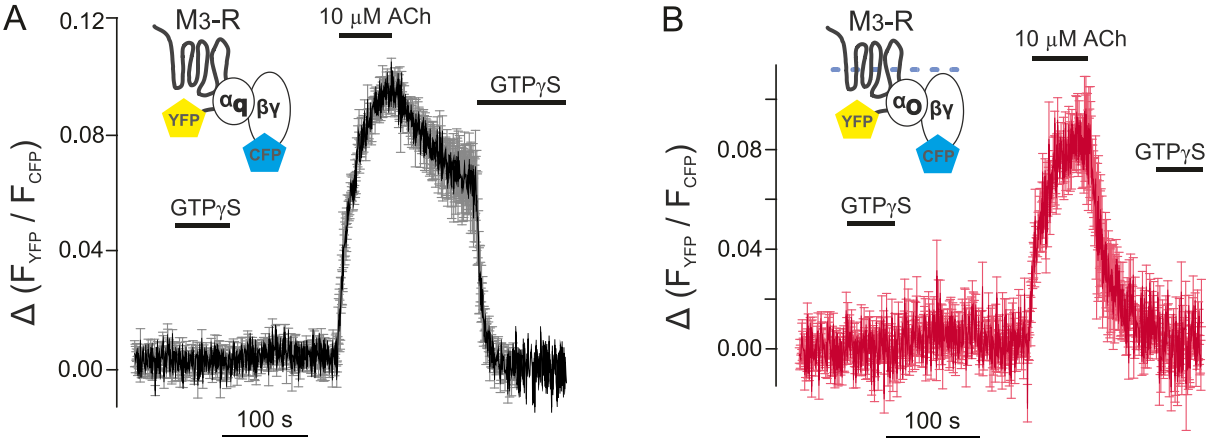

Figure 14. Test for nucleotide sensitive agonist-independent M_3-R-G protein interaction
The figure depicts average FRET traces of M_3-R-G_q **(A)** and M_3-R-G_o **(B)** interaction under nucleotide-free conditions normalized to minimum receptor occupancy state. HEK293T cells were transfected as described in Table 6 section 1. In G_q as well as in G_o transfected cells the application of GTPγS prior to stimulation with the agonist did not lead to a decrease in YFP/CFP emission ratio indicating no preassembly of G proteins with M_3-Rs after membrane permeabilization. All presented data represented as mean ± SEM, with n≥7.

3.2.4 Calculation of M_3-R-G_q and M_3-R-G_o association kinetics

Furthermore, we measured the association kinetics of M_3-R with G_o and G_q proteins under nucleotide-depleted conditions in dependence of the agonist concentration (Figure

7C,D). Based on generally accepted agonist receptor occupancy models (Kenakin, 2008; Pierre, 2011) the rates of receptor-G protein interaction (k_{obs}) should increase with an exponential correlation (E4.1) to the agonist concentration applied. Taking into account that the exponential function is a subcase of a particular hyperbolic sector, k_{on} was calculated as a first derivative of k_{obs} described as hyperbolic function (E4.2).

$$k_{obs} = \frac{P_1 * x}{P_2 + x} \ (s^{-1}) \qquad \text{(E4.1)}$$

$$k_{on} = (k_{obs})' = \frac{P_1 * P_2}{(P_2 + x)^2} \qquad (s^{-1} * mM^{-1}) \qquad \text{(E4.2)}$$

$$k_{on}^{C} = \frac{k_{off}}{EC_{50}} \qquad (s^{-1} * mM^{-1}) \qquad \text{(E4.3)}$$

Moreover, the k_{on} values for the G_q and G_o and G_{i2} were also calculated according to the equation E4.3 (k_{on}^{C}) based on the determined k_{off} values and the apparent EC_{50} values measured under steady-state conditions in permeabilized cells (E4.3, Figure 7, Figure 15, Figure 16, Figure 17A).

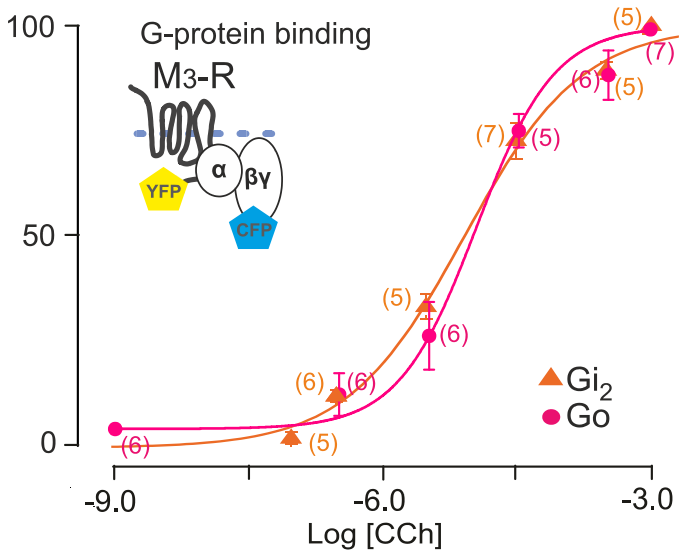

Figure 15. Comparison of carbachol-induced G_{i2} and G_o steady-state binding to M_3-R in absence of nucleotides

Agonist concentration dependent binding of G_{i2} and G_o to M_3-R under nucleotide-depleted conditions were plotted. HEK293T cells were transiently transfected as described in Table 6 section 1, permeabilized and stimulated by increasing concentrations of CCh under conditions close to steady state. CCh-concentration-response curve for G_o binding to M_3-R is given as a reference similar to the one given in Figure 17A. The amplitudes of increase in YFP/CFP emission ratio for both G_o and G_{i2} were normalized to the response of the cell to saturating CCh concentration (1 mM). Curves were fitted according to Hill-Langmuir equation revealing EC_{50}= 8.33 ± 0.22 µM CCh with 0.7 Hill-slope for G_{i2} and 10.68 ± 0.32 µM CCh with 1.0 Hill-slope for Go. All concentration-response data is represented as mean ± SEM for each condition, n of each experiment is shown in brackets.

Based on results shown in Figure 15 the k_{on}^{C} value for the G_{i2} were calculated using equation E4.3 and measured k_{off} data (Table 8), which appeared to be 6.36 $s^{-1}*mM^{-1}$ and 1.5-fold slower as for G_o (Table 8).

Both k_{on} and k_{on}^{C} values for G_q (Figure 7C,D) appeared to be relatively similar (22.40 $s^{-1}*mM^{-1}$ and 14.04 $s^{-1}*mM^{-1}$ respectively). We also attempted to experimentally determine the on-rate for the M_3-R-G_o interaction (Figure 16), however in this case the apparent on-kinetics were faster and if plotted against the agonist concentration we failed to fit the data to a simple one-component hyperbolic function (Table 8).

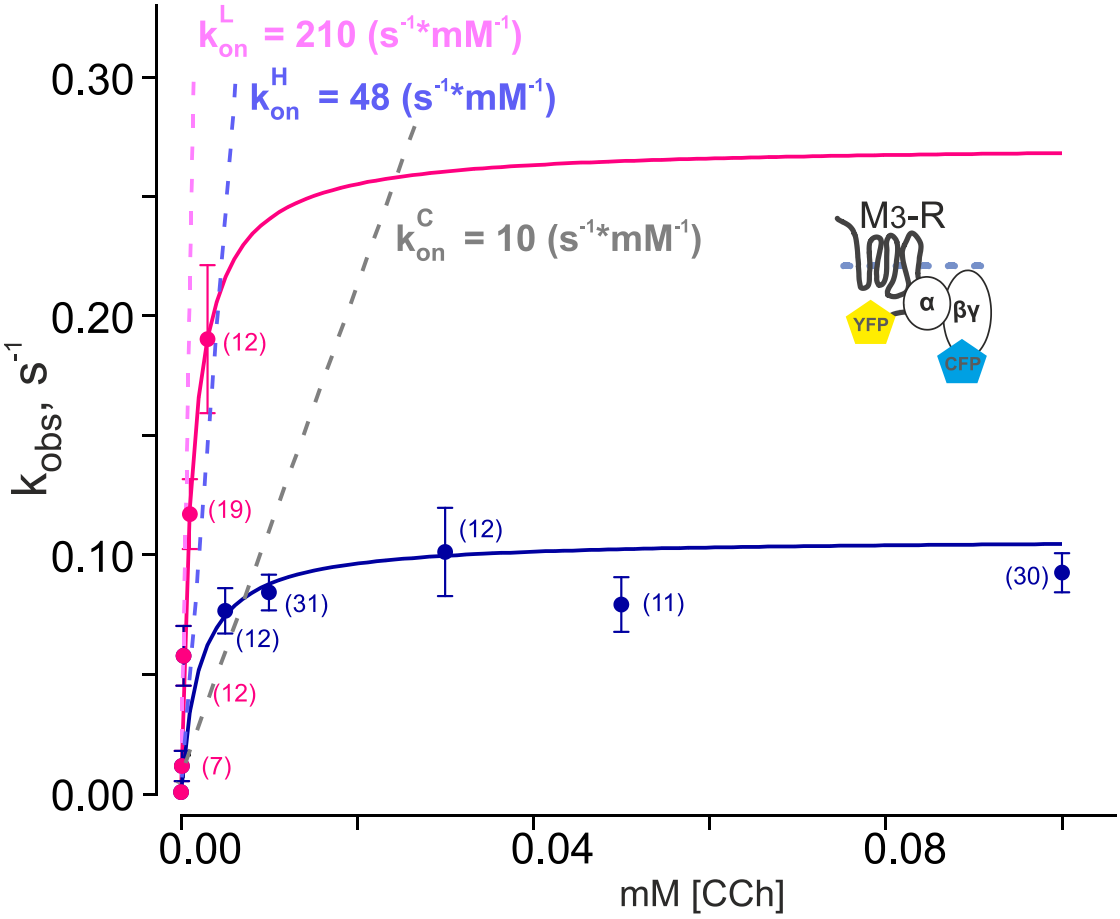

Figure 16. Calculation of M_3-R-G_o protein association kinetics measured in permeabilized cells

The observed association kinetics (k_{obs}) values were calculated by direct fitting of an exponential curve to the increase in the YFP/CFP emission ratio under application of increasing concentrations of CCh and plotted over time. The hyperbolic function was fitted separately to low (magenta, k_{on}^{L}) and high saturating (blue, k_{on}^{H}) concentrations of agonist. The plotted tangents represent the kon values calculated as first derivatives of hyperbolic k_{obs} function. The grey tangent line depict the k_{on} for G_o-M_3-R complex formation calculated based on steady-state experiments and measured dissociation kinetics (k_{off}) for the same complex. Data are shown as mean ± SEM for each condition, n of each experiment is indicated in brackets.

Nevertheless, the measured and calculated association kinetics did not reflect the differences in coupling preference for G_q over G_o proteins suggesting that at least for the M_3-R probably not the k_{on} but rather the lifetimes of the ternary complex play a major role in the determination of receptor-G protein selectivity.

Table 7. Calculated k_{on} (s^{-1}*mM^{-1}) for the association of M_3-R with G_q, G_o and G_{i2} proteins

	k_{on} G_q	k_{on}^{C} G_q	k_{on}^{H} G_o	k_{on}^{L} G_o	k_{on}^{C} G_o	k_{on}^{C} G_{i2}
P1	0.03657	-*	0.271	0.1062	-*	-*
P2	0.00163	-*	0.00129	0.00218	-*	-*
k_{on} (s^{-1}*mM^{-1})	22.4356	14.0625	210.0775	48.715596	10.861423	6.36
k_{off} (s^{-1})	0.009 ± 0.002		0.116 ± 0.019			0.053 ± 0.006
Kd (μM)	0.40115	†	0.55218	2.3812	†	†
EC_{50} binding (μM)	0.64 ± 0.04		10.68 ± 0.32			8.33 ± 0.22
EC_{50} activation (μM)	0.12 ± 0.01		0.79 ± 0.01			-

P1, P2 - hyperbolic function constants of curve amplitude and steepness (equation E1);

k_{on} - quantified k_{on} value based on k_{obs} data using hyperbolic function fit (equation E2);

k_{on}^{C}- calculated k_{on} value based on steady-state experiments (equation E3);

k_{on}^{H} - quantified k_{on} value when higher concentrations of CCh (5 – 100 μM) applied based on k_{obs} data using hyperbolic function fit;

k_{on}^{L}- quantified k_{on} value when lower concentrations of CCh (0.3 – 3 μM) applied based on k_{obs} data using hyperbolic function fit;

*-not hyperbolic fit but Kd calculation was performed;

†-Kd was assumed to be equal to EC_{50} binding;

Empirical data are given as mean ± SEM.

3.2.5 Correlation of G protein affinity to M_3-R with their coupling efficiency

In order to experimentally verify whether the measured k_{on} and k_{off} were realistic, we next determined steady-state binding curves for the carbachol-induced nucleotide-free complex formation of M_3-R with $G\alpha_q$- or $G\alpha_o$-containing G proteins in dependence of agonist concentration, by determining the stable plateau reached after agonist application (Figure 17A black vs pink, B).

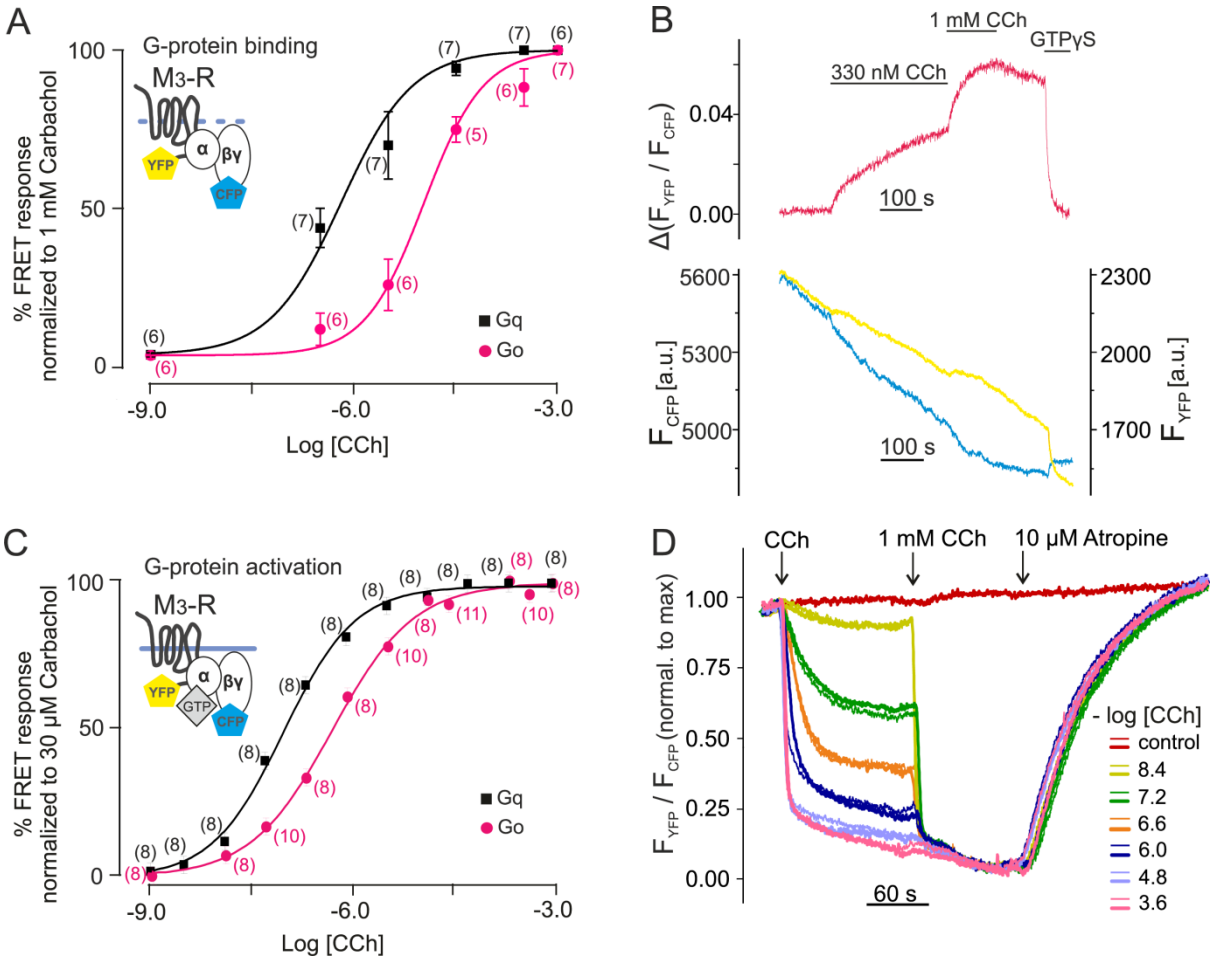

Figure 17. Correlation of M_3-R-G protein binding and G protein coupling efficiency
Concentration-response curves of G_q and G_o binding to M_3-R measured by means of FRET under nucleotide depleted conditions **(A)**. Single-cell imaging was performed on permeabilized HEK293T cells transiently transfected as described in Table 6 section 1. **(B)** The representative trace of G_q binding to M_3-R under application of the sustained increasing concentrations of CCh. Due to the slow association kinetics of G protein-M_3-R complex under application of low concentrations of CCh, the steady-state conditions induced by small amounts of agonist were estimated after incubation of the cells for up to 10 min. **(C)** Concentration-response curves of G_o and G_q protein activation via stimulation of M_3-R were measured by means of FRET. Experiments on G protein coupling efficiency were performed in 96-well format on cells transfected as described in Table 6 section 2. **(D)** A representative experiment for multiple-cell FRET-imaging of G_q activation under M_3-R stimulation with different concentrations of CCh is shown (measured in duplicates). Each trace is derived from one out of 12-wells stimulated simultaneously with overflow technique. All concentration-response data are represented as mean ± SEM for each condition, n of each experiment is shown in brackets. The amplitudes of agonist-induced amplitudes of FRET signal were normalized to the saturating concentrations of CCh (1mM) and in case of G protein binding experiments also to the minimum receptor occupancy state (response to GTPγS).

The concentration-response curve of G_o binding to M_3-R was found to be 16.5-fold right shifted in comparison to G_q (EC_{50} = 10.68 ± 0.32 µM and 0.64 ± 0.04 µM, respectively), which indicates a higher affinity of binding of G_q to M_3-R compared with G_o.

In order to test whether the stability of the ternary complex correlates with the efficiency of G protein activation, we determined G_o and G_q protein coupling efficiency to M_3-R (Figure 17 C,D) by measuring FRET between Gα fused to YFP and CFP-labelled Gβγ subunits (Vilardaga et al. 2003) in thousands of non-permeabilized adherent transiently transfected cells (Figure 17D) in a 96-well format. Similar to the binding data, the concentration-response curve of $G\alpha_o$ activation (EC_{50} = 0.79 ± 0.01 µM) by M_3-R were 6.6-fold right shifted in comparison to $G\alpha_q$ activation (EC_{50} = 0.12 ± 0.01 µM) (Figure 17C pink vs black). Considering our findings regarding the on-kinetics of G_o and G_q binding to activated M_3-R, this result shows that the affinity of the mAChRs-G protein interaction underlying G protein selectivity is primarily reflected by the stability (lifetime) of the complex and correlates closely with the coupling efficiency. In case of G protein activation assays measured by means of FRET the transfected receptor was unlabelled. Taking into account the fact that the expression levels of the receptor influence the agonist sensitivity of G protein activation, radioligand binding assays were performed to compare receptor densities for both conditions, which revealed equal expression levels (Figure 9).

3.2.6 Dissociation rates of different G_i proteins bound to M_1-, M_2-, and M_3-Rs.

Moreover, we measured dissociation kinetics of M_3-R-$G_{i/o}$ proteins complexes in dependence of $G\alpha_i$ subtypes and found no significant differences for $G\alpha_{i1}$, $G\alpha_{i2}$ and $G\alpha_{i3}$ (Figure 18B). Similar results were obtained for M_1-R (Figure 19B,D).

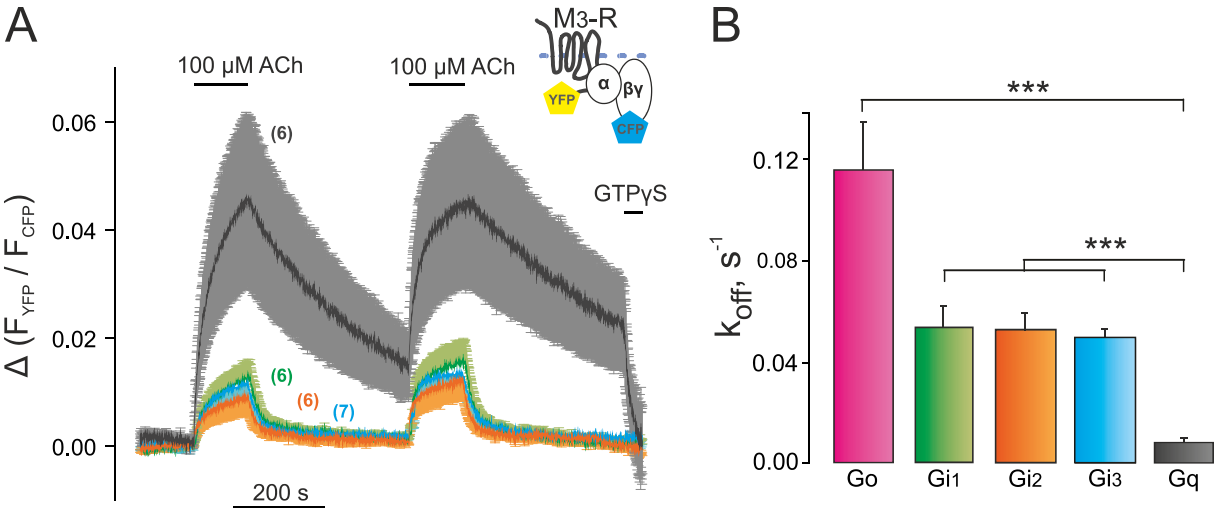

Figure 18. Comparison of the stability of G protein-M_3-R complexes
Decay kinetics of receptor - G protein complexes were determined in response to agonist withdrawal for M_3-Rs and different members of the $G_{i/o}$ and G_q protein family in experiments similar as shown in Figure 7. **(A)** Average traces of the F_{YFP}/F_{CFP} ratio of ACh-induced G proteins interaction with M_3-R under nucleotide-depleted conditions. Examples of exponential curve fittings to the decline in the YFP/CFP emission ratio after agonist withdrawal are shown in Figure 19C. **(B)** Quantified constants of dissociation (k_{off}, s^{-1}) of G_{i1}, G_{i2}, G_{i3}, G_o, and G_q proteins (green, orange, violet, magenta, black respectively in all bar-graphs) M_3-R are

illustrated . Calculated k_{off} (s^{-1}) values including the replication numbers (n) are given in Table 8. The data is represented as mean ± SEM. Normalization of alterations in FRET was performed as described in Figure 7. Statistical analysis was performed by one-way ANOVA with Bonferroni post-hoc test (*P < 0.05).

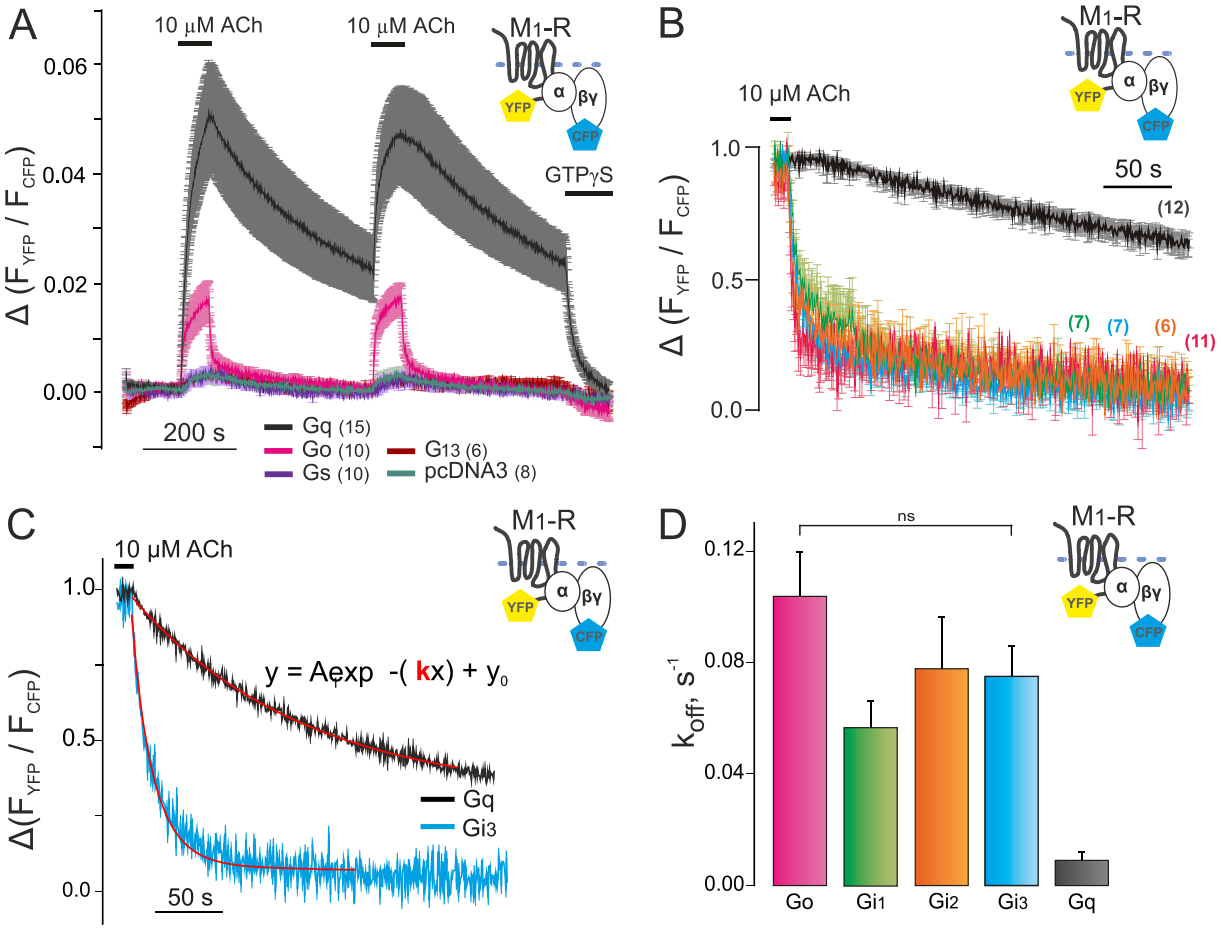

Figure 19. Dissociation kinetics for interactions between M_1-R and specific G proteins
The time course of G_q, G_o, G_s, and G_{13} (black, magenta, violet, dark red respectively) binding to M_1-R was measured in response to short periods of exposure to ACh in nucleotide-depleted cells **(A)** by means of FRET. Binding of G proteins reflected as an increase in F_{YFP}/ F_{CFP} ratio under application of the agonist (10 µM ACh) was compared to the condition when no Gα but empty vector pcDNA3 (dark green) was transfected. Similar to M_3-R, we could not observe binding of G_s and G_{13} proteins to M_1-R as no differences in the amplitudes or kinetics of the F_{YFP}/ F_{CFP} ratio were found compared to M_1-R and pcDNA3 co-transfection. Average traces represented as mean ± SEM, n of each experiment is indicated in brackets. **(B)** Dissociation kinetics of G_i family proteins from M_1-R compared to G_q during the withdrawal of ACh under nucleotide-free conditions plotted as mean ± SEM was calculated by fitting monoexponential function as shown in **(C).** The minimum YFP/CFP emission ratio was measured after GTPγS-induced dissociation of receptor-G protein complexes and was defined as zero. No significant difference was observed among G_i family affinities to M_1-R when k_{off} values were compared **(D).** Statistical analysis was performed by one-way ANOVA with Bonferroni post-hoc test (*P < 0.05).

To test for the $G_{i/o}$ subtype selectivity of M_2-R, we repeated similar experiments for M_2-R. Here we observed a higher amplitude and slightly enhanced complex stability for $G\alpha_o$ and $G\alpha_{i2}$ compared to $G\alpha_{i1}$ and $G\alpha_{i3}$, as the calculated k_{off} values of $G\alpha_o$ and $G\alpha_{i2}$ from M_2-R were

2-fold smaller in comparison to $G\alpha_{i1}$ and $G\alpha_{i3}$, a result that correlates with the G protein homology within the G_i family ((Milligan and Kostenis 2006) Table 1, Table 8, Figure 20).

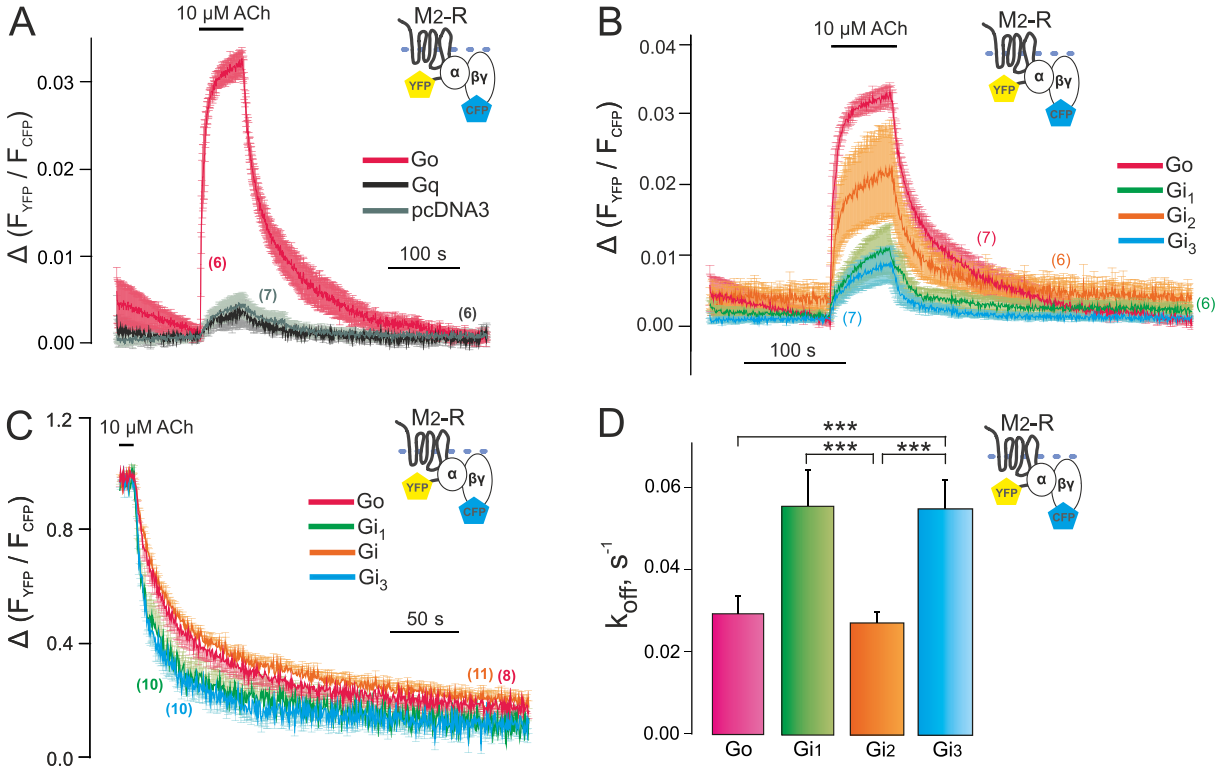

Figure 20. Quantification of the stability of M_2-R G protein complexes
Average traces of FRET recordings reflecting ACh-induced G_o and G_q binding to M_2-R under nucleotide-depleted conditions are shown **(A)**. No binding of G_q proteins to M_2-R was observed as no differences in the amplitudes or kinetics of the F_{YFP}/F_{CFP} ratio were found compared to M_2-R and pcDNA3 co-transfection. **(B)** Similar experiments where performed with M_2-R-YFP to study interactions with G_o, G_{i1}, G_{i2}, and G_{i3} proteins. High or moderate increase of F_{YFP}/F_{CFP} ratio under application of ACh was observed for all investigated M_2-R-G_i family protein pairs. Dissociation kinetics of G_{i1}-, G_{i2}-, G_{i3}-, G_o-, and G_i proteins from M_2-R **(C)** during the withdrawal of ACh derived from experiments shown in **B** were plotted as average traces. The minimum YFP/CFP emission ratio was measured after GTPγS-induced dissociation of receptor-G protein complexes and was defined as zero. The calculated k_{off} values of G_o and G_{i2} proteins were significantly lower compared to G_{i1} and G_{i3} constants of dissociation **(D)**. The data is represented as mean ± SEM for each condition, n of each experiment is given in Table 8. All average traces represented as mean ± SEM, n of each experiment is indicated in brackets. Statistical analysis was performed by one-way ANOVA with Bonferroni post-hoc test (*P < 0.05).

As expected, also no binding of $G\alpha_q$ to M_2-R in absence of nucleotides was detected (Figure 20A). A summary of all k_{off} values is given in Table 8.

Table 8. Calculated k_{off} (s^{-1}) for the dissociation of G proteins from mAChRs

G protein / Receptor	M_1-R	M_2-R	M_3-R
G_q	0.009 ± 0.003 (6)	-* (5)	0.009 ± 0.002 (27)
G_o	0.104 ± 0.016 (6)	0.029 ± 0.004 (8)	0.116 ± 0.019 (21)

G_{i1}	0.057 ± 0.009 (7)	0.056 ± 0.009 (10)	0.054 ± 0.008 (10)
G_{i2}	0.078 ± 0.019 (7)	0.027 ± 0.003 (11)	0.053 ± 0.006 (10)
G_{i3}	0.075 ± 0.011 (7)	0.055 ± 0.007 (10)	0.050 ± 0.004 (12)
G_s	-* (10)	†	-* (6)
G_{13}	-* (6)	†	-* (6)

*The binding of the G protein was not detected under described conditions. Data are given as mean ± SEM (n cells).

†The conditions were not tested.

3.2.7 Effect of PTX on G protein binding to M_3-R

Even though several receptors were crystalized in both active and inactive conformations, the exact mechanism of G protein-receptor coupling selectivity is still unclear. As it was proposed in ternary complex model and later on shown in NMR studies (Kofuku et al. 2012) the specific G protein – receptor complex formation is required for the active receptor conformation stabilization. Based on recent studies, agonist mediated conformational changes in H8 and ICL1 domains of the receptor were suggested to be stabilized by binding of α5 C-terminus domain of Gα subunit of the specific G protein (Sounier et al. 2015). We hypothesized that Gα C-terminus binding to the active GPCR might play an important role in the initial determination of receptor-G protein selectivity. Taking into account that receptor-G protein complex stability depends on intracellular nucleotide concentration (Matesic et al. 1989), we tested the ability of the $G\alpha_i$ protein to bind receptors after Pertussis toxin mediated ADP-ribosilation of the C-terminus of $G\alpha_i$ subunit using FRET method in combination with the controlled nucleotide concentrations technique.

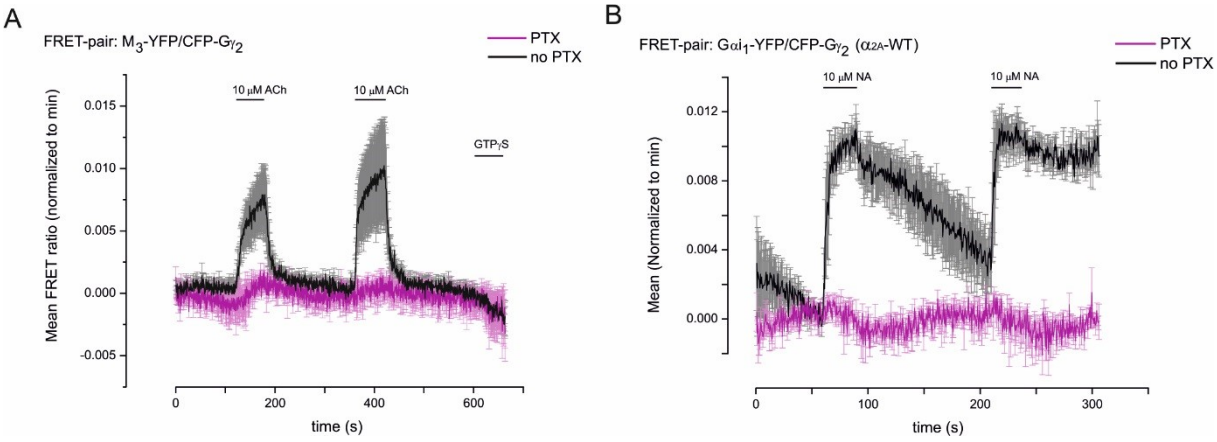

Figure 21. G_i protein binding and activation after PTX treatment
Average YFP/CFP emission traces of G_{i2} binding to M_3-AChR under GTP-depleted conditions in PTX-untreated (black) and untreated (violet) cells plotted over time **(A)**. Cells were transfected as indicated in Table 6 section 1. The significantly reduced amplitudes of

FRET signal upon ACh application in cells incubated with PTX in comparison to PTX-untreated cells indicate the inhibition of G_{i2} binding to the receptor. YFP/CFP emission ratio was normalized to receptor minimum occupancy state (GTPγS application). **(B)** Average traces of G_{i1} activation via α_{2A}-wt in intact cells reflecting an increase of FRET signal are illustrated. Cells were transfected as described in Table 6 section 2. The traces were bleach corrected and normalized to initial values. Perfusion of PTX-untreated with 10 µM NA (black) leads to receptor-mediated G_{i1} activation which was completely diminished by cells preincubation with PTX (violet). All data are represented as mean ± SEM.

Here, we focused on α_{2A} adrenergic receptor and muscarinic acetylcholine receptors M_2 and M_3, as GPCRs known to activate inhibitory G proteins. The binding of PTX-inhibited G_o, G_{i1}, and G_{i2} proteins upon agonist application was investigated by means of FRET-based experiments performed in permeabilized cells transiently transfected with M_3-YFP or α_{2A} – YFP and CFP-$G\gamma_2$ as a FRET-pairs. We also measured the activation of $G\alpha_{i1}$ by α_{2A} -AR as a control of PTX functionality. In order to prevent immediate G protein dissociation after its binding to the receptor, endogenous nucleotides were depleted by brief exposure of the cells to saponin and following washing steps.

Indeed, binding of the G_{i2} to M_3-AChR and α_{2A}-AR in permeabilized cells was completely abolished by overnight incubation with 50 ng/ml PTX and displayed as dramatically reduced FRET amplitudes upon agonist application to PTX-treated cells in comparison to untreated cells (вышеFigure 21).

To sum up, the PTX mediated prevention of G_i binding to the active receptor under GTP-free conditions allows us to conclude that binding of α5 C-terminus of G_i to H8 and ICL1 domains of the receptor plays a crucial role in the mechanism of G protein receptor selectivity.

3.3 Differences in ligand induced GPCR-G protein interaction dynamics

3.3.1 Influence of agonist affinity on M_3-R-G_o and M_3-R-G_q complexes stability

In order to activate mAChRs, we used three different agonists exhibiting different affinities and efficacies towards binding and activation: acetylcholine (ACh), its synthetic analogue carbachol (CCh), and the partial agonist arecoline (Are) (Stamatiou et al. 2014). Thus, we also addressed the question of whether the type of the ligand can affect the affinity of the G protein to the receptor. HEK293T cells were transiently transfected and permeabilized as mentioned above. Single cells were first stimulated with ACh and, after its withdrawal, stimulated a second time with CCh or Are (Figure 22A).

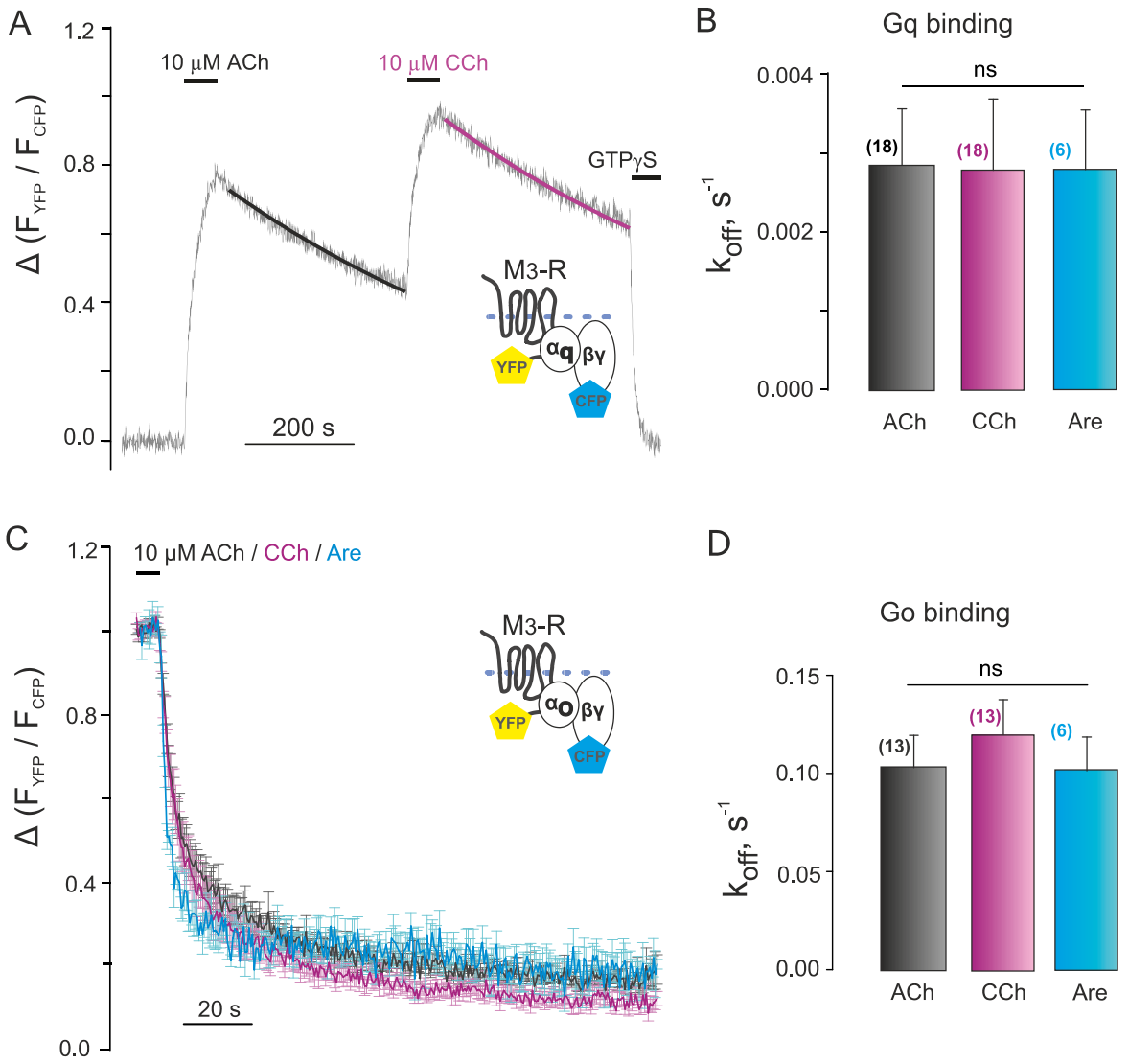

Figure 22. Stability of M_3-R-G protein complexes induced by different agonists Comparison of the averaged decay kinetics of G_q- **(A)** and G_o- **(C)** dissociation from M_3-R under the withdrawal of the agonist when the formation of the respective ternary complex was induced by either acetylcholine (ACh, black), carbachol (CCh, purple) or arecoline (Are, blue). FRET signal was measured on single permeabilized cells transfected as described in Table 6 section 2. The lifetime of the G_q-M_3-R ternary complex **(B)** as well as G_o-M_3-R **(D)** induced by different agonists were found to be similar. The data is shown as mean ± SEM for each condition, n of each experiment is shown in brackets. The traces were normalized to the saturating concentrations of the ligands and to the minimum receptor occupancy state corresponding to the YFP/CFP emission ratio values in presence of GTPγS. Statistical analysis was performed by one-way ANOVA with Bonferroni post-hoc test (*P < 0.05).

This procedure allows a comparison of the dissociation kinetics of G proteins-receptor complexes in the same cell, meaning equal expression levels of interacting proteins. We observed similar dissociation rates of G_q from ACh-, CCh-, and Are-activated M_3-R (Figure 22 A,B). Relatedly, the dissociation kinetics of G_o from M_3-R were not significantly different for all three agonists (Figure 22 C,D). Thus, we could conclude that, at least in the case of

agonists with moderate to low affinity, the stability of the G protein-receptor complex is an intrinsic property of the mAChR-G protein pair and not influenced by the agonist affinity.

3.3.2 Determination of effects of partial, full and super agonists on the dynamics of GPCR-G protein interactions

In this research project, I investigated whether the degree of partial/full agonism can be quantified as the k_{on} of the M_1-R-G_q complex and be used for the ligands characterization. In order to check this hypothesis we calculated the correlation coefficient based on three ligand parameters: 1) association rate of the GPCR-G protein complex induced by the ligand under nucleotide-free conditions, 2) K_d value of the ligand reflecting its affinity to the receptor, and 3) efficiency of the ligand to activate the G protein via the receptor.

I calculated the lifetime of M_1-R-G_q complex induced by pilocarpine compared to ACh and the super agonist Iperoxo (Ipx) in the conditions of nucleotide depletion. In contrast to ACh and pilocarpine, activation of the M_1-R by superagonist iperoxo led to the formation of M_1-R-G_q complex with an enhanced lifetime (Figure 23 C, D). However, the G protein binding rate induced by Ipx and ACh was not significantly different, whereas under pilocarpine application G_q-M_1-R association kinetics was remarkably slower (Figure 23A,B). In this context the on-rate of M_1-R-G_q interaction under nucleotide depleted conditions was suggested to depend not only on the affinity of the G protein to the receptor but mostly on the amount of the receptors stabilized in the active conformation at the particular time point. The stabilization of the receptor in the active conformation preferable for the G protein binding might elucidate the mechanism of action for the weak and superagonists.

Concentration-response curves of G_q activation by M_1-R mediated by ligands of interest was measured in intact cells using established G protein FRET assays with the help of recently developed multiple-cell FRET measurement approach (Professor H. Lemoine, Heinrich Heine University, Düsseldorf, Germany). HEK293T cells were transiently transfected with plasmids for FRET-based G protein activation assay as described in Wolters, et al., 2015. All responses are normalized as previously mentioned to the final application of CCh in saturating concentration (Figure 24).

In summary, the combination of K_d value, EC_{50} of efficiency in G protein activation and the rate of GPCR stabilization will allow us to quantify the degree of partial/full agonism for the agonist.

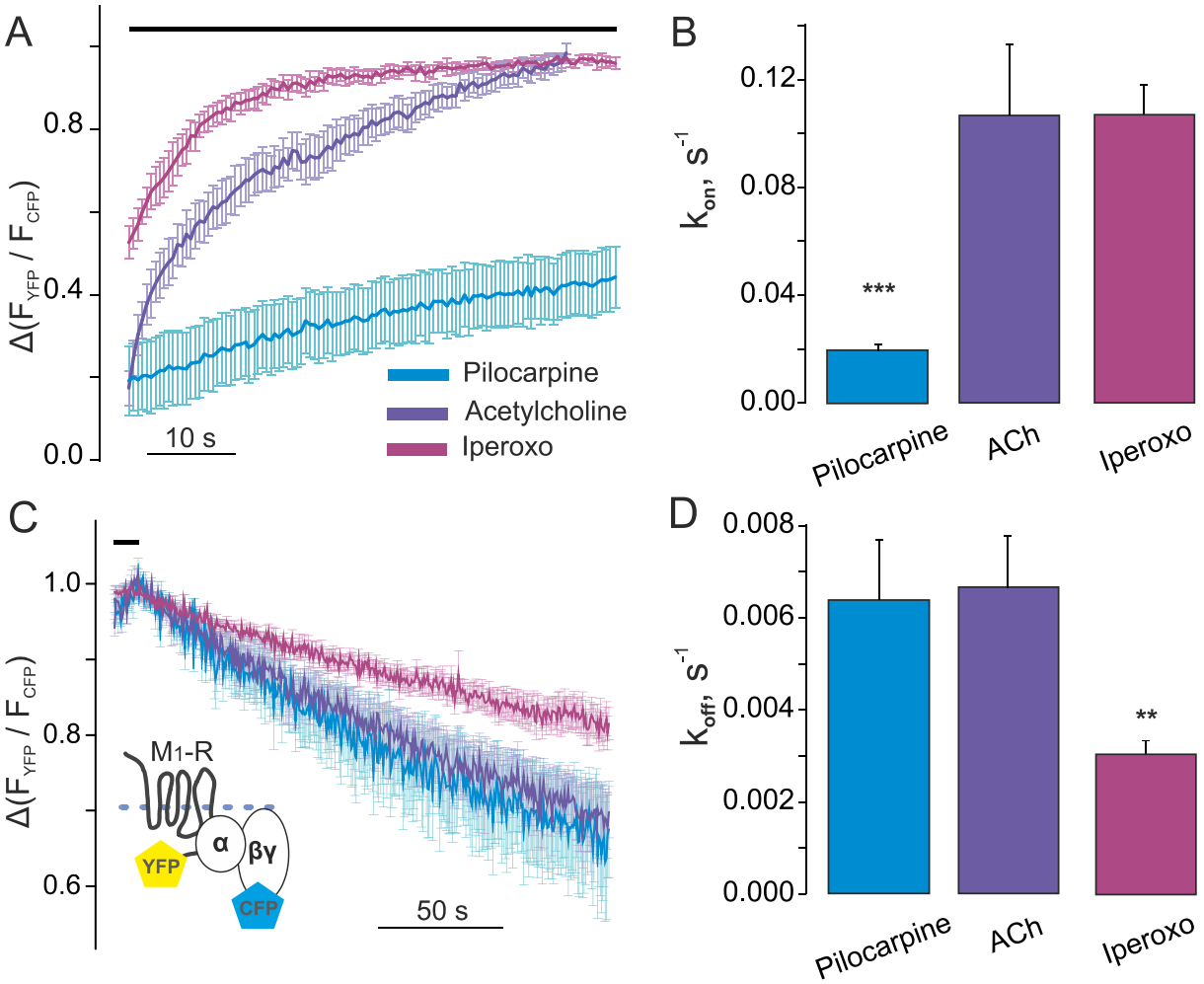

Figure 23. Dynamics of M_1-R G_q protein complexes induced by the partial agonist pilocarpine

The figure depicts comparison of the **(A)** on- and **(C)** off-set kinetics of G_q binding to M_1-R under nucleotide conditions induced by either pilocarpine (blue, n=4), acetylcholine (violet, n=4) or iperoxo (purple, n=4) measured by FRET. HEK293T cells were transfected as described in Table 6 section 1. The constants of **(B)** association (k_{on}, s^{-1}) and **(D)** dissociation (k_{off}, s^{-1}) of M_1-R-G_q complexes induced by different agonist were calculated as indicated in Figure 22. Pilocarpine (blue) mediated G_q binding to M_1-R under nucleotide depleted conditions was significantly slower when compared to the application of both ACh (violet) and Iperoxo (purple). Interestingly, intrinsic G_q protein affinity to pilocarpine-activated M_1-Rs was similar to the ACh-activated receptors, whereas Iperoxo induced higher M_1-R-G_q protein complex stability. All data are plotted as mean ± SEM for each condition. Statistical analysis was performed by one-way ANOVA with Bonferroni post-hoc test (*P < 0.05).

Based on the results of ligand-induced M_1-R-G_q ternary complex association (k_{obs}) and dissociation (k_{off}) kinetics and the data on G_q protein activation (Figure 24), we can suggest that the degree of probability for the receptor to be stabilized in the active conformation with the agonist reflects in receptor-G protein association under nucleotide-depleted conditions and correlates with this agonist efficiency. k_{on} of ternary complex induced by different agonists was calculated by using the following equation:

$$k_{on} = (k_{obs} - k_{off}) = (k_{app} - k_{off}) \qquad \text{(E5.1)}$$

The k_{on} values for all tested agonists are given in Table 9. Moreover, the respective k_{on} values were also calculated based on experiments performed in membranes derived from transiently transfected cells (Table 10, Professor H. Lemoine, Heinrich Heine University, Düsseldorf, Germany). Membranes preparation was performed as described in section 2.2.2.3.

Table 9. Calculated k_{on} of M_1-R-G_q ternary complex induced by different agonists in permeabilzed cells.

Agonist	C	-log [A]	k_{obs}, s^{-1}	k_{off}, s^{-1}	k_{on}
Choline	1 mM	3.0	0.01041 ± 0.00117 (13)	0.00918 ± 0.00118 (11)	0.00123
Bethanechole	100 µM	4.0	0.01423 ± 0.00086 (12)	0.01056 ± 0.00096 (12)	0.00367
Pilocarpine	30 µM	4.5	0.01281 ± 0.00078 (12)	0.00333 ± 0.00062 (12)	0.00948
Methacholine	10 µM	5.0	0.02310 ± 0.00207 (12)	0.00399 ± 0.00083 (12)	0.01911
Arecoline	10 µM	5.0	0.03482 ± 0.00810 (10)	0.00452 ± 0.00093 (10)	0.03030
Carbachol	10 µM	5.0	0.04691 ± 0.02925 (11)	0.00540 ± 0.00098 (7)	0.04151
Acethylcholine	10 µM	5.0	0.08723 ± 0.00601 (7)	0.00317 ± 0.00069 (9)	0.08406
Iperoxo	1 µM	6.0	0.13012 ± 0.00254 (8)	0.00432 ± 0.00094 (10)	0.12580

The agonists are ordered from the lowest to highest k_{on} values,

k_{on} - quantified k_{on} value based on k_{obs} and k_{off} data calculated as indicated in E5.1. Empirical data are given as mean ± SEM, the number of analysed experiments is given in brackets (n).

Table 10. Calculated k_{on} of M_1-R-G_q ternary complex induced by different agonists in membranes.

Agonist	C	-log [A]	k_{app}, s^{-1}	k_{off}, s^{-1}	k_{on}
Carbachol	10 µM	5.0	±		
Bethanechole	10 µM	5.0	0.02845 ± 0.00527 (11)	0.01207 ± 0.00048 (7)	0.01638
Pilocarpine	3 µM	5.5	0.03349 ± 0.00337 (12)	0.00767 ± 0.00032 (10)	0.02582
Choline	1 mM	3.0	0.05007 ± 0.00245 (19)	0.01414 ± 0.00042 (20)	0.03593
Arecoline	3 µM	5.5	0.04903 ± 0.02579 (7)	0.00798 ± 0.00029 (4)	0.04105
Arecoline	3 µM	5.5	0.05725 ± (7)	0.00996 ±(4)	0.04730
Methacholine	3 µM	5.5	0.09350 ± 0.00688 (7)	0.01200 ± 0.00023 (7)	0.08150
Acetylcholine	100 µM	4.0	0.12120 ± 0.03176 ()	0.01565 ± 0.00065 ()	0.10556
Bethanechole	30 µM	4.5	0.12508 ± 0.00751 (19)	0.00495 ± 0.00028 (18)	0.12013
Acetylcholine	30 µM	4.5	0.14270 ± 0.02750 ()	0.01340 ± 0.00110 ()	0.12928

The agonists are ordered from the lowest to highest k_{on} values,

k_{on} - quantified k_{on} value based on k_{obs} and k_{off} data calculated as indicated in E5.1. Empirical data are given as mean ± SEM, the number of analysed experiments is given in brackets (n).

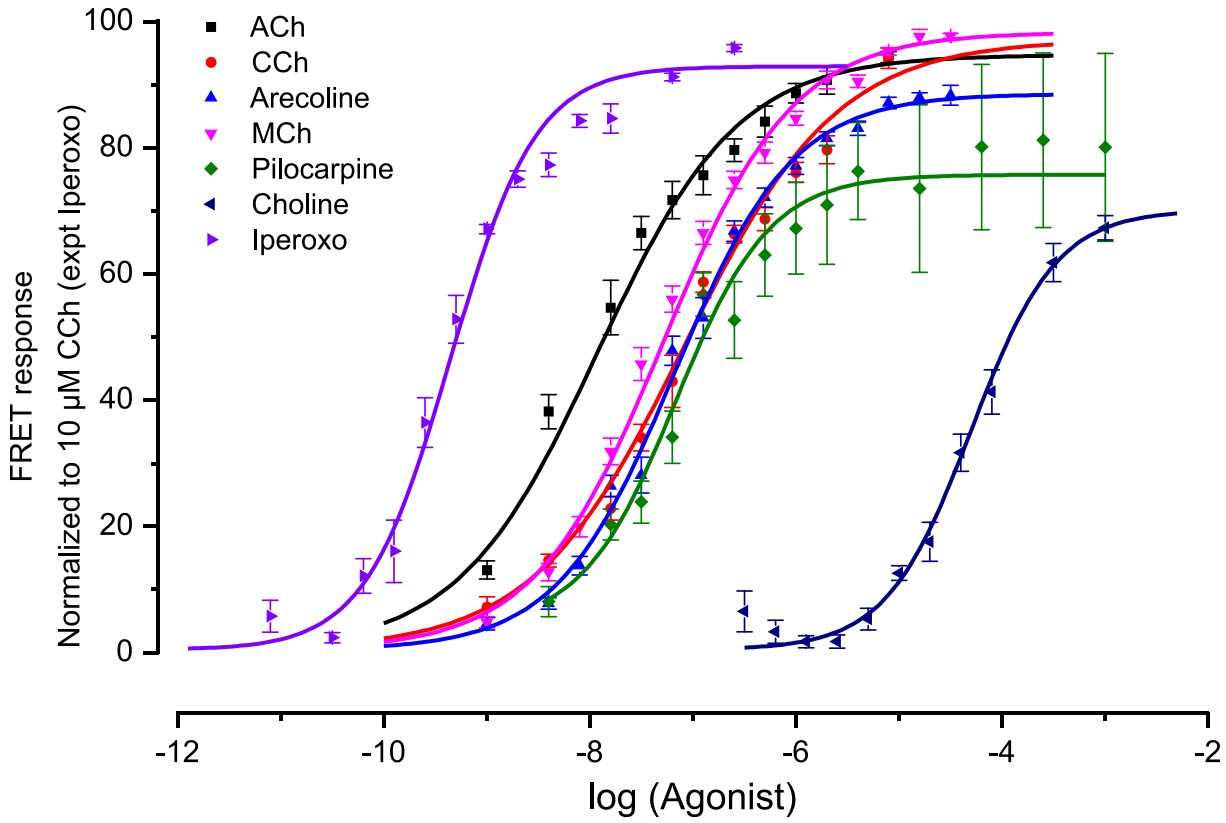

Figure 24. Activation of G_q protein via M_1-R induced by different agonists
The activation of the G protein (Wolters, et al, 2014) via stimulation of M_1-R with agonists exhibiting different potencies was measured using multiple cell FRET assays. HEK293T cells were transiently transfected as described in Methods (G protein activation plasmid mix). Transfected cells were transferred to 12-well strips coated with poly-L-lysine. Ligands were applied using 12-well injection blocks. The artifacts were reduced by holding a constant temperature of the whole system (24℃). All data are plotted as mean ± SEM for each condition.

As previously mentioned, our study focused mainly on M_1-R-G_q dynamic interactions. However, the family of muscarinic acetylcholine receptors also include classical G_i binding GPCRs such as M_2- and M_4Rs (J Wess et al. 1995). The affinity of G_i family protein to M_2-R was shown to be quite low in comparison to stable ternary complexes of other GPCRs binding their typical interaction G protein partners (Figure 20). Furthermore, in pilot experiments for this study, we used iperoxo as a superagonist to activate mAChRs (Schrage et al. 2014; Fredriksson et al. 2003). In contrast to M_1-Rs which exhibited moderate increase in the G_q protein affinity mediated by iperoxo (Figure 23), M_2-R-G_o complex stability induced by iperoxo was found to be 7-fold higher compared to ACh (Figure 25). This phenomena of superagonist induced stabilization of M_2-Rs correlates with the literature data (Kruse et al. 2013).

Taken together, the experiments help to understand the underlying mechanisms of the modulatory effects of high-affinity agonists on the ternary complex stability.

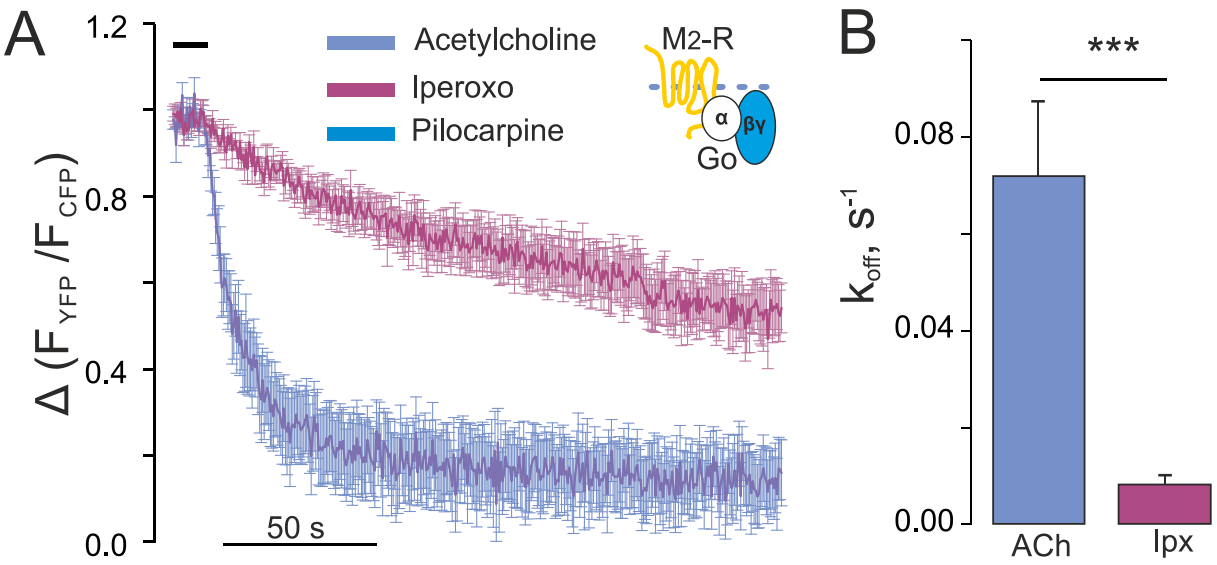

Figure 25. Comparison of the Iperoxo- and ACh-induced M_2-R-G_o complex stability
The average traces of the YFP/CFP emission ratio show the dissociation kinetics of the G_o proteins from M_2-R during the wash out of the agonist under nucleotide-depleted conditions **(A)** M_2-R was activated by either 10 µM ACh or 10 µM Iperoxo (dissociation of the G_o protein shown in violet (n=7) or purple (n=7) respectively). HEK293T cells were transiently transfected as indicated in Table 6 section 1. **(B)** G_o affinity to M_2-R was quantified as dissociation kinetics (k_{off}, s^{-1}) of the G_o protein from M_2-R under nucleotide free conditions as performed in Figure 19C. In comparison to ACh, the M_2-R-G_o ternary complex stability induced by Iperoxo was significantly higher. The data is represented as mean ± SEM. Statistical analysis was performed by one-way ANOVA with Bonferroni post-hoc test (*P < 0.05).

3.3.3 The examination of allosteric ligands effects on mAChR-G protein interaction kinetics

Muscarinic receptors expose a high degree of sequence similarity within the orthosteric binding pocket, making the development of receptor-specific ligands very difficult. Therefore, pharmaceutical research is now shifted to generation of allosteric agents, which can modulate receptor activity subtype-specifically, by targeting non-conserved extracellular regions of the GPCR (Baltos et al. 2016; Birdsall and Lazareno 2005; Katie Leach, Sexton, and Christopoulos 2007). Moreover, since substances only regulate receptor signalling in the presence of natural agonists, the application of allosteric modulators as therapeutical agents potentially result in a reduction of adverse reactions (May et al. 2007).

In this study, BQCA, known to be a selective positive allosteric modulator (PAM) for M_1-R, was used as a positive allosteric modulator (PAM) for the pilot experiments.

In section 3.3.2 it was shown that the agonist efficacy correlated with the probability of mAChR – G protein complex formation. Here I measured the stability of M_1-R-G protein complexes induced by ACh in the presence of BQCA in permeabilized cells. G_q protein

(Figure 26A,B) dissociation kinetics from M_1-R in presence of BQCA during the withdrawal of agonist were slower in comparison when only buffer was used. Similar results were observed for G_o-M_1-R complexes stability (Figure 26C,D). Interestingly, the application of BQCA led to the enhancement of G_q and G_o affinities to M_1-Rs under nucleotide depleted conditions up to the ones induced by iperoxo.

Thus, positive allosteric modulator BQCA not only increases the affinity of M_1-R to ACh, but also increases G_q protein affinity to the M_1-R in concert with ACh, indicating a distinct active M_1-R conformation. It suggests that this allosteric modulator increases the probability of the receptor to be stabilized in active conformation by particular agonist.

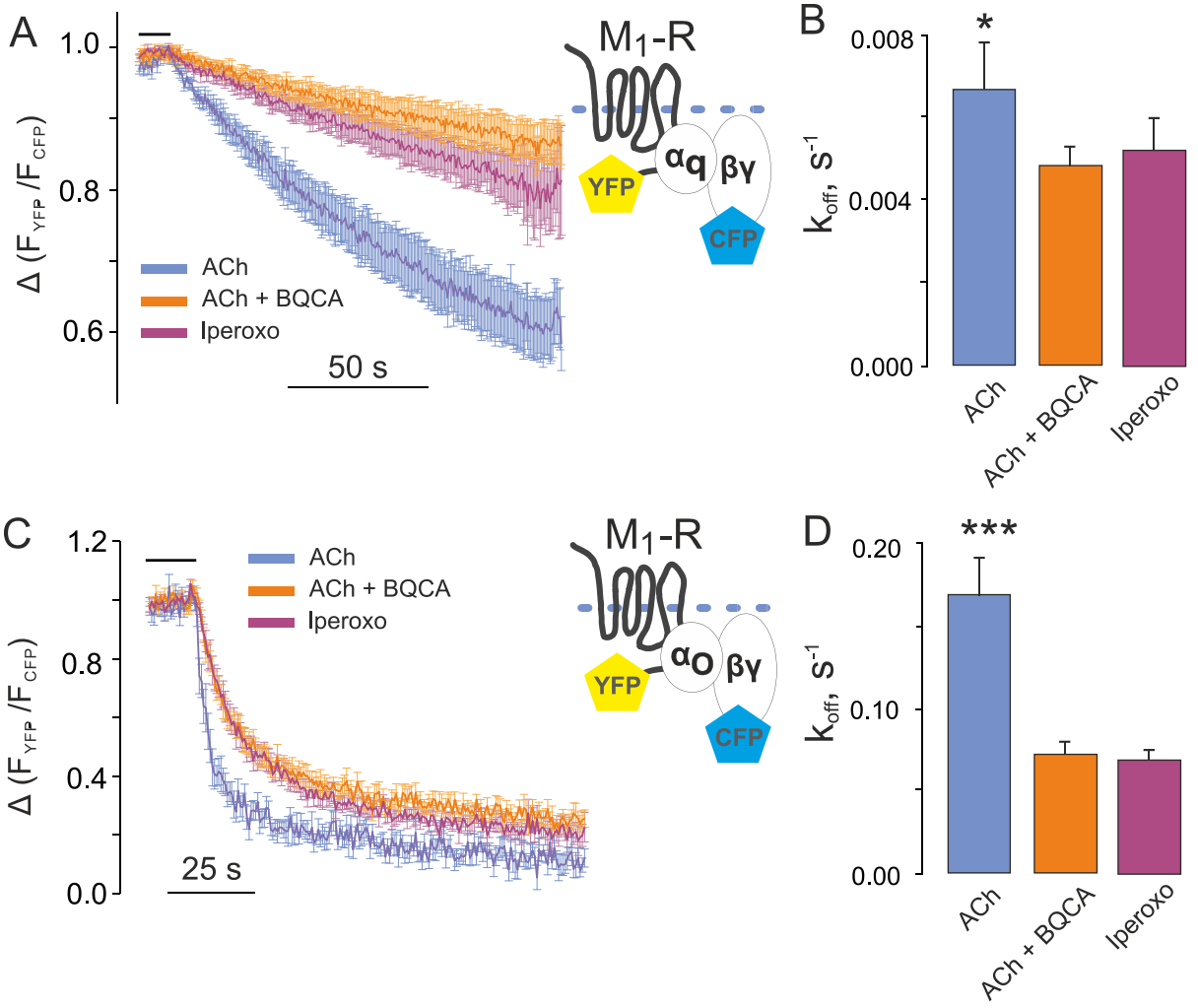

Figure 26. BQCA increases the stability of both M_1-R-G_q and M_1-R-G_o complexes Dissociation of G_o or G_q proteins from M_1-R was measured by means of FRET in response to agonist withdrawal under conditions of nucleotide depletion. Average traces of YFP/CFP emission ratio reflecting FRET between YFP labeled M_1-R and CFP-labeled $G\gamma_2$ subunit show the dissociation rate of G_q **(A)** or G_o **(C)** from M_1-R. The binding of the G proteins to the receptors was induced by application of 10 µM Iperoxo (purple, n=7), 10 µM ACh in absence (violet, n=5) or presence of 1 µM BQCA (orange, n=7). The difference between G_q protein affinity to the M_1-R activated by Iperoxo and ACh was almost completely diminished by stimulation of the receptor with ACh in presence of positive allosteric modulator BQCA.

The constants of dissociation (k_{off}, s^{-1}) for G_q **(B)** and G_o **(D)** proteins from M_1-R were calculated by fitting a monoexponential function as described in Figure 19C. All data are plotted as mean ± SEM for each condition. Statistical analysis was performed by one-way ANOVA with Bonferroni post-hoc test (*P < 0.05).

Interestingly, being an allosteric modulator, BQCA was able to induce G_q protein binding to M_1-R in absence of any orthosteric agonist under nucleotide-depleted conditions. In multi-cell FRET experiments, BQCA alone also led to the activation of small but significant G protein fraction (Figure 27). Thus, BQCA is suggested to act as M_1-R partial agonist probably by shifting the equilibrium of receptor states to higher percentage of active conformations.

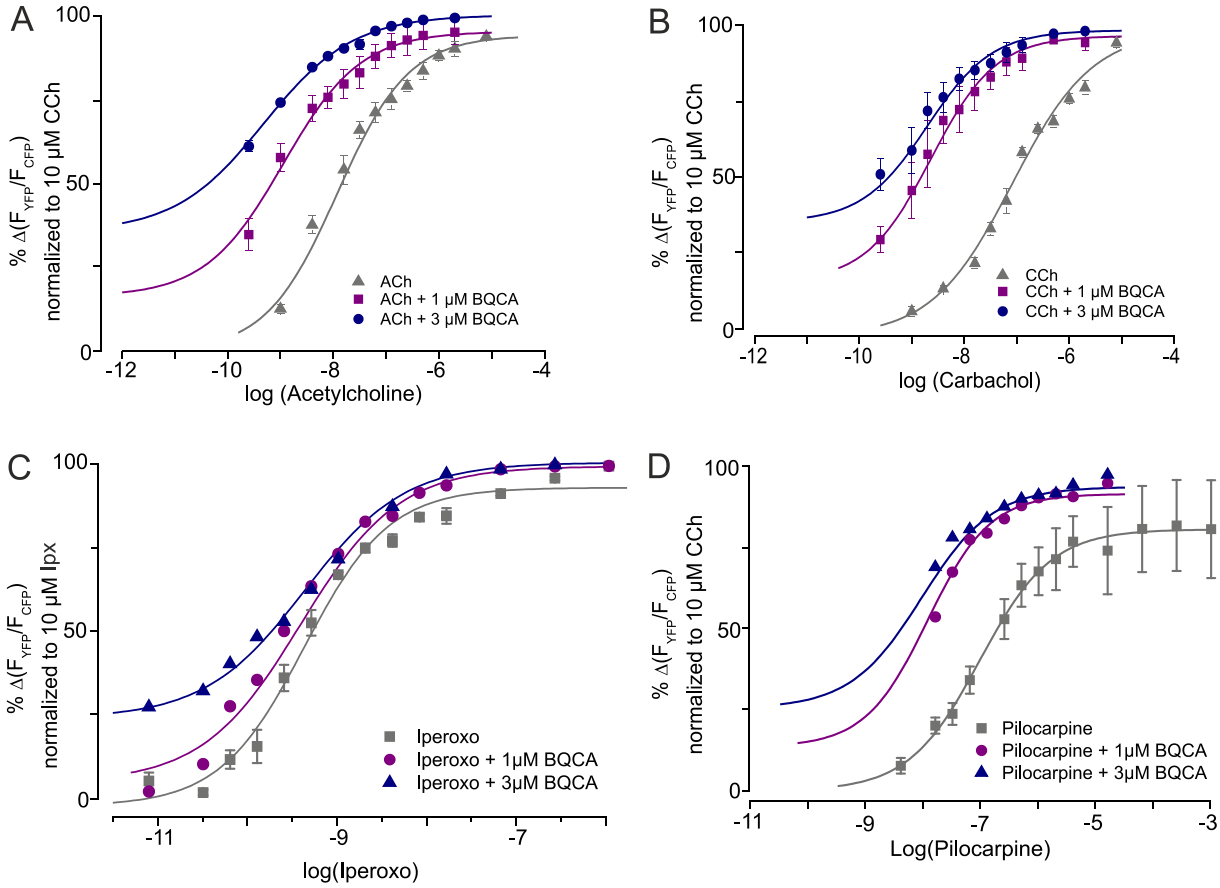

Figure 27. BQCA effect on M_1-R induced G_q activation
G protein activation was measured by means of multiple cell FRET assay. HEK293T cells were handled as described in Table 6 section 2. M_1-R was stimulated with ACh (A), CCh (B), Iperoxo (C), and Pilocarpine (D) alone (grey), in presence of 1 µM BQCA (magenta) or 3 µM BQCA (dark blue). The starting values of the G_q activation concentration-response curves in presence of BQCA were normalized to the effect of BQCA applied without agonist. All data points are presented as mean ± SEM

In my research project, I also tried M_1-R-specific negative allosteric modulator Gallamine. The addition of Gallamine to the buffer during withdrawal of agonist did not lead to the reduction of G_q and G_o proteins binding affinities to M_1-R (Figure 28A-D).

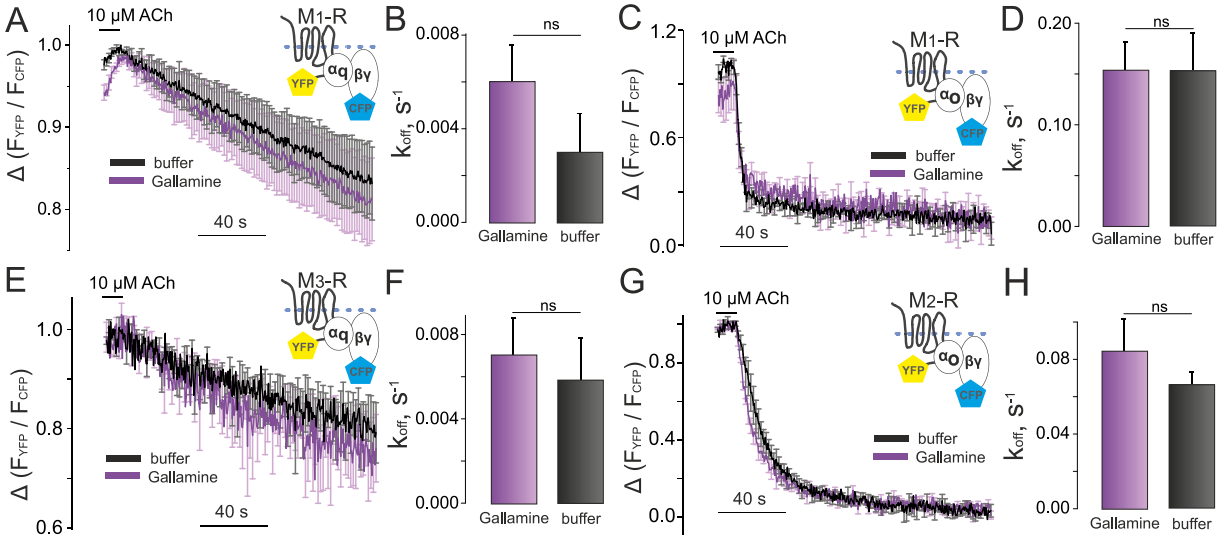

Figure 28. Lifetimes of mAChR - G protein complexes in presence of the negative allosteric modulator Gallamine

Comparison of G_q **(A,B)** and G_o **(C,D)** dissociation kinetics from M_1-R after withdrawal of ACh was measured in absence (black) or presence (violet) of 1 µM Gallamine under conditions of nucleotide depletion. Calculated stabilities (k_{off}) of the M_1-R-G_q complex as well as the M_1-R-G_o complex were not significantly different. Similar results were observed for M_3-R-G_q **(E, F)** and M_2-R-G_o **(G, H)** ternary complex stabilities. Averaged data are represented as mean ± SEM for each condition, n of each experiment is shown in brackets. The minimum state of the receptor is settled to 0 and corresponds to the FRET signal in presence of GTPγS. Statistical analysis was performed by one-way ANOVA with Bonferroni post-hoc test (*P < 0.05).

3.4 Dynamics and selectivity of G protein binding to other GPCRs

3.4.1 G protein binding to α_{2A}-, β_1-, and β_2-adrenergic receptors

Adrenergic receptors play an important role in physiological processes and are of great interest for the pharmaceutical industry as potential drug targets for treating asthma, and cardiovascular diseases such as hypertension and antiarrhythmia. Interactions of members of the G_i protein family with α_{2A}-AR were measured by means of FRET under nucleotide-free conditions. Since α_{2A}-AR is a classical G_i coupled receptor, the detection of specific G_q binding to this receptor was not expected (Figure 29A). In line with this expectation the agonist-evoked increase in FRET between labelled α_{2A}-AR and Gβγ was not increased when Gαq was cotransfected instead of empty pcDNA3. In fact the response was even reduced, presumably by competition with endogenous $G\alpha_{i/o}$ subunits for binding fluorescent Gβγ (Figure 29A). In contrast, co-expression of $G\alpha_i$ enhanced the agonist evoked FRET signal (Figure 29A). The affinities of G_{i1}, G_{i2} and G_{i3} to α_{2A}-AR were quantified by fitting exponential function to G protein decay kinetics (Figure 29B) under the withdrawal of NA.

The G_{i3}-α_{2A}-AR complex stability was higher in comparison to G_{i1}-and G_{i2}-α_{2A}-AR complexes (Figure 29C).

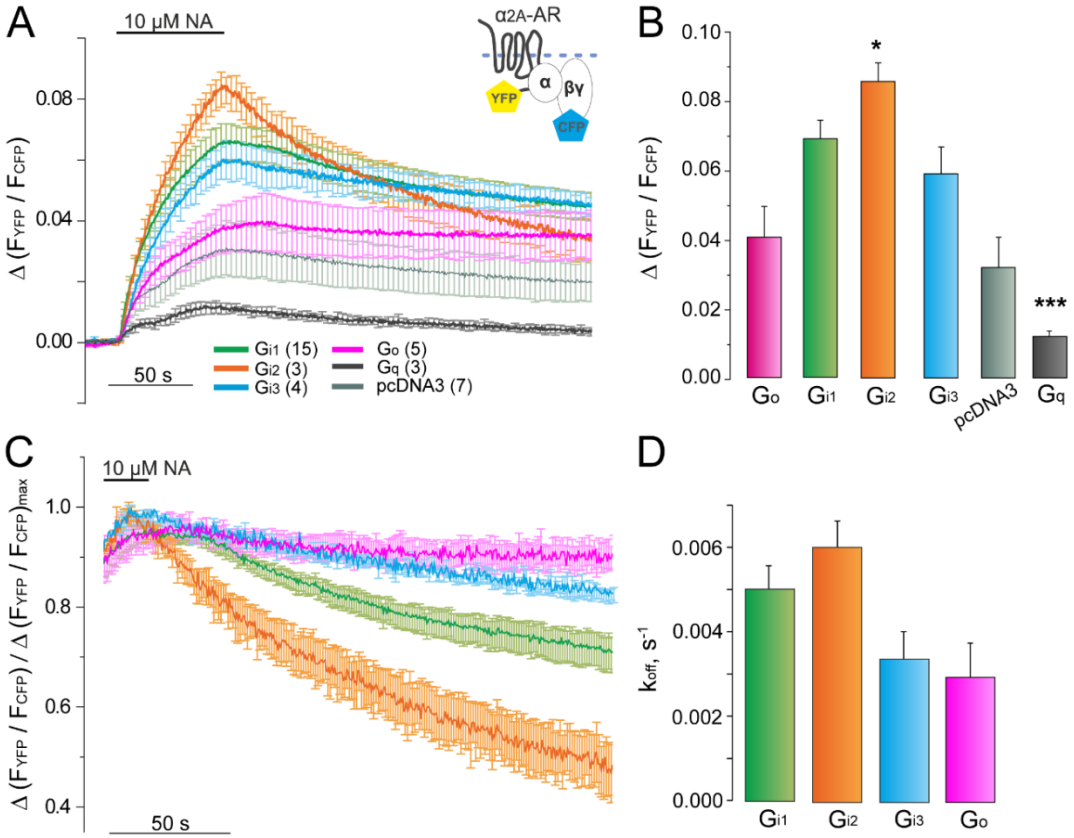

Figure 29. Formation and stability of ternary complexes of α_{2A}-AR-G_i proteins
G proteins binding to α_{2A}-AR **(A)** were measured by means of FRET in permeabilized HEK293T transiently transfected with α_{2A} -YFP, $G\alpha_{i1}$-wt (green), $G\alpha_{i2}$-wt (orange), $G\alpha_{i3}$-wt (blue), $G\alpha_{o}$-wt (magenta), $G\alpha_{q}$-wt (black) or pcDNA3 (light green), $G\beta_1$-wt and CFP-$G\gamma_2$. Average YFP/CFP emission ratios for all conditions were plotted over time. Under the application of 10 µM Noradrenaline (NA) specific G_{i1}, G_{i2}, G_{i3} and G_o binding to the receptor was observed whereas the G_q binding was not detected when compared to pcDNA3. **(B)** The amplitudes of FRET signal evoked by NA were compared. **(C)** Dissociation kinetics of G_{i1}, G_{i2}, G_{i3}, and G_o from α_{2A}-AR under nucleotide depleted conditions and calculated as k_{off} values by fitting a monoexponential curve **(D)**. The values are shown as mean ± SEM. Significance level was determined by one-way ANOVA with Bonferroni post-hoc test (*P < 0.05).

By testing the formation of β_2-AR – G_s complex formation in absence of nucleotides, no change was observed in FRET signal upon stimulation of the receptor by isoproterenol. However, the reintroduction of nucleotides to the cell membrane (GTPγS) led to a dramatic decrease in YFP/CFP emission ratio below the initial base line at the beginning of the measurement (Figure 30A). It suggests the binding of G – protein to the receptor prior to agonist introduction, which correlates with the studies on high β_2-AR basal activity (Yao et al. 2009). In the case of β_1-AR, the superfusion of the cell with isoprenaline evoked a relatively

high increase in FRET signal, indicating agonist-induced G_s binding to the receptor (Figure 30B).

It has been shown in multiple studies in cardiac tissues that in contrast to β_1-AR selective activation of β_2-AR leads to myocyte apoptosis only in the case of G_i inhibition by PTX (Xiao 2001; Devic et al. 2001) which might be interesting for the pharmacological treatment of ischemia and heart failure. Therefore, apart from G_s binding, I also tested the interaction of G_i proteins with β- adrenergic receptors under GTP-free conditions. Rapid increase in YFP/CFP emission ratio under application of 10 µM Iso depicted in Figure 30C suggests agonist-dependent G_o and β_2-AR interaction and corresponds well with literature data (Strohman et al. 2019). Interestingly, I have also detected G_o binding to β_1-AR in absence of nucleotides (Figure 30D).

According to the literature data G_i activation via β_2-AR is less efficient (Strohman et al. 2019). The same was observed in my experiments. Dissociation kinetics of G_o from both β_2-AR and β_1-AR is faster indicating its lower affinity to β-adrenergic receptors in comparison to G_s (Figure 30C and D vs. Figure 30A and B, respectively).

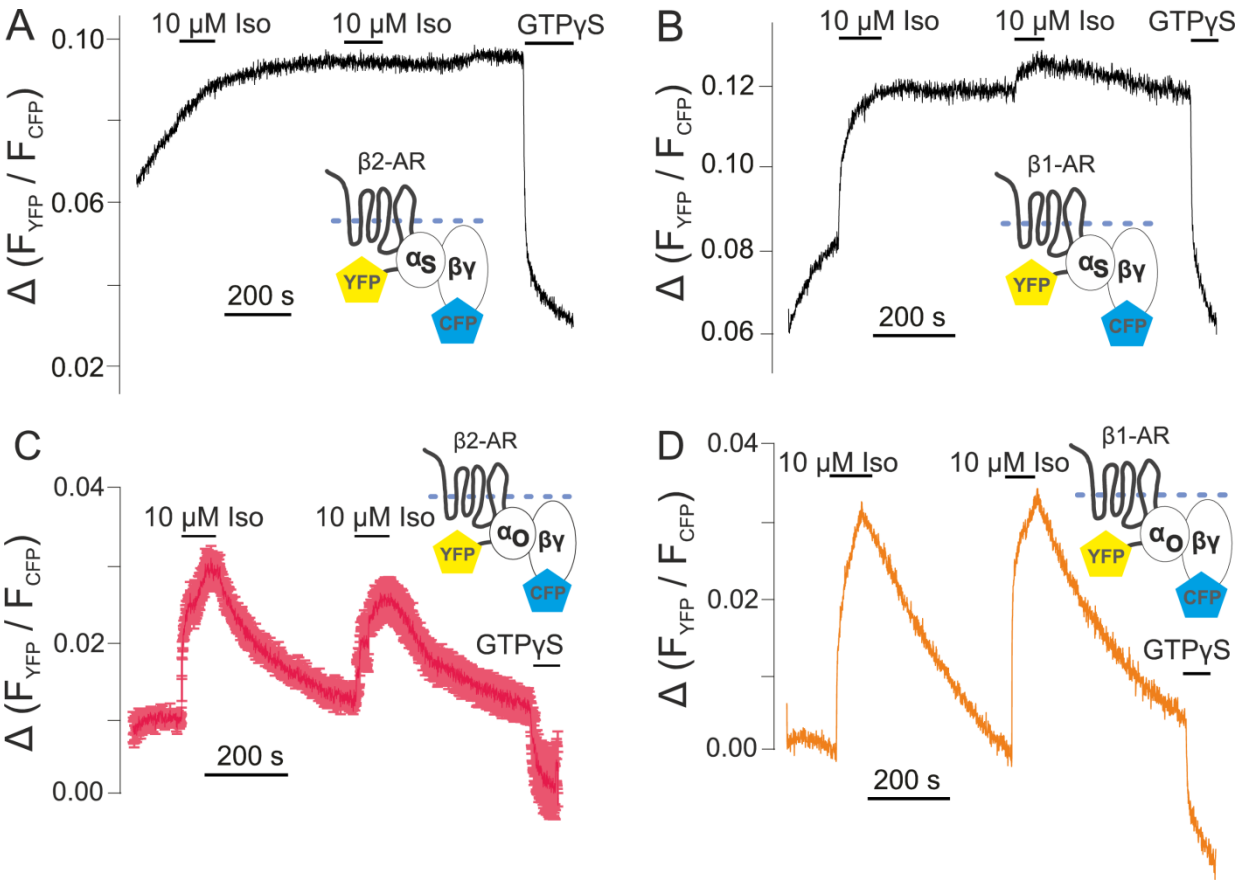

Figure 30. β-adrenergic receptor-G protein complexes
Single cell YFP/CFP emission ratio of isoprenaline-induced G_s binding to β_2-AR **(A)** and β_1-

AR **(B)** was measured in absence of nucleotides. Small increase in FRET signal under stimulation of β_2-AR with Iso and rapid decrease under application of GTPγS stands for a high basic activity of the receptor. Both β_2-AR and β_1-AR showed a very strong affinity to G_s which reflected in dramatically slow dissociation of the G protein from these receptors during ligand withdrawal. **(C)** Average YFP/CFP intensities ratio of G_o binding to β_2-AR upon isoprenalin application under nucleotide-free conditions. **(D)** Representative trace depicts isoprenalin induced G_{i2}- β_1-AR ternary complex formation in absence of nucleotides. All represented data were normalized and if averaged shown as mean ± SEM for each condition.

3.4.2 Binding of G_i and G_q proteins to Endothelin B receptor

For the following experiments I used HEK293T cells transiently transfected with ET_BR-YFP and heterotrimeric G_i or G_q proteins labelled with CFP on the Gγ subunit as described in the Methods part. In order to account for the endogenous expression of G_i family proteins in HEK293T, empty vector pcDNA3 was transfected instead of Gα subunit as a negative control for the specificity of the G protein-ET_BR binding measured by means of FRET between receptor and Gβγ. The experiments were done under nucleotide-depleted conditions. As expected from the literature, agonist-induced binding of G_{i1} protein to ET_BR lead to the higher increase in the F_{YFP}/F_{CFP} ratio compared to G_q (Figure 31).

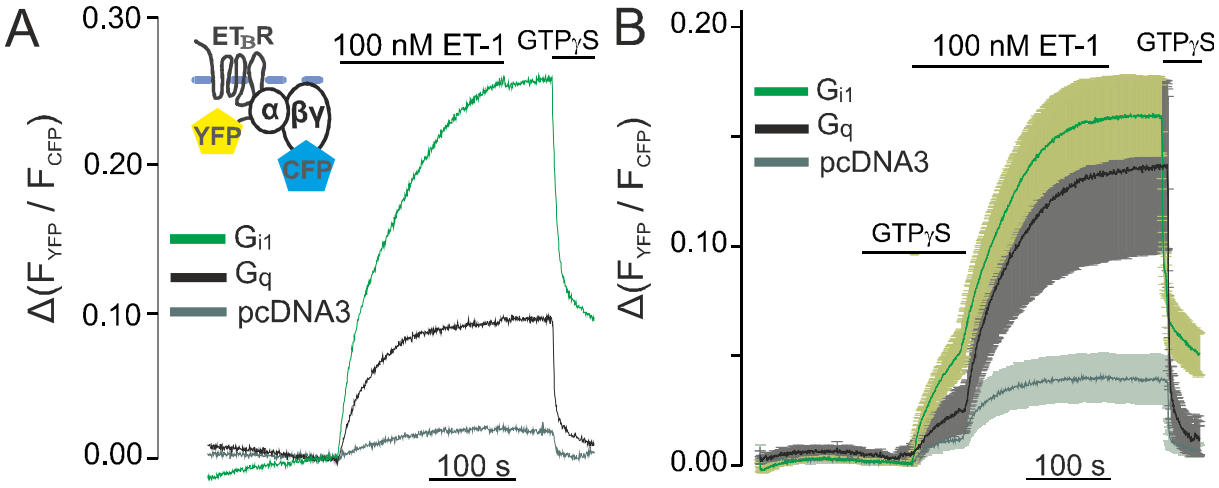

Figure 31. Stability of ET_BR-G protein complexes
(A) Representative YFP/CFP emission ratio of G_{i1} and G_q binding to ET_BR induced by ET-1 under nucleotide-free conditions. High G_{i1} affinity binding to ET_BR results in very slow dissociation kinetics of G protein during agonists wash out. **(B)** Average YFP/CFP emission ratio of G_{i1} and G_q binding to ET_BR depicts also a small initial increase in YFP/CFP emission ratio under application of agonist in presence of 1 µM GTPγS and reduced amplitude of the response to the final application of GTPγS. All represented data were normalized and if averaged shown as mean ± SEM for each condition, with n of least 6 independent experiment.

Interestingly, the GTPγS-triggered G_{i1} protein activation and its dissociation from ET_BR did not result in complete ternary complex degradation (Figure 31A). We repeated the experiment with an altered protocol. Application of agonist in presence of nucleotides led to

ET_BR-G_{i1} ternary complex formation but not ET_BR-G_q (Figure 31B), which shows a very high affinity of G_{i1} protein to the ET_BR. Moreover, these results are in accordance with literature data and computational experiments claiming that agonists with a very high affinity to the receptor, such as endothelin 1, increase the affinity of G protein to GTP (DeVree, et al., 2016).

3.4.3 Investigation of GPCR-G protein selectivity in high affinity GPCR-G protein complexes

Although, nucleotide-free conditions allowed the lifetime of ternary complexes to be prolonged, the quantification of dissociation rates of the G proteins exhibiting very high affinities to certain GPCRs in absence of nucleotides is limited by experimental restraints regarding the stability of FRET recordings on cover slips. Based on mAChRs as a model system we were able to quantify ternary complex stability and proved the intrinsic affinity of G proteins to the active receptor to be a major determinant of their coupling efficiency. In this study we modulated the stability of ternary complex by low GTP concentrations.

3.4.3.1 G protein selectivity of thromboxane A_2 receptor

The differences in G_{12}, G_{13}, and G_q protein affinity to thromboxane TP-R were depicted by calculating the k_{off} values in the presence of nucleotides in nM concentration range. Interestingly, G_{13} was found to have more than a 4-fold higher affinity to the TP-R under nucleotide depleted conditions compared to G_q (Figure 32), which has reflected in steady-state experiments under nucleotide-free conditions as a 5-fold difference of EC_{50} of G_{13} and G_q binding to TP-R and correlated with coupling efficiency (Figure 33). The determined dissociation rate as well as EC_{50} values of G_{12} from TP-R was very similar to G_q.

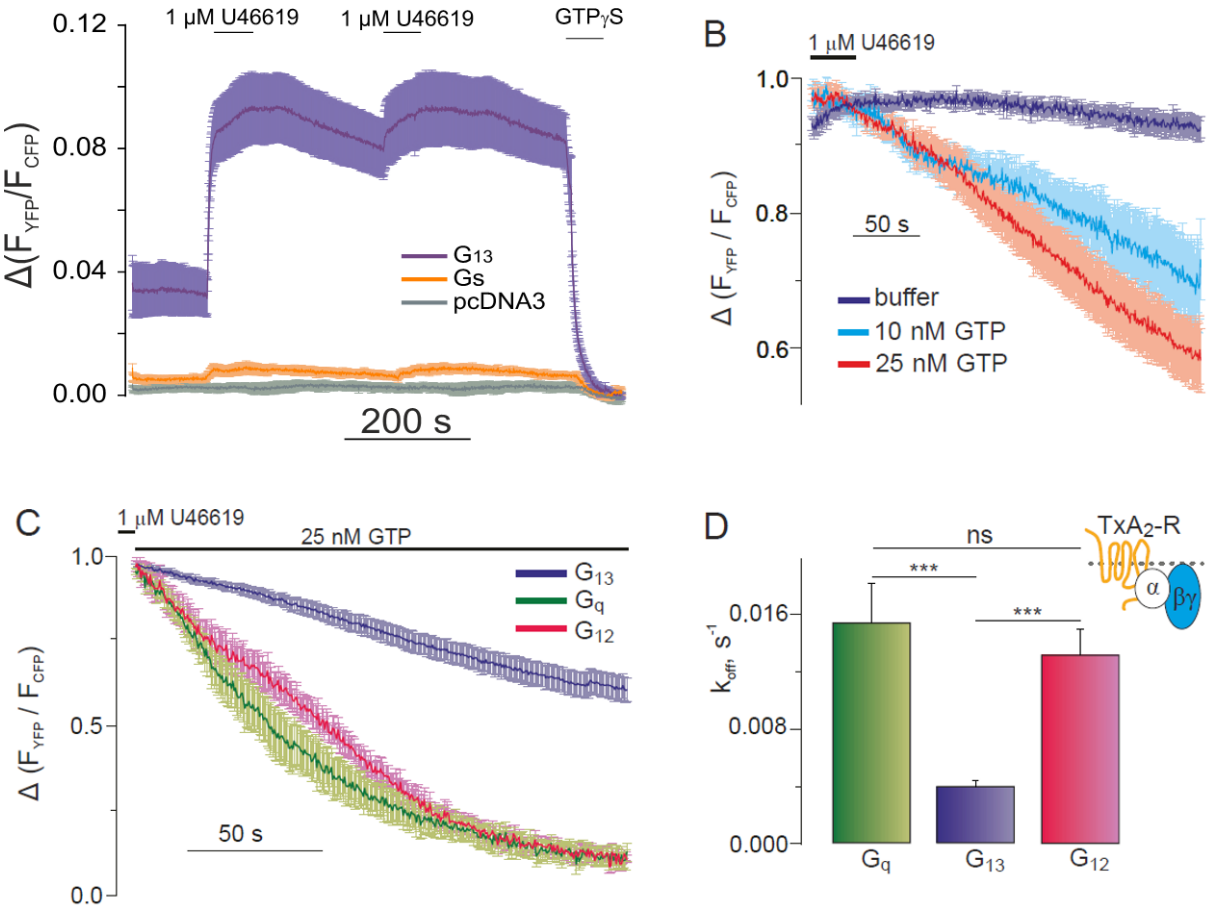

Figure 32. Modulation of the lifetime of G_q-, G_{13}- and G_{12} - TP-R complexes
Average YFP/CFP emission ratio traces of G_{13} binding to TP-R after nucleotide depletion **(A)** was compared to binding of endogenous G proteins. As no difference to negative control (pcDNA3 transfection instead of Gα subunit) was observed, G_s did not bind to TP-R. Dissociation rate indicate for a high stability of G_{13}-TP-R complex and it was modulated by application of different GTP concentrations **(B)**. Comparison of dissociation kinetics of G_q, G_{13} and G_{12} proteins from TP-R in presence of 25 nM GTP **(C)** and their calculated k_{off} values **(D)** revealed the 5-fold difference in G_q and G_{13} affinities to TP-R. Interestingly, G_q and G_{12} affinities were found to be similar. All data shown as mean ± SEM for each condition, with n ≥7 independent experiments. The minimum receptor occupancy state is settled to 0 and corresponds to the FRET signal in presence of GTPγS. Statistical analysis was performed by one-way ANOVA with Bonferroni post-hoc test (*P < 0.05).

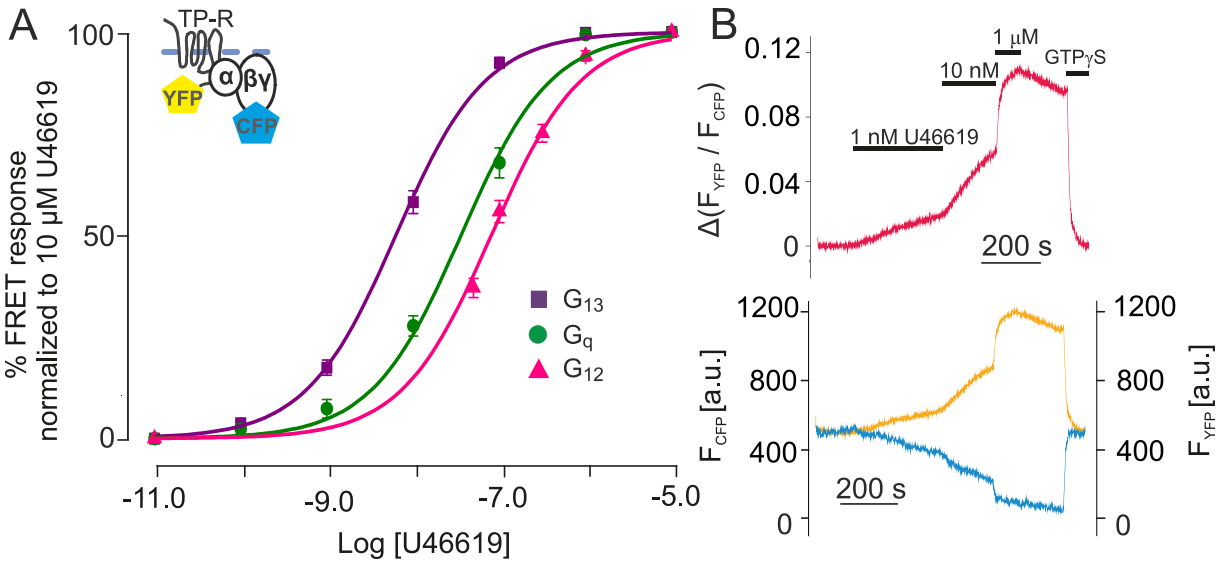

Figure 33. Binding of G_{12}, G_{13} and G_q to TP-R in dependence of agonist concentration
Concentration – response curve of U46619 induced G_q binding to TP-R (EC_{50}= 6,82 ± 0,08 nM U46619) under GTP-depleted conditions (A) measured by means of FRET (B) is 6-fold right shifted when compared to G_{13} binding (EC_{50}= 35,94 ± 0,13 nM U46619). The factor difference in EC_{50} correlated with the difference in k_{off} values. All data shown as mean ± SEM for each condition, with n ≥6 independent experiments.

The dissociation kinetics data on G_{13} and G_q protein binding to TP-R under nucleotide depleted conditions correlates with the coupling efficiency of these G proteins which has been previously described in Bodmann et al. 2017. Thus, the quantification of intrinsic G protein affinity to the receptor determines the GPCR degree of selectivity not only for mAChRs but also for other types of GPCRs.

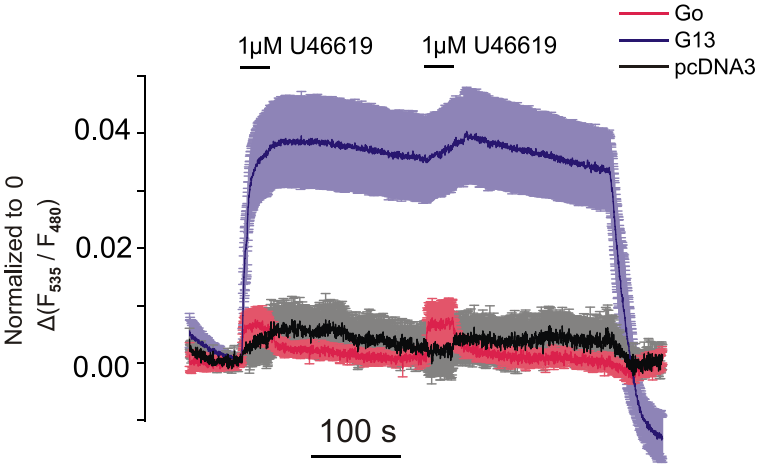

Figure 34. Binding of G_o to TP-R under nucleotide-depleted conditions
Mean traces of YFP/CFP intensities ratio of G_o binding to TP-R after nucleotide depletion are compared to binding of endogenous G proteins (pcDNA3, negative control) and G_{13} (positive control). G_o binding to TP-R was observed but differed from pcDNA3 condition only by fast dissociation kinetics after agonist withdrawal. The data is represented as mean ± SEM for each condition. The minimum state of the receptor is settled to 0 and corresponds to the FRET signal in presence of GTPγS.

Next, I investigated the interaction of TP-R with members of the G_i family, in particular with G_o, under conditions of nucleotide-depletion (Figure 34, Figure 35). In order to increase the number of Ns and calculate the difference in G_{13} and G_o interaction kinetics with TP-R, the experiments depicted in Figure 34 were repeated. Unfortunately, interactions between G_o and TP-R were only observed in a few instances, whereas the majority of cells did not respond (Figure 35A, B). The possible explanation is the difference in the endogenous G proteins expression in HEK293T due to the lower or high passage as well as the batch of the cell line.

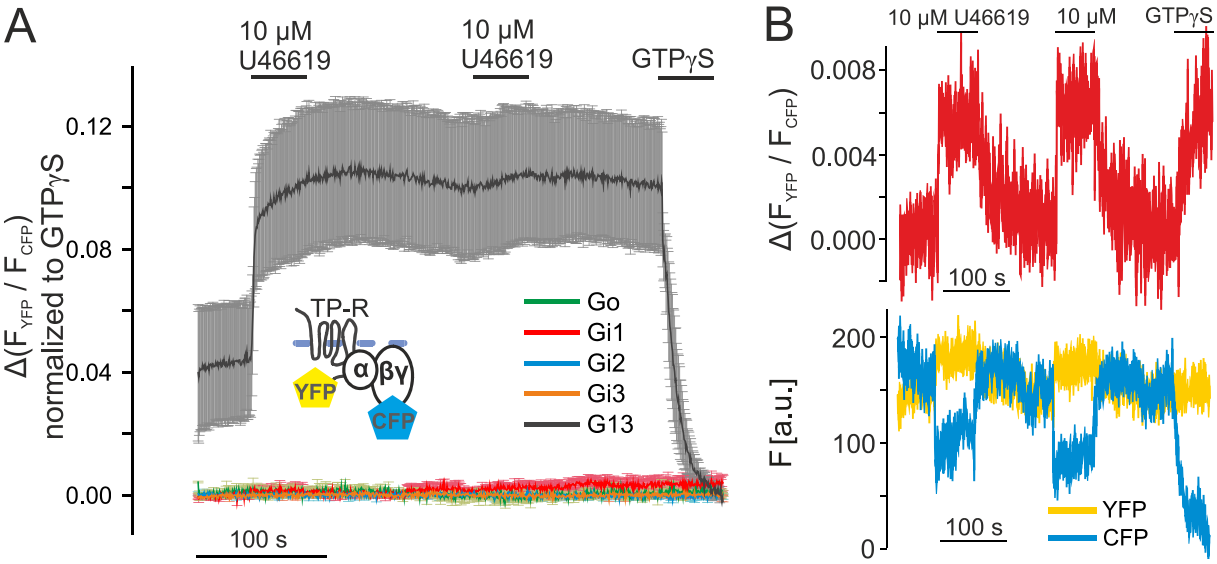

Figure 35. Test for interaction of TP-R with members of the G_i family under conditions of nucleotide-depletion
Averages of normalized YFP/CFP emission ratio traces (upon 430 nM excitation) of agonist-induced binding of G_{i1}, G_{i2}, G_{i3}, G_o and G_{13} to TP-R in the absence of nucleotides **(A)** are depicted. Go binding to TP-R was detectable but differed from pcDNA3 condition only by fast dissociation kinetics after agonist withdrawal. The data is represented as mean ± SEM for each condition. The minimum state of the receptor is settled to 0 and corresponds to the FRET signal in presence of GTPγS. **(B)** Representative YFP/CFP emission ratio trace of the G_o binding to TP-R under nucleotide conditions. Application of U46619 triggered the G_o binding to TP-R. Dissociation of G_o was rather fast, as previously was observed with mAChRs. **(C)** Individual traces of YFP and CFP intensities reflecting the change in FRET signal depicted in B.

Although, on average no specific binding of G_i family proteins to TP-R were observed, the activation of G_o via TP-R was shown by means of FRET G protein activation assay (Figure 36). The amplitudes of G_o activation traces were comparible with G_{13} activation under TP-R stimulation with U46619.

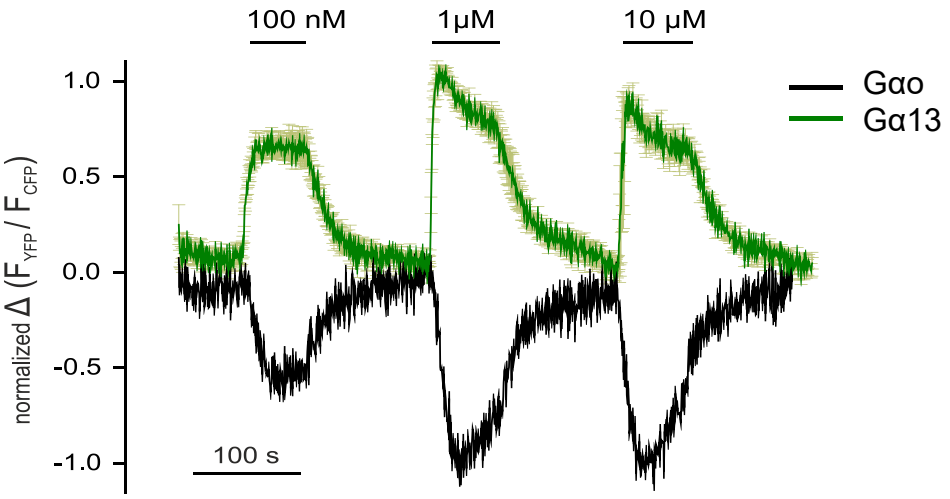

Figure 36. Activation G_o protein via TP-R
YFP/CFP emission ratio traces of U46619-induced activation of G_o and G_{13} via TP-R **(A)** were obtained in intact cells and are plotted as mean ± SEM normalized to initial values for each condition. HEK293T cells were transiently transfected with TP-R labelled with mVenus and G proteins labelled with CFP on Gβγ subunit as described in Table 6 section 2.

I also tested the stability of TP-R-G_{13} ternary complex induced by a different agonist. The partial agonist Daltroban was chosen as a ligand with high affinity but low potency for TP-R (Figure 37) (Bertolino et al. 1997; John, Colpaert, and Valentin 1998; Miki, Kase, and Ishii 1992). The Daltroban concentration-response curve was right shifted compared to U46619 (Figure 37A) whereas no difference in U46619- or Daltroban-induced TP-R-G_{13} complex stability was observed (Figure 37B).

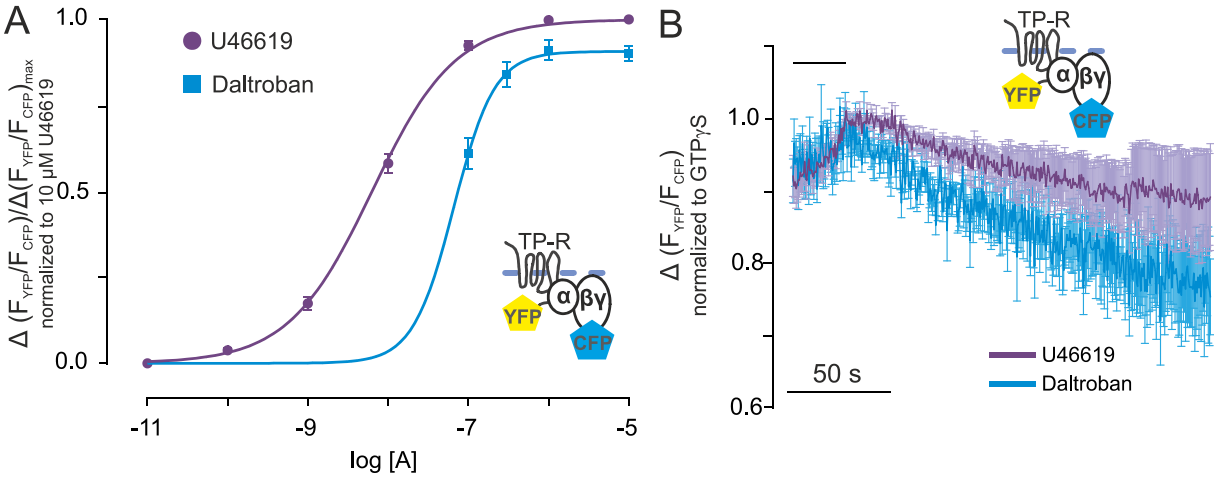

Figure 37. Binding of G_{13} to TP-R induced by Daltroban
(A) Concentration – response curve of G_{13} binding to TP-R induced by U46619 (EC_{50}= 6.82 ± 0.08 nM) and Daltroban (EC_{50}= 65.84 ± 1.9 nM under GTP-depleted conditions were measured by means of FRET. **(B)** G_{13} dissociation from TP-R stimulated with U46619 compared to those stimulated with Daltroban was measured under nucleotide-free conditions and shown as average traces. The data is represented as mean ± SEM normalized to receptor maximum (agonist stimulation) and receptor minimum state (GTPγS application).

3.4.3.2 Characterization of μ-OR-G_i proteins complex stability

One of the aims of this dissertation/my research was to investigate the μ-OR selectivity for different Gα subunits. It is still unknown, which of the G proteins has the highest affinity to the μ-OR. I focused on G_o, G_{i1} and G_{i2} members of G_i family. In order to determinate that, FRET measurements were performed on HEK293T cells transiently transfected with μ-OR-YFP, $G\beta_1$, CFP-$G\gamma_2$ and either $G\alpha_o$, $G\alpha_{i1}$ or $G\alpha_{i2}$ constructs.

The binding of G_i proteins to the μ-OR was measured under GTP-depleted conditions on single HEK293T cells, transfected with three different Gα subunits: G_o, G_{i1}, G_{i2}. Following washing steps with internal buffer ensured the depletion of nucleotides through saponin mediated pores. FRET changes under the application GTPγS, 10 μM DAMGO and 20 nM GTP modulating concentration were observed in all conditions (Figure 38).

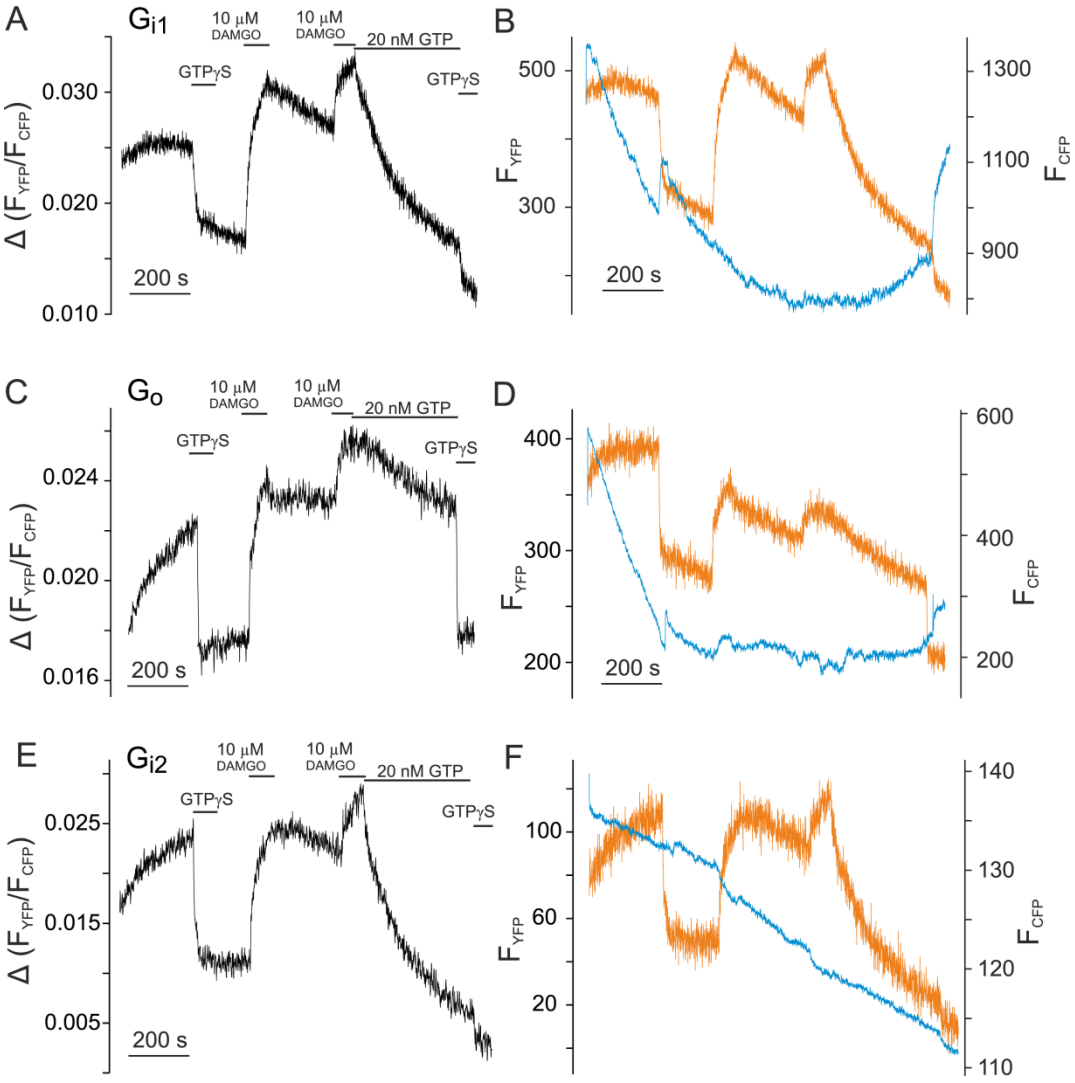

Figure 38. Example traces of G_{i1}, G_o, and G_{i2} binding to μ-OR in permeabilized cells
The figure represents individual F_{YFP} / F_{CFP} ratios of single cells transfected with μ-OR-YFP and G_{i1}, Go or G_{i2} proteins labelled with CFP on the $G\gamma_2$ **(A, C, E)** and their individual F_{YFP} and F_{CFP} intensities **(B, D, F)**.

The overlaid traces of G_{i1} protein binding to μ-OR are depicted in Figure 39A. I also tested the interaction of G_s protein with μ-OR by means of FRET in absence of nucleotides (Figure 39B). Although the application of saturating concentrations of DAMGO induced increases in the YFP/CFP emission ratio when $G\alpha_s$ was cotransfected with the receptor, the amplitude of the response evoked in cells with no transfected Gα (pcDNA3 plasmid replacement) was also similarly high probably due to high expression of endogenous G_i family protein in HEK293T batch of cells used in this study. However, the increase in the YFP/CFP emission ratio of the conditions mentioned above was significantly lower in comparison to the DAMGO-induced signal of Go binding to μ-OR used as positive control (Figure 39B).

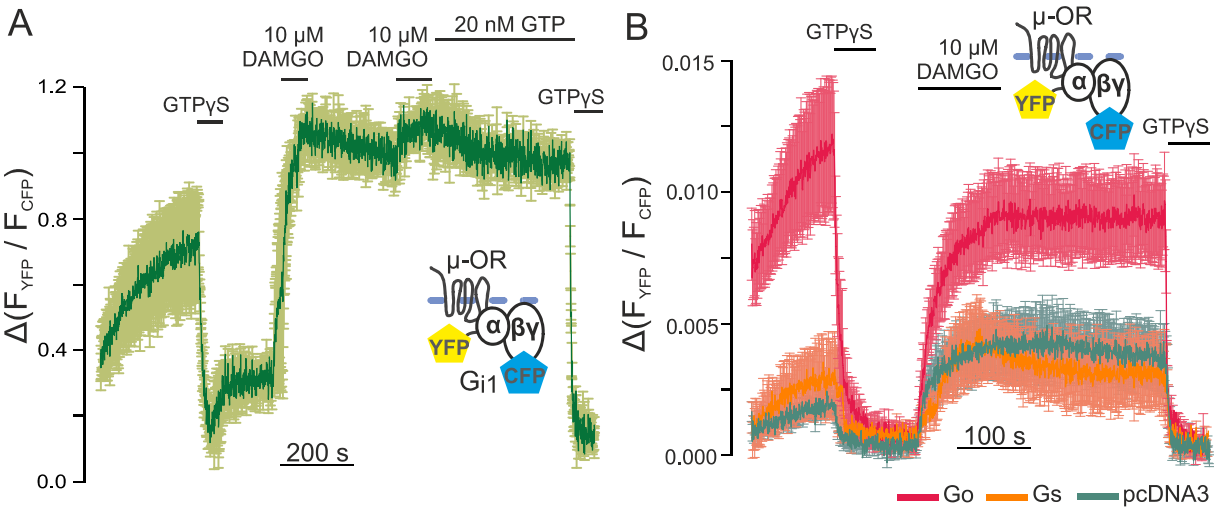

Figure 39. Test for binding of G_s proteins to μ-OR under nucleotide-free conditions
The figure **(A)** depicts an average YFP/CFP emission ratio of G_{i1} binding to μ-OR under nucleotide-depleted conditions. Single-cell FRET recording was done in HEK293T cells transfected with μ-OR-YFP and G protein subunits. **(B)** In comparison to G_o transfected cells and cells transfected with pcDNA3 instead of Gα, no binding of G_s to μ-OR under nucleotide-depleted conditions was detected. Data are normalized to minimum and maximum receptor occupancy state and presented as mean ± SEM.

GTPγS was applied twice: at the beginning and at the end of each experiment for further bleaching correction by receptor minimum state (receptor with no G protein coupled). Decrease in YFP/CFP emission ration under initial application of GTPγS prior to agonist application as well as a relatively small increase in YFP/CFP emission ratio under application of 10 μM DAMGO and dramatic response to the final addition of GTPγS indicates high basal interaction of Go with μ-OR in the absence of nucleotides. This can be explained by the known high degree of μ-OR basic activity (Huang et al. 2015). The level of intrinsic affinity of the G_i family proteins to μOR was calculated as k_{off} of the ternary complexes. Due to the

high affinities, observed in previous experiments, the off-rate of FRET response upon wash out of the agonist has to be accelerated. Therefore, 20 nM GTP was applied during second agonist wash-out to achieve the rate of G protein-receptor dissociation optimal for quantification. Calculated k_{off} of G_{i1}, G_{i2} and G_o were found to be not significantly different, which indicates similar affinities of these G_i family proteins to μ-OR (Figure 40).

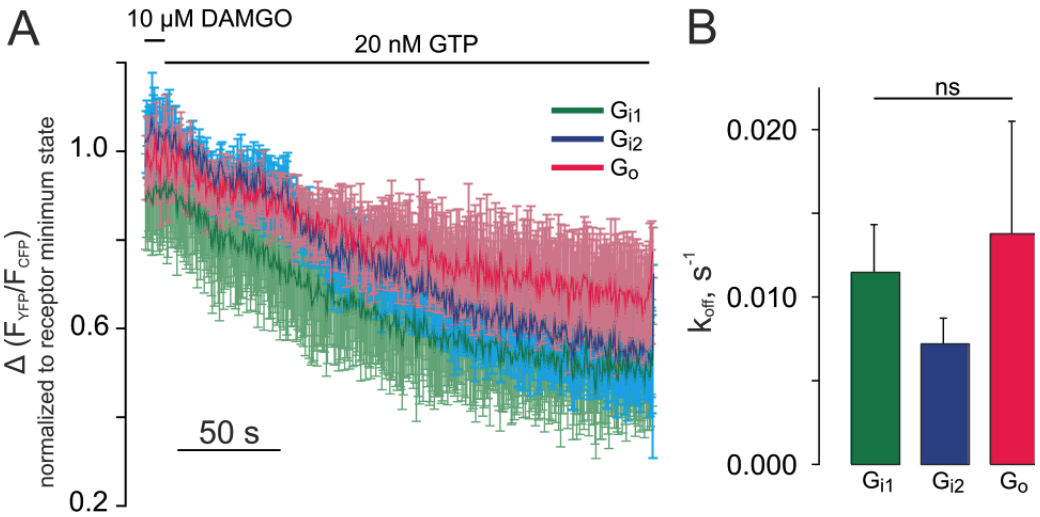

Figure 40. Dissociation kinetics of G_{i1}, G_{i2} and G_o from μ-OR
Off-rates of Gi_1 (green curve), Gi_2 (blue curve) and G_o (red curve) from μ-OR **(A)** were determined after withdrawal of 10 μM DAMGO in the presence of 20 nM GTP (to moderately shorten complex lifetimes). Data are plotted as mean ± SEM. The traces were normalized to maximum (10 μM DAMGO) and minimum (GTPγS). **(B)** Calculated dissociation kinetics (k_{off}) for HEK293T cells transfected either with G_o (n=5), G_{i1} (n=5) or G_{i2} (n=6) are illustrated. The values are shown as mean ± SEM. Significance level was determined by one-way ANOVA.

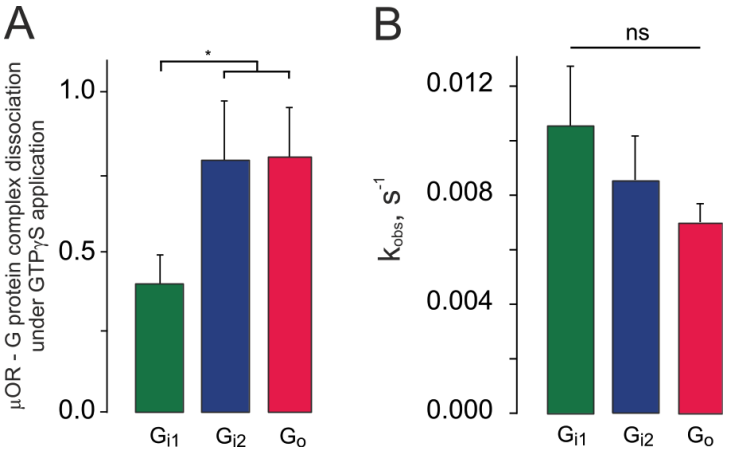

Figure 41. Agonist independent association of μ-OR with different G proteins
To test for the agonist independent association of μ-OR with the indicated G protein subtypes induced by nucleotide depletion **(A)**, the amplitude of the decrease in F_{YPF} / F_{CFP} ratio upon GTPγS (1 μM) application was determined and plotted as averaged data for G_o (n=5), G_{i1} (n=5) and G_{i2} (n=6) proteins. Kinetics of the FRET increase reflecting association (k_{obs}) between μ-OR and G_o, G_{i1}, and G_{i2} proteins were measured after application of internal buffer

(B). Data are normalized to maximum (F_{YFP} / F_{CFP} ratio in presence of 1 µM DAMGO) and minimum (F_{YFP} / F_{CFP} ratio upon final application of GTPγS) receptor occupancy state as depicted in Figure 39A. The values are shown as mean ± SEM. Significance level was determined by one-way ANOVA.

Under the initial application of GTPγS a fast decrease of the FRET signal indicates the dissociation of G protein-receptor complexes which have formed right after permeabilization in absence of agonist. Although, the k_{obs} of DAMGO-independent G protein-receptor association were similar for all proteins (Figure 41B), the amplitude of the GTPγS triggered G_{i1} protein dissociation from the µOR was found to be significantly different from G_{i2} and G_o (Figure 41A). This defines the higher stability G_{i2}-, G_o-µ-OR complexes compared to G_{i1}.

It has been previously shown in Figure 29, that no difference in G_{i3} and G_o affinity to α_{2A}-AR was revealed, probably due to the high stability of their ternary complexes. Therefore, the dissociation rate was accelerated by the addition of low GTP concentrations as described for TP-R and µ-OR. Interestingly, the significant difference in the affinities of G_{i3} and G_o to α_{2A}-AR was observed in presence of low GTP concentration (Figure 42).

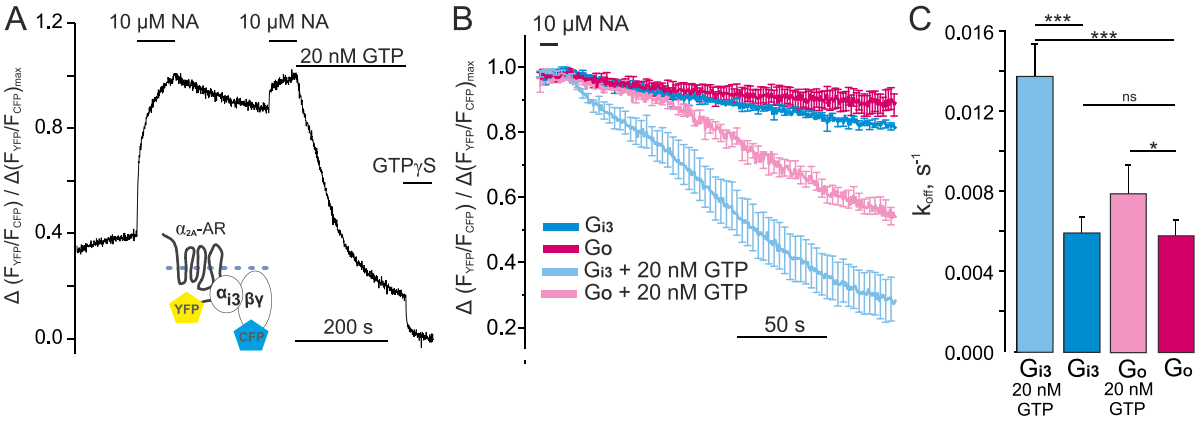

Figure 42. α_{2A}-AR - G_i protein complex stability in presence of low GTP concentrations
Representative trace of G_{i3} binding to α_{2A}-AR under nucleotide-depleted conditions **(A)** derived from a single permeabilized cell transiently transfected as described in Table 6. **(B)** Off-rates of G_{i3} (blue curve), and G_o (pink curve) from α_{2A}-AR were determined after withdrawal of 10 µM NA in the presence of 20 nM GTP and absence of nucleotides. Data are plotted as mean ± SEM. The traces were normalized to maximum (10 µM NA) and minimum (GTPγS). **(C)** Calculated dissociation kinetics (k_{off}) for HEK293T cells transfected either with G_o (n=9) or G_{i3} (n=7) under nucleotide-free conditions are illustrated. Data are normalized to maximum (F_{YFP} / F_{CFP} ratio in presence of 10 µM NA) and minimum (F_{YFP} / F_{CFP} ratio upon final application of GTPγS) receptor occupancy state as depicted in Figure 39A. The values are shown as mean ± SEM. Significance level was determined by one-way ANOVA with additional Boferroni test ($P < 0.05$).

4 Discussion

4.1 The stability of mAChR-G protein complexes

Understanding the molecular mechanism of selectivity and efficiency of receptor-mediated G protein activation is one of the key research topics in the field of GPCR physiology and pharmacology. However, crystal structures of GPCR-G protein complexes do not resolve any common linear epitopes which could determine receptor selectivity for a particular G protein family (Rasmussen et al. 2011; Koehl et al. 2018). In this research, I have experimentally addressed the hypothesis that the specificity of G protein-receptor coupling depends on a complex three-dimensional interaction and might be specific for every receptor-G protein pair. We therefore hypothesised that the degree of selectivity is dependent on the intrinsic affinity of the G protein to a particular receptor. Based on the fact that agonist-receptor-G protein complexes exhibit the highest stability in absence of nucleotides (Christopoulos and Kenakin 2002; Roberts and Waelbroeck 2004), we quantified the affinity of different G proteins to M_1-, M_2-, and M_3-Rs (Jürgen Wess 1998; Burford, Tobin, and Nahorski 1995; Kostenis, Zeng, and Wess 1998) by means of FRET imaging on permeabilized membranes of single cells. By laminar superfusion of these membranes we ensured excellent control of agonist and nucleotides (Figure 6, Figure 13) and resolved the dynamics of interactions between nucleotide-free G proteins with several different receptors.

The ternary complex formation was defined as a high amplitude of response upon ACh application in permeabilized cells when compared to the small change in FRET signal measured in intact cells (Figure 6C). The minor increase in F_{YFP}/F_{CFP} ratio induced by agonist in intact cells was assumed to be a balance between G proteins bound to the receptor and the activated G proteins which have been dissociated from the receptor by GDP/GTP exchange. In contrast, in cells depleted from nucleotides by exposure to permeabilization agent and constant superfusion, the stimulation with agonist led to a higher amplitude of response and a slow decrease in FRET signal during agonist withdrawal confirming the formation of the ternary complex in absence of nucleotides und full receptor-G protein occupancy state (Figure 6F). Although several previously published biochemical and radioligand-binding experiments suggest the inability to rescue the ternary complex without nucleotides, the re-exposition of the permeabilized cell to the agonist as depicted in Figure 6F results in repeating G protein recruitment to the receptor. One can argue, that this could indicate the unsustainable nucleotide depletion leading to binding of the previously activated and perhaps nucleotide-free G proteins to the receptor. However, there are several observations against this argument. Firstly, the results show that even low concentrations of nucleotides lead to significant

changes in the receptor-G protein interaction dynamics (Figure 12, Figure 13), which makes the developed system rather nucleotide-sensitive. Although the multiple recruitment event of G protein to the receptor under agonist application can occur due to the excess of G proteins to the receptor (Figure 10), the amplitude of receptor-G protein interaction did not diminish substantially over the time course of the experiment. The excess of G_q-protein over M_1-R or M_3-R receptor was measured to be only 2-3-fold. Therefore, a loss of half of the G protein population after the first stimulation (assuming full receptor occupancy) should have led to, at least, a detectable reduction of the second amplitude compared to the first one, which was not observed. Secondly, as depicted in Figure 13 agonist-induced M_3-R-G_q interaction subsequent to exposing the cell membranes to 100 nM GDP after an initial period of nucleotide withdrawal, resulted in a transiently enhanced receptor-G protein interaction signal compared to a second application of the same concentration of agonist. This can be best explained by GDP-binding being somewhat rate limiting under these conditions (100 nM), causing -still nucleotide-free- G proteins to bind to the receptor followed by the release from the receptor due to receptor-induced GDP binding (Dror et al. 2015).

The lifetime of receptor-G protein complexes was determined by measuring complex dissociation in response to withdrawal of agonist and was longest for those complexes that contained G protein subtypes that are known to be activated best by the respective receptor (Figure 7, Table 8). Since the active conformation of the receptor is maintained by the presence of the agonist, the determination of the association kinetics of G proteins to the receptor in the continuous presence of the agonist would be preferable in order to get direct access to the binding kinetics. Unfortunately, in current experimental settings with biological membranes it is impossible to add G proteins in a defined fashion. However, it has been shown, that kinetics of agonist binding to muscarinic as well as adrenergic receptors are considerably faster (Hoffmann et al. 2012; Vilardaga et al. 2003) than the binding of receptors and G proteins under current nucleotide free experimental conditions (τ value for about 0.1 s for M_3-R activation with 1 mM CCh, and about 28 s for M_3-R-G_q binding induced by 1 mM CCh under nucleotide-depeleted conditions) (Hommers et al., JBC 2010). The receptor-G protein dissociation kinetics were dramatically accelerated by applying nucleotides (Figure 13). In accordance with known similar binding affinities of GDP and GTP for a given G protein, major differences in the dissociation rate of receptor G protein complexes upon GDP versus GTP application were not observed. Therefore, the performed analysis of dissociation kinetics of G protein receptor complexes is not affected by the activity state of the G protein and reflects exclusively the nucleotide free state of the G protein. It is also important to note,

that all signal-transducing GTP-binding proteins bind and hydrolyse GTP, properties that are crucial to their function as a molecular switch for diverse cellular functions. Each GTP-binding protein, however, has its own dissociation constant for guanine nucleotides, K_d value for GTP and GDP, and rate constant for GTP hydrolysis ($k_{cat.GTP}$) (Kaziro et al. 1991). One has to keep in mind, that ternary complex association includes at least 2 step pattern of the receptor-G protein interaction: initially GDP-loaded heterotrimeric G protein binding to the activate receptor and following after GDP release from the Gα subunit nucleotide-free G protein-receptor complex formation. The association kinetic of G_q and G_o proteins with M_3-R, which has been measured in the current nucleotide-free assay, is probably a mixture of those GDP-bound and nucleotide-free G protein-receptor interaction dynamics, since both were measured: initial low affinity phase of fast on-kinetics and high affinity state reached by the "empty" G protein-receptor complex after GDP release. Regarding G_o-M_3-R complex formation, the fast GDP dissociation from Go might affect the on-rate which could be a reason why I was unable to successfully fit the onset-kinetics to a monoexponential function (Figure 16).

Preliminary data has provided further evidence that no replenishing GDP under current conditions occurs from the interaction of G_i family proteins with μ-OR (Figure 38). The μ-OR interaction with G_i proteins was quite stable (Figure 39), and had a tendency to form even in the absence of agonist under conditions of nucleotide depletion. In this context withdrawal of the agonist led to only a very slow receptor-G protein dissociation, however exposure to as little as 20 nM GTP accelerated the complex dissociation (Figure 40), suggesting the non-existence of relevant concentrations of nucleotides in our preparation.

In my studies I focused mainly on the dynamics of the receptor-G protein complex formation. Based on crystallography data (Rasmussen et al. 2011) receptors interact with G proteins by binding to the Gα subunits, whereas Gβγ subunits come in close proximity but without direct contact to any of receptor intracellular loops. However, the established FRET-based assay cells were transiently transfected with C-terminus labelled receptor and the G protein labelled on the Gγ subunit. Since the insertion sites for GFP variants on Gα subunits differ substantially for the individual Gα subtypes, in order to achieve an accurate comparison between receptor-G protein coupling, the native Gα subunits were transfected. Importantly, only a very small signal due to endogenous Gα subunits (as a control pcDNA3 was transfected instead of Gα subunit) was observed, therefore high selectivity for transfected untagged Gα is guaranteed.

Moreover, the labelling of the $G\gamma_2$ subunit on its N-terminus with a flexible linker far away from the receptor-G protein interaction surface was chosen to minimize the influence of a fluorescent tag on Gα subunit interaction with the receptor. Nevertheless, in order to test whether the dissociation kinetics of fluorescent Gα subunits and M_3-R will differ from those obtained with fluorescent $G\gamma_2$, additional experiments were performed. Despite having to deal with much lower FRET amplitudes by measuring FRET between YFP-labelled receptor and CFP-labelled Gα, association and dissociation kinetics of G_q and G_o proteins to M_3-R were very similar when either $G\gamma_2$ or respective Gα subunits were labelled (Figure 8). Furthermore, the robust expression of heterologously transfected G proteins was confirmed by means of Western Blot. No major differences in the expression levels of Gβγ were obtained when either $G\alpha_o$ or $G\alpha_q$ subunits were co-transfected (Figure 11).

As has been mentioned in the introduction, only $G\gamma_2$ and $G\beta_1$ subunits and no other isoforms were transfected as they are known to be not very selective in respect to heterotrimer formation with different Gα subtypes (Cook et al. 2001; Hillenbrand et al. 2015). However, influence of different Gβ and Gγ isoforms on the receptor-G protein complex stability can be an interesting topic for further investigation.

One more interesting point for discussion is the preassembly of GPCRs and G proteins. Previous studies have reported basal FRET between some GPCRs and G protein subunits that may reflect some level of constitutive association or pre-coupling. One possible reason for agonist-independent receptor-G protein interaction is a specific anchoring mechanism such as described for the receptor C-terminus mediated tethering of M_3 receptor and G_q proteins (Qin et al. 2011). The described mechanism of pre-coupling requires an unmodified C-terminus of the receptor, the described pre-association might be relevant physiologically, however it can be neglected under current study conditions since the receptor is labelled with YFP on the C-terminus, which abolishes the described pre-association (Qin et al. 2011). Since pre-association may enhance the probability of G_q activation over G_o, the additional experiments were performed for both G_o and G_q binding to M_3-R under nucleotide depleted conditions applying GTPγS before the agonist. As no significant reductions in FRET signal under application of the GTPγS was observed, the phenomenon of pre-association of the G protein and the receptor in current studies was excluded (Figure 14).

However, the comparable fast association of G_o and G_q with M_3-R could be connected to the intrinsic nucleotide exchange rates of the G proteins themselves. Although, it was not considered the intrinsic GDP release rates to be a major factor influencing M_3-R-G_q and M_3-R-G_o association and dissociation kinetics, this issue was experimentally tested. It has been

described that $G\alpha_o$ exhibits a about fourfold higher GDP release rate compared to $G\alpha_{i2}$ (Rubenstein, Linder, and Ross 1991), therefore Go and G_{i2} steady-states binding to M_3-R were compared. No significant differences were observed, as the obtained EC_{50} values (10.68 ± 0.32 µM and 8.33 ± 0.08 µM for G_o and G_{i2} respectively, Figure 15) were quite similar based on the approximately 2-fold difference in the complex dissociation rate (Table 8) and 2-fold faster association rate for G_o over G_i (Table 7).

Unlike the dissociation kinetics of the nucleotide-free receptor-G protein complex, one has to be aware that steady-state and on-rate measurements might not exclusively be restricted to complexes after GDP release, but also include initially GDP-bound G proteins. GDP release is much faster for G_o (Higashijima et al. 1987) than for G_q (Mukhopadhyay and Ross 1999), which needs to be considered. Nevertheless, we attempted to measure the k_{on} of GPCR-G protein interactions in native cell membranes. The correlation of apparent M_3-R-G_q association kinetics and agonist concentration are consistent with a hyperbolic function (Figure 7C), allowing us to determine the k_{on} directly. The resulting value of k_{on} = 22.4 s^{-1}*mM^{-1} was remarkably close to the k_{on} = 14.0 s^{-1}*mM^{-1} calculated by division of k_{off} by the EC_{50} value (Figure 7D, Figure 17C), clearly indicating the applicability of our method. Based on the much faster equilibration kinetics of agonist binding to non-G protein bound muscarinic receptors (Hoffmann et al. 2012) the kinetics of agonist-induced receptor-G protein complex formation under nucleotide-free conditions is probably a close approximation to the optimal situation of G protein binding to equilibrated agonist-receptor complexes. In the case of M_3-R-G_o interaction, the correlation of apparent association kinetics of G_o proteins and M_3-R with the agonist concentration is best explained by a 2-component hyperbolic function (Figure 16). A comparison of the correspondingly determined on-rates with $k_{on,}$ (calculated based on k_{off} and EC_{50} values) revealed, even with the slower on-rate, a 5-fold deviation from the calculated k_{on} (Table 7). Possible reasons for this could be effects attributable to the above-mentioned multistep binding reaction. This might affect the apparent association kinetics of receptors and G proteins and complicates interpretation of the measured k_{on} rates. Therefore, at the current research stage, measuring the off-rates of the complex together with steady-state association gives a more robust quantitative correlate of the affinity of the subtype specific receptor-G protein complex. However, the association rate of the G protein and the receptor in our FRET assay could also be affected by the expression levels of the proteins. Therefore, as previously mentioned, the relative expression levels of fluorescent receptor versus fluorescent G protein were measured. Although in all cases only a 2-6-fold excess of G protein versus receptor was observed (Figure 10), the difference in the

relative expression of the different G proteins for each receptor tested was at most approx. 2-fold (Figure 10), which excludes a major influence of the expression ratio on the measured kinetics. Thus, based on theoretical considerations the expression ratio of receptor versus G protein should not affect the dissociation of the complex.

The results of my research project show that both the steady-state curves of G protein binding to the M_3-Rs as well as the dissociation kinetics of this complex quantitatively reflect M_3-R-G protein selectivity (Table 7, Table 8, Figure 17). Specifically, the dissociation kinetics of G_o protein from M_3- and M_1-Rs were 13-fold faster in comparison to G_q (Figure 7, Figure 18, Figure 19). Similarly, I have observed an approximate 16.5-fold right-shift of the concentration-response curves of G_o proteins binding to M_3-R in comparison to G_q (Figure 17A). A quantitatively similar 6.6-fold difference in coupling efficiency of G_o and G_q to M_3-R, measured in a FRET-based G protein activation assay in intact cells (Figure 17C), suggests that the efficacy of coupling to a certain G protein subtype is indeed reflected in the relative M_3-R-G protein affinity, and can thus be detected by measurement of the lifetime of the G protein-receptor complex. For moderate to low affinity agonists with different efficacies we could so far not detect any differences in the stability of M_3-R-G_q or G_o complexes. The effect of ligands on the dynamics of G protein-receptor interaction has been additionally investigated and the findings are discussed in more details in section 4.3. An important finding was that the G_q-coupled and evolutionary close M_1- and M_3-Rs were found to be very similar in respect to their ternary complex stabilities and selectivity pattern for the different G protein subtypes (Figure 18, Figure 19, Table 8). Remarkably, the stability of the GPCR-G protein complexes varied over at least two orders of magnitude for the different receptors, being lowest for M_2-R-G_o protein complexes (lifetime only a few seconds, Table 8) and highest for TP-R-G_{13} complexes and β-AR-Gs complexes (lifetime > 200 s, Figure 32, Figure 30), which likely reflects the parallel evolution of the coupling mechanism (Flock, et al., 2017). In light of recent advances in understanding the allosteric effect of G protein binding (or mimicking nanobodies) to the M_2-R-agonist interaction, specifically the closure of a tyrosine lid on the extracellular side of the agonist exit path (Haga K, et al., 2012; Kruse AC, et al., 2013; DeVree BT, et al.,2016), the results that M_2-R-G_o interaction is very short lived may be somewhat unexpected. However, they are not contradictory to published results, as the lifetime of M_2-R-G_o complexes were not addressed in previous studies. The reliability of the method we developed was also confirmed by testing other G protein classes. For instance, I was unable to detect G_s or G_{13} binding to M_3-R or M_1-R under nucleotide-depleted

conditions (Figure 7A), or to observe activation of these G proteins measured by means of FRET (Figure 9A,C).

Furthermore, other G_i family proteins were screened, and although no significant differences in the affinities of G_i proteins to M_3- or M_1-Rs could be observed, M_2-R did show a higher specificity for G_o and G_{i2} over G_{i1} and G_{i3} (Figure 18B, Figure 19D, Figure 20D). This distinct affinity profile of GPCR is also supported by recently delineated GPCR fingerprints determined as the efficiency of G protein activation by different GPCRs (Carr III R, et al. ,2015). Moreover, recent computational and evolutionary studies assume that the selectivity mechanism of GPCRs is likely disclosed on the G protein level (Flock, et al.,2015; Flock, et al.,2017). Thus, one can conclude that receptor-G protein affinity represents a major determinant for receptor-G protein subtype selectivity. The observed differences in the affinity of G_o vs G_q towards active M_3-Rs can be essentially attributed to the differences in the lifetime of the complex, suggesting that the apparent on-rate of complex formation is less important for defining coupling selectivity.

The potential and distinctive advantage of our FRET-based nucleotide-free method over biochemical assays is the ability to perform experiments in a regular membrane environment. By excluding the steps of protein purification and protein reconstitution (Lee, Linder, and Gilman 1994; M E Linder et al. 1990) a remarkably high degree of signal specificity is still exhibited. This is particularly important as G proteins are well known to be very sensitive to detergents (Sýkora, 2009). Furthermore, this method is easily accessible to all GPCRs and G proteins and can be used as a reliable way to quantify GPCR-G protein specificity.

The calculation of the k_{on} based on the equation E3 was done based on steady-state experiments on G protein binding to M_3-R under nucleotide-depleted conditions. We assumed that the EC_{50} of these dose-response curves reflected the K_d values since the amplitudes of the YFP/CFP intensities ratio reflect the occupancy of the active M_3-Rs by nucleotide-free G proteins bound with a high affinity under application of different agonist concentrations.

Taken together, the performed detailed analysis of M_3-R revealed that the lifetime of the nucleotide-free GPCR-G protein complex rather than the association kinetics is the major determinant for the differences in affinity of these complexes.

4.2 Insights of G protein-receptor selectivity mechanism

Taking into account that receptor-G protein complex stability depends on intracellular nucleotide concentration (Matesic et al. 1989) the ability of $G\alpha_i$ protein to bind relative GPCR after modifying the C-terminus of $G\alpha_i$ subunit by Pertussis toxin was tested. The FRET

method described above in combination with the controlled nucleotide concentrations technique was used to address this issue.

In this part of my research project I have focused on M_2 and M_3 muscarinic acetylcholine receptors and additionally on α_{2A} adrenergic receptor, as GPCRs known to activate inhibitory G proteins. According to the recent computational experiments, the interaction of μ-OR with G_i protein is a multistep process which involves first low affinity contact as initial recognition phase followed by high affinity binding of G protein to the receptor (Sounier et al. 2015). The aim of the study was to reveal the involvement of the α5 C-terminus of the Gα subunit in the selectivity of receptor-G protein interaction. Pertussis toxin was used to covalently modify the last amino acids of the $G\alpha_i$ subunit in order to prevent coupling to the receptor (Quist, Satumtira, and Vasan 1999). The binding G_i proteins to M_3-R and to α_{2A}-AR under nucleotide-depleted conditions as well as their activation was completely abolished in cells treated with PTX (Figure 21). Although inhibition of G_i with Pertussis toxin might indicate the complete blockage of G protein-receptor binding, it is also possible to suggest that α5 C-terminus of G_i binding to H8 and ICL1 domains of the receptor plays a crucial role in the mechanism of G protein-receptor selectivity and might be the first step in G protein-receptor low-affinity contact.

4.3 Alterations in ternary complex stability induced by different ligands

Previously in this study, I investigated whether the selectivity of the receptor-G protein interaction depends on intrinsic affinity of the G protein to the receptor. It was also of great interest to test the influence of agonist on ternary complex stability using the mAChR-G protein complex model. As no difference in the ternary complex stability was observed when the receptor-G protein binding was induced by agonists with several fold differences in affinity to the receptor such as ACh, CCh or Are (Figure 23), it was concluded that agonist affinity does not affect ternary complex stability once it is formed. However, we extended our studies on the complex stability by also comparing agonists with different efficacies to activate mAChRs. Taking into account that stimulation of M_3-R with partial agonists such as pilocapine or choline evoked rather small amplitudes in FRET signal, further detailed experiments were done analyzing the M_1-R-G_q interaction. Interestingly, the ligand specific differences in the dynamics of M_1-R-G_q complex formation were rather observed for the association kinetics than for the dissociation of the G protein from the receptor (Figure 23). These data suggest that the efficacy but not affinity of the ligand to the receptor influence the speed of ternary complex formation in absence of nucleotides. Indeed, in the range of the agonists, tested in this part of my project, the row of ligands ordered by the k_{on} values of the

M_1-R-G_q complex (Table 9) correlated with the ability of the respective agonist to activate G proteins (Figure 24). Therefore, it is assumed that calculated k_{on} values reflect the probability of the receptor to be stabilized in active conformation by a particular ligand. Thus, the established method can further help to quantitatively characterize the degree of partial agonism of different pharmacological agents.

Moreover, I have tried to assess the contribution of allosteric modulators to the ternary complex stability. It was shown, that at least in case of BQCA the positive allosteric effect occurs due to the change in BQCA-agonist-induced efficiency of G protein coupling rather than alteration of ligand affinity to the receptor (Figure 26, Figure 27). Although, negative allosteric modulator Gallamine did not affect M_1-R-G protein complexes stability, the additional experiments such as steady-state measurements and k_{on} kinetics calculation should be done.

4.4 Quantification of high affinity GPCR-G protein complex stability

In order to investigate whether the correlation of mAChR-G protein complex stability with receptor-G protein selectivity can be expanded for other GPCRS, in this part of the research project I studied the dynamics of G protein interaction with thromboxane 2A receptor, α_{2A}-, β_1-, and β_2-adrenergic receptors, as well as with ET_BR - and μ-ORs. In all cases we observed that the receptors bind with the highest affinity (reflected in the longest lifetime of the complex) to those G proteins that are known to be activated best by the respective receptor. The complexes of G_s-β_1-AR and G_s-β_2-AR as well as TP-R-G_{13} (Figure 29, Figure 30, Figure 32) were found to be very stable and therefore their dissociation rate was too slow to be quantified by fitting an exponential curve. For some receptors such as the β_1- and β_2-ARs and μ-ORs the basal activity and the long lifetime of the receptor-G protein receptors complex did not allow for an accurate determination of the lifetime of the complex, however until now, all data on the receptor-G protein lifetime of our measured receptor-G protein complexes are in line with the generalization proposed in Ilyaskina et al., 2018 Even though all the novel data correlate with the assumption that the conclusions of our in depth study on muscarinic receptors can be generalized, this generalization requires testing of many more members of different GPCR families.

It was hypothesized that G_i family proteins might have various affinities to μ-OR due to the differences in their structural homology. In this study I have particularly focused on G_o, G_{i1} and G_{i2} proteins. In previous experiments on permeabilized cells it was shown that these proteins form very stable ternary complexes (agonist-receptor-G protein) with μ-OR under application of DAMGO. Therefore, we decided to use constant GTP concentration to

modulate the dissociation rate of G protein from the receptor during the agonist removal. This allowed us to calculate the k_{off} for each tested G protein. The sufficient concentration of GTP to depict the differences in dissociation kinetics was empirically established (data not shown). The defined relative affinities of G_o, G_{i1} and G_{i2} to μ-OR were found to be similar. However, the pattern of higher G_o affinity to μ-OR compared to other G proteins might obtain the higher significance level if more experiments were performed, which would correlate with the G_o properties described in literature (Oldham et al., 2008). The complexity of the experimental protocol is also increased by membrane permeabilization procedure as well as the instability of GTP under room temperature in the perfusion system.

Interestingly, the initial application of GTPγS led to a decrease in FRET signal, indicating for the agonist-independent G protein – receptor complex formation directly after permeabilization. This effect can be explained by the high affinity of G_i family proteins to μ-OR and their ability to couple to the receptor in absence of agonist under GTP-free conditions. Although, the rate of association kinetics did not differ within the group of tested G proteins, significant differences in the amplitude of the decrease in FRET signals under application of GTPγS was observed. In contrast to G_{i1}, G_o and G_{i2} were observed to form more stable complexes with μ-OR as GTPγS triggered a larger decrease of FRET reflecting a larger fraction of G protein occupied receptors prior to dissociation. In order to diminish agonist-independent μ-OR-G_i protein complex formation prior to permeabilization, cells can be incubated with μ-OR antagonists to such as naloxone.

To sum up, the established FRET assay on permeabilized cells is applicable for quantification of GPCR-G protein selectivity for the G proteins with high intrinsic affinity. The differences in the dissociation kinetics of G_q, G_{13} and G_{12} proteins from TP-R in the presence of 25 nM GTP correlated with steady-state experiments under GTP-depleted conditions measured by means of FRET (Figure 32, Figure 33). Interestingly, relative affinities for G_q and G_{12} were found to be similar. Moreover, the acceleration of relatively slow G_{i3} and G_o dissociation rates from α_{2A}-AR revealed a significant difference in G_{i3} and G_o binding affinities to α_{2A}-AR (Figure 42).

Although, modulation of μ-OR-G_i family proteins complex stability by 20 nM GTP concentration did not reveal any significant difference between G_i family members, the calculation of the amplitude of the FRET decrease under application of GTPγS could be useful for the assessment of the stability of the ternary complex (Figure 40, Figure 41).

Similar to experiments with mAChRs, it would be interesting to investigate the stability of high affinity G protein-receptor complexes in dependence of receptor agonists with

different properties. For instance, it would be interesting to compare the G_i family members affinity to μ-OR under application of partial agonists such as morphine and buprenorphine and investigate dissociation kinetics of G_{13}-, G_{12}-, and G_q-TP-R in respond to daltroban (Figure 37). Also, the modulation of G protein-receptor dissociation rate by low GTP concentration can be used to elucidate the differences in G_s-β adrenergic receptors complexes stability induced by various ligands.

In summary, the FRET-based method developed in my research work allows to quantify the degree of G protein-receptor complex stability in a regular membrane environment. Using this approach, I have shown that the intrinsic G protein affinity is a major determinant of the receptor-G protein selectivity for different receptor families. Moreover, screening over different GPCR ligands revealed the certain pattern of G-protein-receptor ternary complex stability mediated by low and high affinity agonists as well as allosteric modulators.

5 Summary

G protein coupled receptors (GPCR) regulate many important physiological functions by converting extracellular stimuli into the variety of biological responses. The spectrum of induced signalling pathways depends on the type of heterotrimetric G protein coupling to the receptor. A number of recent structural and computational studies could visualize and define motifs important for G protein-GPCR complex formation. However, the essential factor for the receptor-G protein selectivity has not been fully elucidated. In this research project it was hypothesized that G protein-receptor selectivity can be determined by G protein affinity, which can be numerically assessed as ternary complex stability.

Interaction of G protein with the receptor can be subdivided into three major phases: G protein binding to the ligand-activated receptor, nucleotides exchange (GDP to GTP) on the Gα subunit which leads to ternary complex formation (ligand-receptor-G protein), and finally activation of the heterotrimeric G protein resulting in rearrangement of Gα and Gβγ subunits. Taking into account that ternary complex is stable only in the absence of nucleotides, I have developed a broadly applicable FRET-based assay to study receptor-G protein interaction in permeabilized transiently transfected cells under nucleotide depleted conditions. This approach allowed to quantitatively as both association and dissociation rates of G proteins from agonist-activated GPCRs.

Activated by similar agonists, members of muscarinic acetylcholine receptor family (mAChRs) have been known to couple to different G protein classes. Therefore, mAChRs were taken as a model to study GPCR-G protein selectivity. G protein affinity was calculated as dissociation kinetics in response to withdrawal of agonist. Remarkably, the dissociation rate was the slowest for those complexes that contained G protein subtypes that are known to be most efficiently activated by the respective receptor. Specifically, dissociation of G_q protein from M_3- and M_1-Rs was significantly slower in comparison to G_o, Importantly, the shift in concentration-response curves in steady-state experiments correlated well with the calculated G_q and G_o affinities. Moreover, G protein activation measurements revealed quantitative correlation between coupling efficiency and affinity of G_o and G_q to M_3-R. This suggests that the stability of the receptor-G protein complex is an inherent property of both interaction partners and closely correlates with the ability of the receptor to activate the corresponding G protein subtype. In addition, by calculating the constants of association and dissociation, it has been shown that the affinity of the G protein to the receptor, but not the rate of ternary complex formation, determines the degree of GPCR-G protein selectivity.

Apart from mAChRs, this principle was also applicable for other GPCRs: μ-OR, β_1-, β_2-, and α_{2A}-adrenegic receptors, TP-R and ETR_B. Interestingly, each receptor revealed an individual pattern of G protein affinities. It was also observed that receptors known for high basal activity form extremely stable complexes with their regular interacting G proteins. The characterization of G protein affinities spectrum for such GPCRs was challenging. In this case, in order to quantify the ternary complex stability, the dissociation rate was modulated by the addition of constant low GTP concentrations. Thus, it was possible to show the difference between the affinities of individual members of G protein families.

Moreover, the developed nucleotide-free method was used to test a range of orthosteric and allosteric mAChRs agonists with different affinities and efficiencies in terms of ternary complex stability. It was shown that the efficiency, but not the affinity, of the ligand to the receptor can be estimated as the rate of GPCR-G protein complex association. Calculated constant of association correlated with the efficiency of G protein activation and reflected the probability of the receptor to be stabilized in the active conformation by the particular agonist. Interestingly, the results of FRET experiments on permeabilized cells correlated with the data derived from FRET measurement on membranes. The last technique can be further used as a cell-free screening of different pharmacological agents effecting GPCR-G protein dynamics.

To conclude, my findings shed new light on the mechanisms which determine the receptor-G protein selectivity.

Keywords: Förster resonance energy transfer (FRET), G protein coupled receptor (GPCR), ternary complex, G protein affinity, G protein selectivity, permeabilization

5 Zusammenfassung

G-Protein-gekoppelte Rezeptoren (GPCR) regulieren viele wichtige physiologische Funktionen, indem sie extrazelluläre Stimuli in eine Vielzahl biologischer Reaktionen umwandeln. Das Spektrum der induzierten Signalwege hängt von der Art der heterotrimetrischen G-Protein-Kopplung an den Rezeptor ab. Eine Reihe von aktuellen strukturellen Studien und Computersimulationen ermöglichte die Visualisierung und Bestimmung von Motiven, die für die Bildung von G-Protein-GPCR-Komplexen wichtig sind. Der wesentliche Faktor für die Rezeptor-G-Protein-Selektivität wurde jedoch nicht vollständig aufgeklärt. In diesem Forschungsprojekt wurde die Hypothese aufgestellt, dass die Rezeptor-G-Protein-Selektivität durch die G-Protein-Affinität bestimmt wird, die als Stabilität des ternären Komplexes quantifiziert werden kann.

Die Interaktion eines G-Proteins mit einem Rezeptor kann in drei Hauptphasen unterteilt werden: G-Protein-Bindung an den ligandenaktivierten Rezeptor, Nukleotidaustausch (GDP zu GTP) an der Gα-Untereinheit, was zur Bildung des ternären Komplexes führt (Ligand-Rezeptor-G-Protein) und schließlich Aktivierung des heterotrimeren G-Proteins, was zur Umlagerung von Gα- und Gβγ-Untereinheiten führt. Unter Berücksichtigung der Tatsache, dass der ternäre Komplex nur in Abwesenheit von Nukleotiden stabil ist, habe ich einen breit anwendbaren FRET-basierten Assay entwickelt, um die Rezeptor-G-Protein-Interaktion in Abwesenheit von Nukleotiden zu untersuchen. Dieser Ansatz ermöglichte die quantitative Abschätzung sowohl der Assoziations- als auch der Dissoziationsrate von G-Proteinen aus durch Agonisten aktivierten Rezeptor-G-Protein-Komplexen.

Es ist bekannt, dass Mitglieder der muscarinischen Acetylcholin-Rezeptor-Familie (mAChRs), die von ähnlichen Agonisten aktiviert werden, an verschiedene G-Protein-Klassen koppeln. Daher wurden mAChRs als Modell zur Untersuchung der GPCR-G-Proteinselektivität herangezogen. Die G-Protein-Affinität wurde als Dissoziationskinetik der Reaktion auf den Entzug des Agonisten berechnet. Bemerkenswerterweise war die Dissoziationsrate für jene Komplexe am langsamsten, die G-Protein-Subtypen enthielten, von denen bekannt ist, dass sie vom jeweiligen Rezeptor am effizientesten aktiviert werden. Insbesondere war die Dissoziation des G_q-Proteins von M_3- und M_1-Rs im Vergleich zu G_o signifikant langsamer. Wichtig ist, dass die Verschiebung der Konzentrations-Reaktions-Kurven in stationären Experimenten gut mit den berechneten G_q- und G_o-Affinitäten korrelierte. Darüber hinaus zeigten G-Protein-Aktivierungsmessungen eine quantitative Korrelation zwischen der Kopplungseffizienz und der Affinität von G_o und G_q zu M_3-R. Dies

deutet darauf hin, dass die Stabilität des Rezeptor-G-Proteinkomplexes eine inhärente Eigenschaft beider Interaktionspartner ist und eng mit der Fähigkeit des Rezeptors korreliert, den entsprechenden G-Protein-Subtyp zu aktivieren. Zusätzlich wurde durch Berechnung der Konstanten der Assoziation und Dissoziation gezeigt, dass die Affinität des G-Proteins zum Rezeptor, jedoch nicht die Bildungsrate des ternären Komplexes den Grad der GPCR-G-Protein-Selektivität bestimmt.

Außer mAChRs galt dieses Prinzip auch für andere GPCRs: μ-OR-, β_1-, β_2- und α_{2A}-adrenegische Rezeptoren, TP-R und ET_B-R. Interessanterweise zeigte jeder Rezeptor ein individuelles Muster der G-Protein-Affinitäten. Es wurde auch beobachtet, dass Rezeptoren, die für ihre hohe Basalaktivität bekannt sind, mit ihren regulär interagierenden G-Proteinen extrem stabile Komplexe bilden. Die Charakterisierung des G-Protein-Affinitätsspektrums für solche GPCRs war schwierig. In diesem Fall wurde zur Quantifizierung der ternären Komplexstabilität die Dissoziationsrate durch Zugabe konstant niedriger GTP-Konzentrationen moduliert. Somit konnte der Unterschied zwischen den Affinitäten einzelner Mitglieder von G-Protein-Familien gezeigt werden.

Darüber hinaus wurde die entwickelte nukleotidfreie Methode verwendet, um eine Reihe von orthosterischen und allosterischen mAChRs-Agonisten mit unterschiedlichen Affinitäten und Effizienzen hinsichtlich der Stabilität des ternären Komplexes zu testen. Es wurde gezeigt, dass die Effizienz, aber nicht die Affinität des Liganden zum Rezeptor, als Rate der GPCR-G-Proteinkomplexassoziation abgeschätzt werden kann. Die berechnete Assoziationskonstante korrelierte mit der Effizienz der G-Protein-Aktivierung und spiegelte die Wahrscheinlichkeit wider, dass der Rezeptor durch den jeweiligen Agonisten in der aktiven Konformation stabilisiert wird. Die Ergebnisse von FRET-Experimenten an permeabilisierten Zellen korrelierten mit den Daten, die aus der FRET-Messung an Membranen erhalten wurden. Die letzte Technik kann ferner als ein zellfreies System für Screening verschiedener pharmakologischer Wirkstoffe verwendet werden, die die GPCR-G-Proteindynamik beeinflussen.

Zusammenfassend werfen meine Ergebnisse ein neues Licht auf die Mechanismen, die die Rezeptor-G-Protein-Selektivität bestimmen.

Literature

Ahles, A., and S. Engelhardt. 2014. “Polymorphic Variants of Adrenoceptors: Pharmacology, Physiology, and Role in Disease.” *Pharmacological Reviews* 66 (3): 598–637.

Al-hasani, Ream, and Michael R Bruchas. 2011. “Molecular Mechanism of Opioid Receptor-Dependent Signaling and Behavior.” *Journal of Anesthesiology* 115 (6): 1363–81.

Albert, P.R., Robillard, L. 2002. “G Protein Specificity: Traffic Direction Required.” *Cellular Signalling* 14 (5): 407–18.

Allgeier, Anouk, Stefan Offermanns, Jacqueline Van Sande, Karsten Spricher, Günter Schultz, and J.E. Dumont. 1994. “The Human Thyrotropin Receptor Activates G-Proteins Gs and Gq/11.” *Journal of Biological Chemistry* 269 (19): 13733–35.

Aronstam, R.S, and P. Patil. 2009. *Encyclopedia of Neuroscience*.

Baker, Jillian G. 2010. “The Selectivity of β-Adrenoceptor Agonists at Human B1-, B2- and B3-Adrenoceptors.” *British Journal of Pharmacology* 160 (5): 1048–61.

Baltos, Jo-Anne, Silvia Paoletta, Anh Tn Nguyen, Karen J. Gregory, Dilip K. Tosh, Arthur Christopoulos, Kenneth A. Jacobson, and Lauren T. May. 2016. “Structure-Activity Analysis of Biased Agonism at the Human Adenosine A3 Receptor.” *Molecular Pharmacology*.

Berstein, G., J. L. Blank, A. V Smrcka, T. Higashijima, J. H. Exton, and E.M. Ross. 1992. “Reconstitution of Agonist-Stimulated Phosphatidylinositol 4,5- Bisphosphate Hydrolysis Using Purified M1 Muscarinic Receptor, Gq/11, and Phospholipase Cβ1.” *Journal of Biological Chemistry* 267 (4): 8081–88.

Bertolino, Frédéric, Jean-Pierre Valentin, Jean-François Patoiseau, Jean-pPerre Rieu, Francis C Colpaert, and Gareth W John. 1997. “Evidence for Partial Agonist Properties of Daltroban (BM 13 , 505) at TP Receptors in the Anæsthetized Open-Chest Rat.” *Naunyn-Schmiedeberg´s Arch Pharmacol* 356: 462–66.

Birdsall, N J M, and S Lazareno. 2005. “Allosterism at Muscarinic Receptors : Ligands and Mechanisms.” *Medicinal Chemistry* 5: 523–43.

Bodmann, Eva Lisa, Anna Lena Krett, and Moritz Bünemann. 2017. “Potentiation of Receptor Responses Induced by Prolonged Binding of Ga13 and Leukemia-Associated RhoGEF.” *FASEB Journal* 31 (8): 3663–76.

Booe, Jason M., Christopher S. Walker, James Barwell, Gabriel Kuteyi, John Simms, Muhammad A. Jamaluddin, Margaret L. Warner, et al. 2015. “Structural Basis for Receptor Activity-Modifying Protein-Dependent Selective Peptide Recognition by a G Protein-Coupled Receptor.” *Molecular Cell* 58 (6): 1040–52.

Brodde, O E, and M C Michel. 1999. “Adrenergic and Muscarinic Receptors in the Human Heart.” *Pharmacological Reviews* 51 (4): 651–90.

Broussard, Joshua A., Benjamin Rappaz, Donna J. Webb, and Claire M. Brown. 2013a. “Fluorescence Resonance Energy Transfer Microscopy as Demonstrated by Measuring the Activation of the Serine/Threonine Kinase Akt.” *Nature Protocols* 8 (2): 265–81.

Broussard, Joshua A., Benjamin Rappaz, Donna J Webb, and Clarie M. Brown. 2013b. “Fluorescence Resonance Energy Transfer Microscopy as Demonstrated by Measuring the Activation of the Serine/Threonine Kinase Akt.” *Nature Protocols* 8 (2): 265–81.

Bünemann, Moritz, Monika Frank, and Martin J Lohse. 2003. “Gi Protein Activation in Intact Cells Involves Subunit Rearrangement Rather than Dissociation.” *Proceedings of the National Academy of Sciences of the United States of America* 100 (26): 16077–82.

Burford, N.T., and S.R. Nahorski. 1996. “Muscarinic M1 Receptor-Stimulated Adenylate Cyclase Activity in Chinese Hamster Ovary Cells Is Mediated by Gsα and Is Not a Consequence of Phosphoinositidase C Activation.” *The Biochemical Journal* 315: 883–88.

Burford, N.T., A.B. Tobin, and S.R. Nahorski. 1995. “Differential Coupling of M1, M2 and M3 Muscarinic Receptor Subtypes to Inositol 1,4,5-Trisphosphate and Adenosine 3’,5’-Cyclic Monophosphate Accumulation in Chinese Hamster Ovary Cells.” *J Pharmacol Exp Ther* 274 (1): 134–42.

Bylund, David B., Douglas C. Eikenberg, J. Paul Hieble, Salomon Z. Langer, Robert J. Lefkowitz, Kenneth P. Minneman, Perry B. Molinoff, Robert R. Ruffolo, JR, and Ulrich Trendelenburg. 1994. “International Union of Pharmacology Nomenclature of Adrenoceptors.” *Trends in Pharmacological Sciences* 46 (2): 121–36.

Carr III, R., C. Koziol-White, J. Zhang, H. Lam, S. S. An, G. G. Tall, R. a. Panettieri, and J. L. Benovic. 2015. “Interdicting Gq Activation in Airway Disease by Receptor-Dependent and Receptor-Independent Mechanisms.” *Molecular Pharmacology* 89 (1):

Caulfield, M. P. 1993. “Muscarinic Receptors-Characterization, Coupling and Function.” *Pharmacology and Therapeutics* 58 (3): 319–79.

Cembala, T.M., J.D. Sherwin, M.D. Tidmarsh, B.L. Appadu, and D.G. Lambert. 1998. “Interaction of Neuromuscular Blocking Drugs with Recombinant Human M1-M5 Muscarinic Receptors Expressed in Chinese Hamster Ovary Cells.” *British Journal of Pharmacology* 125 (5): 1088–94.

Cerione, R. A., C. Staniszewski, J. L. Benovic, R. J. Lefkowitz, M. G. Caron, P. Gierschik, R. Somers, A. M. Spiegel, J. Codina, and L. Birnbaumer. 1985. “Specificity of the

Functional Interactions of the β-Adrenergic Receptor and Rhodopsin with Guanine Nucleotide Regulatory Proteins Reconstituted in Phospholipid Vesicles." *Journal of Biological Chemistry* 260 (3): 1493–1500.

Cerione, R a, J Codina, J L Benovic, R J Lefkowitz, L Birnbaumer, and M G Caron. 1984. "The Mammalian B2-Adrenergic Receptor: Reconstitution of Functional Interactions between Pure Receptor and Pure Stimulatory Nucleotide Binding Protein of the Adenylate Cyclase System." *Biochemistry* 23 (20): 4519–25.

Christopoulos, Arthur, and Terry Kenakin. 2002. "G Protein-Coupled Receptor Allosterism and Complexing." *Pharmacological Reviews* 54 (2): 323–74.

Chung, C. T., Suzanne. L. Niemela, and Roger. H. Miller. 1989. "One-Step Preparation of Competent Escherichia Coli: Transformation and Storage of Bacterial Cells in the Same Solution." *Proceedings of the National Academy of Sciences* 86: 2172–75.

Coleman, R A, W L Smith, and S Narumiya. 1994. "Classification of Prostanoid Receptors: Properties, Distribution, and Structure of the Receptors and Their Subtypes." *Pharmacological Reviews* 46 (2): 205–29.

Conklin, Bruce R., Zvi Farfelt, Kevin D. Lustig, David Julius, and Henry R. Bourne. 1993. "Substitution of Three Amino Acids Switches Receptor Specificity of Gqa to That of Gia." *Nature* 363 (May): 274–76.

Cook, Lana A., Kevin L. Schey, John H. Cleator, Michael D. Wilcox, Jane Dingus, and John D. Hildebrandt. 2001. "Identification of a Region in G Protein γ Subunits Conserved across Species but Hypervariable among Subunit Isoforms." *Protein Science* 10: 2548–55.

Dell'Acqua, M L, Reed C Carroll, and E G Peralta. 1993. "Transfected M2 Muscarinic Acetylcholine Receptors Couple to Gαi2 and Gαi3 in Chinese Hamster Ovary Cells. Activation and Desensitization of the Phospholipase C Signaling Pathway." *The Journal of Biological Chemistry* 268 (8): 5676–85.

Devic, Eric, Yang Xiang, Dianna Gould, and Brian Kobilka. 2001. "β-Adrenergic Receptor Subtype-Specific Signaling in Cardiac Myocytes from B1 and B2 Adrenoceptor Knockout Mice." *Molecular Pharmacology* 60 (3): 577–83.

DeVree, Brian T., Jacob P. Mahoney, Gisselle A. Vélez-Ruiz, Soren G. F. Rasmussen, Adam J. Kuszak, Elin Edwald, Juan-Jose Fung, et al. 2016. "Allosteric Coupling from G Protein to the Agonist-Binding Pocket in GPCRs." *Nature* 535: 182–86.

Dingus, Jane, and John D Hildebrandt. 2012. "Synthesis and Assembly of G Protein Bγ Dimers: Comparison of in Vitro and in Vivo Studies." In *GPCR Signalling Complexes* –

Synthesis, Assembly, Traffi Cking and Specifi City, 63:155–80.

Dippel, E., F. Kalkbrenner, B. Wittig, and G. Schultz. 1996. "A Heterotrimeric G Protein Complex Couples the Muscarinic M1 Receptor to Phospholipase C-β." *Proceedings of the National Academy of Sciences of the United States of America* 93 (4): 1391–96.

Dohlman, H. G. 1991. "Model Systems for the Study of Seven-Transmembrane-Segment Receptors." *Annual Review of Biochemistry* 60 (1): 653–88.

Doi, Tomoko, Hiromi Sugimoto, Ikuyo Arimoto, Yoko Hiroaki, and Yoshinori Fujiyoshi. 1999. "Interactions of Endothelin Receptor Subtypes A and B with Gi, Go, and Gq in Reconstituted Phospholipid Vesicles." *Biochemistry* 38 (10): 3090–99.

Dorn, Gerald W. 2010. "Adrenergic Signaling Polymorphisms and Their Impact on Cardiovascular Disease." *Physiological Reviews* 90 (3): 1013–62.

Dorsch, Sandra, Karl-Norbert Klotz, Stefan Engelhardt, Martin J Lohse, and Moritz Bünemann. 2009. "Analysis of Receptor Oligomerization by FRAP Microscopy." *Nature Methods* 6 (3): 225–30.

Downes, Gerald B., Debra J. Gilbert, Neal G. Copeland, N. Gautam, and Nancy A. Jenkins. 1999. "Chromosomal Mapping of Five Mouse G Protein γ Subunits." *Genomics* 57: 173–76.

Dror, Ron O, Thomas J Mildorf, Daniel Hilger, Aashish Manglik, David W Borhani, Daniel H Arlow, Ansgar Philippsen, et al. 2015. "Structural Basis for Nucleotide Exchange in Heterotrimeric G Proteins." *Science* 348 (6241): 1361–65.

Dupré, Denis J., Mélanie Robitaille, R. Victor Rebois, and Terence E. Hébert. 2008. "The Role of Gβγ Subunits in the Organization, Assembly, and Function of GPCR Signaling Complexes." *Annual Review of Pharmacology and Toxicology* 49 (1): 31–56.

Eason, Margaret G., Hitoshi Kurose, Brian D. Holt, John R. Raymond, and Stephen B. Liggett. 1992. "Simultaneous Coupling of A2-Adrenergic Receptors to Two G-Proteins with Opposing Effects: Subtype-Selective Coupling of A2C10, A2C4, and A2C2 Adrenergic Receptors to Gi and Gs." *Journal of Biological Chemistry* 267 (22): 15795–801.

Eglen, Richard M., and Nikki Watson. 1996. "Selective Muscarinic Receptor Agonists and Antagonists." *Pharmacology and Toxicology* 78 (2): 59–68.

Eps, Ned Van, Anita M Preininger, Nathan Alexander, Ali I Kaya, Scott Meier, Jens Meiler, Heidi E Hamm, and Wayne L Hubbell. 2011. "Interaction of a G Protein with an Activated Receptor Opens the Interdomain Interface in the Alpha Subunit." *Proceedings of the National Academy of Sciences* 108 (23): 9420–24.

Filep, János G., Martine Clozel, Alain Fournier, and Éva Fóldes-Filep. 1994. "Characterization of Receptors Mediating Vascular Responses to Endothelin-1 in the Conscious Rat." *British Journal of Pharmacology* 113 (3): 845–52.

Flock, T., C.N. Ravarani, D. Sun, A.J. Venkatakrishman, M. Kayikci, C.G. Tate, D.B. Veprintsev, and M.M. Babu. 2015. "Universal Allosteric Mechanism for Gα Activation by GPCRs." *Nature* 524 (7564): 173–79.

Flock, Tilman, Alexander S. Hauser, Nadia Lund, David E. Gloriam, Santhanam Balaji, and M. Madan & Babu. 2017. "Selectivity Determinants of GPCR-G-Protein Binding." *Nature* 545 (7654): 317–22.

Forster, Th. 1948. "Intermolecular Energy Migration and Fluorescence." *Annalen Der Physik* 6 (2): 55–75..

Fredriksson, R., Malin C. Lagerström, Lars-Gustav Lundin, and Helgi B. Schiöth. 2003. "The G-Protein-Coupled Receptors in the Human Genome Form Five Main Families. Phylogenetic Analysis, Paralogon Groups, and Fingerprints." *Molecular Pharmacology* 63 (6): 1256–72.

Gautam, D. 2004. "Cholinergic Stimulation of Salivary Secretion Studied with M1 and M3 Muscarinic Receptor Single- and Double-Knockout Mice." *Molecular Pharmacology* 66 (2): 260–67.

Gautam, D., S. J. Han, A. Duttaroy, D. Mears, F. F. Hamdan, J. H. Li, Y. Cui, J. Jeon, and Jürgen Wess. 2007. "Role of the M3 Muscarinic Acetylcholine Receptor in β-Cell Function and Glucose Homeostasis." *Diabetes, Obesity and Metabolism* 9: 158–69.

Gilman, A G. 1987. "G Proteins: Transducers of Receptor-Generated Signals" 56: 615–49.

Goh, Joanne W, and Peter S Pennefather. 1989. "A Pertussis Toxin-Sensitive G Protein in Hippocampal Long-Term Potentiation." *Science* 244: 980–83.

Goricanec, David, Ralf Stehle, Pascal Egloff, Simina Grigoriu, Andreas Plückthun, Gerhard Wagner, and Franz Hagn. 2016. "Conformational Dynamics of a G-Protein α Subunit Is Tightly Regulated by Nucleotide Binding." *Proceedings of the National Academy of Sciences* 113 (26): E3629–38.

Gudermann, T, F Kalkbrenner, and G Schultz. 1996. "Diversity and Selectivity of Receptor-G Protein Interaction." *Annual Review of Pharmacology and Toxicology* 36: 429–59.

Haga, K., A.C. Kruse, H. Asada, T. Yuruqi-Kobayashi, M. Shiroshi, C. Zhang, W.I. Weis, et al. 2012. "Structure of the Human M2 Muscarinic Acetylcholine Receptor Bound to an Antagonist." *Nature* 482 (7386): 547–51

Halushka, Perry V. 2000. "Thromboxane A2 Receptors: Where Have You Gone?"

Prostaglandins and Other Lipid Mediators 60 (4–6): 175–89.

Hamm, Heidi E. 1998. "The Many Faces of G Protein Signaling." *The Journal of Biological Chemistry* 273 (2): 669–72.

Hamm, Heidi E, Dusanka Deretic, Anatol Arendt, Paul A Hargrave, Bernd Koenig, and Klaus P Hofmann. 1988. "Site of G Protein Binding to Rhodopsinmapped with Synthetic Peptides from the α Subunit." *Science* 241 (4867): 832–36.

Hein, Peter, and Moritz Bünemann. 2009. "Coupling Mode of Receptors and G Proteins." *Naunyn-Schmiedeberg's Archives of Pharmacology* 379 (5): 435–43..

Hermans, E. 2003. "Biochemical and Pharmacological Control of the Multiplicity of Coupling at G-Protein-Coupled Receptors." *Pharmacology and Therapeutics* 99 (1): 25–44..

Herrlich, A., B. Kühn, R. Grosse, A. Schmid, G. Schultz, and T. Gudermann. 1996. "Involvement of Gs and Gi Proteins in Dual Coupling of the Luteinizing Hormone Receptor to Adenylyl Cyclase and Phospholipase C." *Journal of Biological Chemistry* 271 (28): 16764–72.

Higashijima, Tsutomu, Kenneth M Ferguson, Paul C Sternweis, Murray D Smigel, and Alfred G Gilman. 1987. "Effects of Mg2+ and the Bγ-Subunit Complex on the Ineraction of Guanine Nucleotides with G Proteins." *Journal of Biological Chemistry* 262 (2): 762–66.

Hildebrandt, John D. 1997. "Role of Subunit Diversity in Signaling by Heterotrimeric G Proteins." *Biochemical Pharmacology* 54 (3): 325–39.

Hillenbrand, M., C. Schori, J. Schöppe, and A Plückthun. 2015. "Comprehensive Analysis of Heterotrimeric G-Protein Complex Diversity and Their Interactions with GPCRs in Solution." *Proceedings of the National Academy of Sciences of the United States of America* 112 (11): E1181-90.

Hoffmann, Carsten, Susanne Nuber, Ulrike Zabel, Nicole Ziegler, Christiane Winkler, Peter Hein, Catherine H Berlot, Moritz Bünemann, and Martin J Lohse. 2012. "Comparison of the Activation Kinetics of the M3 Acetylcholine Receptor and a Constitutively Active Mutant Receptor in Living Cells." *Molecular Pharmacology* 82 (2): 236–45.

Hommers, Leif G., Christoph Klenk, Christian Dees, and Moritz Bünemann. 2010. "G Proteins in Reverse Mode: Receptor-Mediated GTP Release Inhibits G Protein and Effector Function." *Journal of Biological Chemistry* 285 (11): 8227–33.

Horiguchi, Takahiko, Soichi Tachikawa, Rieko Kondo, Mamoru Shiga, Masahiro Hirose, and Koji Fukumoto. 2002. "Study on the Usefulness of Seratrodast in the Treatment of Chronic Pulmonary Emphysema." *Arzneimittelforschung* 52 (10): 764–68.

Huang, Weijiao, Aashish Manglik, A. J. Venkatakrishnan, Toon Laeremans, Evan N. Feinberg, Adrian L. Sanborn, Hideaki E. Kato, et al. 2015. “Structural Insights into μ-Opioid Receptor Activation.” *Nature* 00 (7565): 315–21.

Hughes, John. 1975. “Isolaton of an Endogenous Compound from the Brain with Pharmacological Properties Similar to Morphine.” *Brain Research* 88: 295–308.

Hurowitz, Evan. H., M. Melnyk, James, Yu-Juin Chen, Hosein Kouros-Mehr, Melvin. I. Simon, and Hiroaki Shizuya. 2000. “Genomic Characterization of the Human Heterotrimeric G Protein α, β, and γ and Subunit Genes.” *DNA Research* 7: 111–20..

Ilyaskina, Olga S., Horst Lemoine, and Moritz Bünemann. 2018. “Lifetime of Muscarinic Receptor–G-Protein Complexes Determines Coupling Efficiency and G-Protein Subtype Selectivity.” *Proceedings of the National Academy of Sciences* 115 (19): 5016–21.

Iniguez-Lluhi, Jorge, Christiane Kleuss, and Alfred G. Gilman. 1993. “The Importance of G-Protein Bγ Subunits.” *Trends in Cell Biology* 3: 230–36.

Insel, Paul A., Krishna Sriram, Shu Z. Wiley, Andrea Wilderman, Trishna Katakia, Thalia McCann, Hiroshi Yokouchi, et al. 2018. “GPCRomics: GPCR Expression in Cancer Cells and Tumors Identifies New, Potential Biomarkers and Therapeutic Targets.” *Frontiers in Pharmacology* 9 (431): 1–11.

Ishikawa-Ankerhold, Hellen C., Richard Ankerhold, and Gregor P.C. Drummen. 2012. “Advanced Fluorescence Microscopy Techniques-FRAP, FLIP, FLAP, FRET and FLIM.” *Molecules* 17 (4): 4047–4132.

John, Gareth W, Francis C Colpaert, and Jean Pierre Valentin. 1998. “Overview of the Pharmacological Properties of Daltroban, a Thromboxane A2/Prostanoid-Receptor Partial Agonist.” *Cardiovascular Drug Reviews* 16 (3): 264–87.

Jones, S V, C J Heilman, and M R Brann. 1991. “Functional Responses of Cloned Muscarinic Receptors Expressed in CHO-K1 Cells.” *Molecular Pharmacology* 40 (2): 242–47.

Kaziro, Yoshito, Hiroshi Itoh, Tohru Kozasa, Masato Nakafuku, and Takaya Satoh. 1991. “Signal transducing, structure and function of GTP-binding proteins.” *Annual Review of Biochemistry* 60: 349–400.

Kelly, P., B. J. Moeller, J. Juneja, M. A. Booden, C. J. Der, Y. Daaka, M. W. Dewhirst, T. A. Fields, and P. J. Casey. 2006. “The G12 Family of Heterotrimeric G Proteins Promotes Breast Cancer Invasion and Metastasis.” *Proceedings of the National Academy of Sciences* 103 (21): 8173–78.

Kenakin, Terry. 2008. “Receptor Theory,” no. June: 1–28.

Kilts, J. D., M.A. Gerhardt, M.D. Richardson, G. Sreeram, G.B. Mackensen, H.P. Grocott,

W.D. White, et al. 2000. “B2-Adrenergic and Several Other G Protein–Coupled Receptors in Human Atrial Membranes Activate Both Gs and Gi.” *Circulation Research* 87: 705–9.

Kisselev, Oleg, and Narasimhan Gautamsb. 1993. “Specific Interaction with Rhodopsin Is Dependent on the γ Subunit Type in a G Protein.” *The Journal of Biological Chemistry* 268 (33): 24159–522.

Kleuss, C, H Scherübl, J Hescheler, G Schultz, and B Wittig. 1993. “Selectivity in Signal Transduction Determined by g Subunits of Heterotrimeric G Proteins.” *Science* 259 (February): 832–34.

Knaus, Anne E., Verena Muthig, Stefanie Schickinger, Eduardo Moura, Nadine Beetz, Ralf Gilsbach, and Lutz Hein. 2007. “A2-Adrenoceptor Subtypes-Unexpected Functions for Receptors and Ligands Derived from Gene-Targeted Mouse Models.” *Neurochemistry International* 51 (5): 277–81.

Knezevic, Irina, Catherine Borg, and Guy C. Le Breton. 1993. “Identification of Gq as One of the G-Proteins Which Copurify with Human Platelet Thromboxane A2/Prostaglandin H2 Receptors.” *Journal of Biological Chemistry* 268 (34): 26011–17.

Koehl, Antoine, Hongli Hu, Shoji Maeda, Yan Zhang, Qianhui Qu, Joseph M. Paggi, Naomi R. Latorraca, et al. 2018. “Structure of the μ-Opioid Receptor-G i Protein Complex.” *Nature* 558 (7711): 547–52.

Kofuku, Yutaka, Takumi Ueda, Junya Okude, Yutaro Shiraishi, Keita Kondo, Masahiro Maeda, Hideki Tsujishita, and Ichio Shimada. 2012. “Efficacy of the B2-Adrenergic Receptor Is Determined by Conformational Equilibrium in the Transmembrane Region.” *Nature Communications* 3: 1045–49.

Kostenis, E., F. Y. Zeng, and J. Wess. 1998. “Structure-Function Analysis of Muscarinic Acetylcholine Receptors.” *Journal of Physiology Paris* 92 (3–4): 265–68.

Krief, Stéphane, Fredrik Lönnqvist, Serge Raimbault, Beatrice Baude, Anke Van Spronsen, Peter Amer, A Donny Strosberg, Daniel Ricquier, and Laurent J Emorine. 1993. “Tissue Distribution of β3-Adrenergic Receptor MRNA in Man.” *Journal of Clinical Investigation* 91 (1): 344–49.

Kruse, Andrew C, Aaron M Ring, Aashish Manglik, Jianxin Hu, Kelly Hu, Katrin Eitel, Harald Hübner, et al. 2013. “Activation and Allosteric Modulation of a Muscarinic Acetylcholine Receptor.” *Nature* 504 (7478): 101–6.

Kuravi, Sudhakiranmayi, Tien Hung Lan, Arnab Barik, and Nevin A. Lambert. 2010. “Third-Party Bioluminescence Resonance Energy Transfer Indicates Constitutive Association of

Membrane Proteins: Application to Class a g-Protein-Coupled Receptors and g-Proteins." *Biophysical Journal* 98 (10): 2391–99.

Lambright, David G., John Sondek, Andrew Bohm, Nikolai P. Skiba, Heidi E. Hamm, and Paul B. Sigler. 1996. "The 2.0 Å Crystal Structure of a Heterotrimeric G Protein." *Nature* 379 (6563): 311–19.

Leach, K., J. Simms, P.M. Sexton, and A. Christopoulos. 2012. "Structure–Function Studies of Muscarinic Acetylcholine Receptors." In *Handbc Exp Pharmacol (208)*, 29–48.

Leach, Katie, Patrick M Sexton, and Arthur Christopoulos. 2007. "Allosteric GPCR Modulators: Taking Advantage of Permissive Receptor Pharmacology." *Trends in Pharmacological Sciences* 28 (8): 382–89.

Lean, A. De, J. M. Stadel, and R. J. Lefkowitz. 1980. "A Ternary Complex Model Explains the Agonist-Specific Binding Properties of the Adenylate Cyclase-Coupled β-Adrenergic Receptor." *Journal of Biological Chemistry* 255 (15): 7108–17.

Lee, E, M E Linder, and A G Gilman. 1994. "Expression of G-Protein α Subunits in Escherichia Coli." *Methods in Enzymology* 237 (1992): 146–64.

Leung, Susan Wai Sum, Su Lin Lim, Catherine Cheuk Ying Pang, and Ricky Ying Keung Man. 2002. "Use of A-192621 and IRL-2500 to Unmask the Mesenteric and Renal Vasodilator Role of Endothelin ETb Receptors." *Journal of Cardiovascular Pharmacology* 39 (4): 533–43.

Li, Z., X. Zhou, Z. Dai, and X. Zou. 2012. "Classification of G Proteins and Prediction of GPCRs-G Proteins Coupling Specificity Using Continuous Wavelet Transform and Information Theory." *Amino Acids* 43 (2): 793–804.

Linder, M E, D A Ewald, R J Miller, and A G Gilman. 1990. "Purification and Characterization of Go α and Three Types of Gi α after Expression in Escherichia Coli." *The Journal of Biological Chemistry* 265 (14): 8243–51.

Linder, Maurine E, Iok-hou Pang, Robert J Duroniotii, Jeffrey I Gordon, P C Sternweis, Paul C Sternweis, and Alfred G Gilman. 1991. "Lipid Modifications of G Protein Subunits." *Journal of Biological Chemistry* 266 (7): 4654–59.

Liu, Bo, and Dianqing Wu. 2003. "The First Inner Loop of Endothelin Receptor Type B Is Necessary for Specific Coupling to Gα13." *Journal of Biological Chemistry* 278 (4): 2384–87.

Liu, Songling, Richard T. Premont, Christopher D. Kontos, Jianhua Huang, and Don C. Rockey. 2003. "Endothelin-1 Activates Endothelial Cell Nitric-Oxide Synthase via Heterotrimeric G-Protein Bγ Subunit Signaling to Protein Kinase B/Akt." *Journal of*

Biological Chemistry 278 (50): 49929–35.

Lymperopoulos, Anastasios, Giuseppe Rengo, and Walter J. Koch. 2013. "The Adrenergic Nervous System in Heart Failure: Pathophysiology and Ttherapy." *Circulation Research* 113 (6): 1–6.

Maeda, Shoji, Qianhui Qu, Michael J. Robertson, Georgios Skiniotis, and Brian K. Kobilka. 2019a. "Structures of the M1 and M2 Muscarinic Acetylcholine Receptor/G-Protein Complexes." *Science* 364 (6440): 552–57.

Matesic, D. F., D. R. Manning, B. B. Wolfe, and G. R. Luthin. 1989. "Pharmacological and Biochemical Characterization of Complexes of Muscarinic Acetylcholine Receptor and Guanine Nucleotide-Binding Protein." *Journal of Biological Chemistry* 264 (36): 21638–45.

May, Lauren T, Katie Leach, Patrick M Sexton, and Arthur Christopoulos. 2007. "Allosteric Modulation of G Protein – Coupled Receptors." *Annual Reviews of Toxicology* 47: 1–53.

McCudden, C. R., M. D. Hains, R. J. Kimple, D. P. Siderovski, and F. S. Willard. 2005. "G-Protein Signaling: Back to the Future." *Cellular and Molecular Life Sciences* 62: 551–77.

McIntire, William E. 2009. "Structural Determinants Involved in the Formation and Activation of G Protein Bγ Dimers." *NeuroSignals* 17 (1): 82–99.

McIntire, William E., Gavin MacCleery, and James C. Garrison. 2001. "The G Protein β Subunit Is a Determinant in the Coupling of G s to the B1-Adrenergic and A2a Adenosine Receptors." *Journal of Biological Chemistry* 276 (19): 15801–9.

Mende, Ulrike, Carl J. Schmidt, Fei Yi, Denise J. Spring, and Eva J. Neer. 1995. "The G Protein γ Subunit." *The Journal of Biological Chemistry* 270 (26): 15892–98.

Mervine, Stacy. M, Evan A. Yost, Jonathan L. Sabo, Thomas R. Hynes, and Catherine H. Berlot. 2006. "Analysis of G Protein Bγ Dimer Formation in Live Cells Using Multicolor Bimolecular Fluorescence Complementation Demonstrates Preferences of B1 for Particular γ Subunits." *Molecular Pharmacology* 70 (1): 194–205.

Miki, Ichiro, Hiroshi Kase, and Akio Ishii. 1992. "Differences in Activities of Thromboxane A2 Receptor Antagonists in Smooth Muscle Cells." *European Journal of Pharmacology* 227: 199–204.

Milde, Markus, Andreas Rinne, Frank Wunder, Stefan Engelhardt, and Moritz Bünemann. 2013. "Dynamics of Gαi1 Interaction with Type 5 Adenylate Cyclase Reveal the Molecular Basis for High Sensitivity of Gi-Mediated Inhibition of CAMP Production." *The Biochemical Journal* 454 (3): 515–23.

Milligan, Graeme, and Evi Kostenis. 2006. “Heterotrimeric G-Proteins: A Short History.” *British Journal of Pharmacology* 147 (SUPPL. 1): S46–55.

Mixon, M. B., E. Lee, D. E. Coleman, A. M. Berghuis, A. G. Gilman, and S. R. Sprang. 1995. “Tertiary and Quaternary Structural Changes in Gialpha Induced by GTP Hydrolysis.” *Science* 270 (5238): 954–60.

Moers, Alexandra, Bernhard Nieswandt, Steffen Massberg, Nina Wettschureck, Sabine Grüner, Ildiko Konrad, Valerie Schulte, et al. 2003. “G13 Is an Essential Mediator of Platelet Activation in Hemostasis and Thrombosis.” *Nature Medicine* 9 (11): 1418–22.

Mukhopadhyay, Suchetana, and Elliott M Ross. 1999. “Rapid GTP Binding and Hydrolysis by Gq Promoted by Receptor and GTPase-Activating Proteins.” *Proc Natl Acad Sci USA* 96 (August): 9539–44.

Offermanns, S., K. L. Laugwitz, K. Spicher, and G. Schultz. 1994. “G Proteins of the G12 Family Are Activated via Thromboxane A2 and Thrombin Receptors in Human Platelets.” *Proceedings of the National Academy of Sciences* 91 (2): 504–8.

Oldham, William M., Ned Van Eps, Anita M. Preininger, Wayne L. Hubbell, and Heidi E. Hamm. 2006. “Mechanism of the Receptor-Catalyzed Activation of Heterotrimeric G Proteins.” *Nature Structural and Molecular Biology* 13 (9): 772–77.

Oldham, William M, and Heidi E Hamm. 2008. “Heterotrimeric G Protein Activation by G-Protein-Coupled Receptors.” *Nature Reviews. Molecular Cell Biology* 9 (1): 60–71.

Pasternak, Gavril W., and Ying-Xian Pan. 2013. “M-Opioids and Their Receptors: Evolution of a Concept.” *Pharmacological Reviews* 65: 1257–1317.

Pasternak, Gavril W., and Solomon H. Snyder. 1975. “Identification of Novel High Affinity Opiate Receptor Binding in Rat Brain.” *Nature* 253: 563–65.

Patel, Maulik, Takeharu Kawano, Nobuchika Suzuki, Takao Hamakudo, Andrei V. Karginov, and Tohru Kozasa. 2014. “Gα13/PDZ-RhoGEF/RhoA Signaling Is Essential for Gastrin Releasing Peptide-Receptor Mediated Colon Cancer Cell Migration.” *Molecular Pharmacology* 86: 252–62.

Piascik, M T, and D M Perez. 2001. “A1-Adrenergic Receptors: New Insights and Directions.” *The Journal of Pharmacology and Experimental Therapeutics* 298 (2): 403–10.

Pierre, Nicolas. 2011. “Determination of Association (Kon) and Dissociation (Koff) Rates of Spiperone on the Dopamine D2 Receptor Using a Platform for GPCR Applications.” *American Laboratory*, 2–4.

Qin, Kou, Chunmin Dong, Guangyu Wu, and Nevin A. Lambert. 2012. “Inactive-State

Preassembly of Gq-Coupled Receptors and Gq Heterotrimers." *Nature Chemical Biology* 7 (10): 740–47.

Qin, Kou, Chunmin Dong, Guangyu Wu, and Nevin A Lambert. 2011. "Inactive-State Preassembly of Gq-Coupled Receptors and G q Heterotrimers." *Nature Chemical Biology* 7 (10): 740–47.

Quist, E, N Satumtira, and R Vasan. 1999. "Regulation of Guanine Nucleotide Turnover on Gi/Go by Agonist-Stimulated and Spontaneously Active Muscarinic Receptors in Cardiac Membranes." *Arch Biochem Biophys* 361 (1): 57–64.

Ramachandran, J, E G Peralta, A Ashkenazi, J W Winslow, D H Smith, and D J Capon. 1989. "Structural and Functional Diversity of Muscarinic Acetylcholine Receptor Subtypes." *Prog Clin Biol Res* 289 (March): 327–39.

Rasmussen, Sŏren G.F., Brian T. Devree, Yaozhong Zou, Andrew C. Kruse, Ka Young Chung, Tong Sun Kobilka, Foon Sun Thian, et al. 2011. "Crystal Structure of the B2adrenergic Receptor-Gs Protein Complex." *Nature* 477: 549–57.

Reihsaus, Ellen, Michael Innis, Neil MacIntyre, and Stephen D. Ligget. 1993. "Mutations in the Gene Encoding for the Beta2-Adrenergic Receptor in Normal and Asthmatic Subjects." *American Journal of Respiratory Cell and Molecular Biology* 8 (3): 334–39.

Remuzzi, G., G.A. Fitzgerald, and C. Patrono. 1992. "Thromboxane Synthesis and Action within the Kidney." *Kidney International* 41 (6): 1483–93.

Richter, Martin, Solange Cloutier, and Pierre Sirois. 2007. "Endothelin, PAF and Thromboxane A2 in Allergic Pulmonary Hyperreactivity in Mice." *Prostaglandins Leukotrienes and Essential Fatty Acids* 76 (5): 299–308.

Roberts, David J., and Magali Waelbroeck. 2004. "G Protein Activation by G Protein Coupled Receptors: Ternary Complex Formation or Catalyzed Reaction?" *Biochemical Pharmacology* 68 (5): 799–806.

Rubenstein, R C, M E Linder, and E M Ross. 1991. "Selectivity of the β-Adrenergic Receptor among Gs, Gi's, and Go: Assay Using Recombinant Alpha Subunits in Reconstituted Phospholipid Vesicles." *Biochemistry* 30 (44): 10769–77.

Schrage, Ramona, Janine Holze, Jessica Klöckner, Aileen Balkow, Anne S. Klause, Anna-Lena Schmitz, Marco De Amici, et al. 2014. "New Insight into Active Muscarinic Receptors with the Novel Radioagonist [3H]Iperoxo." *Biochemical Pharmacology* 90 (3): 307–19.

Shenker, A., P. Goldsmith, C. G. Unson, and A. M. Spiegel. 1991. "The G Protein Coupled to the Thromboxane A2 Receptor in Human Platelets Is a Member of the Novel Gq

Family." *Journal of Biological Chemistry* 266 (14): 9309–13.

Shraga-Levine, Zurit, and Mordechai Sokolovsky. 2000. "Functional Coupling of G Proteins to Endothelin Receptors Is Ligand and Receptor Subtype Specific." *Cellular and Molecular Neurobiology* 20 (3): 305–17.

Shrestha, Dilip, Attila Jenei, Péter Nagy, György Vereb, and János Szöllősi. 2015. "Understanding FRET as a Research Tool for Cellular Studies." *International Journal of Molecular Sciences* 16 (4): 6718–56.

Siderovski, David .P., and Francis.S. Willard. 2005. "The GAPs, GEFs, and GDIs of Heterotrimeric G-Protein α Subunits." *International Journal of Biological Sciences* 1 (2): 51–66.

Simon, Melvin I., Michael P. Strathmann, and Narasimhan Gautam. 1991. "Diversity of G Proteins in Signal Transduction." *Science* 252 (5007): 802–8.

Slessareva, Janna E., Hongzheng Ma, Karyn M. Depree, Lori A. Flood, Hyunsu Bae, Theresa M. Cabrera-Vera, Heidi E. Hamm, and Stephen G. Graber. 2003. "Closely Related G-Protein-Coupled Receptors Use Multiple and Distinct Domains on G-Protein α-Subunits for Selective Coupling." *Journal of Biological Chemistry* 278 (50): 50530–36.

Smrcka, A.V., J. R. Hepler, K. O. Brown, and P. C. Sternweis. 1991. "Regulation of Polyphosphoinositide-Specific Phospholipase C Activity by Purified Gq." *Science (New York, N.Y.)* 251 (4995): 804–7.

Sounier, Rémy, Camille Mas, Jan Steyaert, Toon Laeremans, Aashish Manglik, Weijiao Huang, Brian K Kobilka, Héléne Déméné, and Sébastien Granier. 2015. "Propagation of Conformational Changes during M-Opioid Receptor Activation." *Nature* 524: 375–79.

Stamatiou, Rodopi, Efrosini Paraskeva, Anna Vasilaki, Ilias Mylonis, Paschalis Adam Molyvdas, Konstantinos Gourgoulianis, and Apostolia Hatziefthimiou. 2014. "Long-Term Exposure to Muscarinic Agonists Decreases Expression of Contractile Proteins and Responsiveness of Rabbit Tracheal Smooth Muscle Cells." *BMC Pulmonary Medicine* 14:39: 1–12.

Strathmann, Michael P, and Narasimhan Gautam. 1991. "Diversity of G Proteins." *Science* 252 (1971): 802–8.

Strohman, M.J., S. Maeda, D Hilger, M. Masureel, Y. Du, and B.K. Kobilka. 2019. "Local Membrane Charge Regulates B2 Adrenergic Receptor Coupling to Gi3." *Nature Communications* 10: 1–10.

Stumpf, A. D., and C. Hoffmann. 2016. "Optical Probes Based on G Protein-Coupled Receptors - Added Work or Added Value?" *British Journal of Pharmacology* 173 (2):

255–66.

Sýkora, J., L. Bouřová, M. Hof, and P. Svoboda. 2009. “The Effect of Detergents on Trimeric G-Protein Activity in Isolated Plasma Membranes from Rat Brain Cortex: Correlation with Studies of DPH and Laurdan Fluorescence.” *Biochimica et Biophysica Acta - Biomembranes* 1788 (2): 324–32.

Syrovatkina, Viktoriya, Kamela O Alegre, Raja Dey, and Xin-Yun Huang. 2016. “Regulation, Signaling, and Physiological Functions of G-Proteins.” *Journal of Molecular Biology* 428 (19): 3850–68.

Takigawa, Miho, Takeshi Sakurai, Yoshitoshi Kasuya, Yoichiro Abe, Tomoh Masaki, and Katsutoshi Goto. 1995. “Molecular Identification of Guanine-nucleotide-binding Regulatory Proteins Which Couple to Endothelin Receptors.” *European Journal of Biochemistry* 228 (1): 102–8.

Thal, D. M., B. Sun, D. Feng, V. Nawaratne, K. Leach, C.C. Felder, M.G. Bures, et al. 2016. “Crystal Structures of the M1 and M4 Muscarinic Acetylcholine Receptors.” *Nature* 531 (7594): 335–40.

Thomas, Thomas C., Carl J. Schmidt, and Eva J. Neer. 1993. “G-Protein Ao Subunit: Mutation of Conserved Cysteines Identifies a Subunit Contact Surface and Alters GDP Affinity.” *Proc Natl Acad Sci USA* 90: 10295–99.

Vilardaga, Jean-Pierre, Moritz Bünemann, Cornelius Krasel, Mariàn Castro, and Martin J Lohse. 2003. “Measurement of the Millisecond Activation Switch of G Protein-Coupled Receptors in Living Cells.” *Nature Biotechnology* 21 (7): 807–12.

Wall, M a, D E Coleman, E Lee, J a Iñiguez-Lluhi, B a Posner, a G Gilman, and S R Sprang. 1995. “The Structure of the G Protein Heterotrimer Gi Alpha 1 Beta 1 Gamma 2.” *Cell* 83 (6): 1047–58.

Wess, J, N Blin, E Mutschler, and K Blüml. 1995. “Muscarinic Acetylcholine Receptors: Structural Basis of Ligand Binding and G Protein Coupling.” *Life Sciences* 56: 915–22.

Wess, Jürgen. 1993. “Molecular Basis of Muscarinic Acetylcholine Receptor Function.” *Trends in Pharmacological Sciences* 14 (8): 308–13.

. 1998. “Molecular Basis of Receptor / G-Protein-Coupling Selectivity.” *Parmacology & Therapeutics* 80 (3): 231–64.

. 2004. “Muscarinic Acetylcholine Receptor Knock-out Mice: Novel Phenotypes and Clinical Implications.” *Annual Review of Pharmacology and Toxicology* 44 (1): 423–50.

Wong, Stephen K - F. 2003. “G Protein Selectivity Is Regulated by Multiple Intracellular Regions of GPCRs.” *Neuro-Signals* 12 (1): 1–12.

Worzfeld, Thomas, Nina Wettschureck, and Stefan Offermanns. 2008. “G12/G13-Mediated Signalling in Mammalian Physiology and Disease.” *Trends in Pharmacological Sciencees* 29(11): 582-89.

Xiao, Rui-ping. 2001. “β -Adrenergic Signaling in the Heart: Dual Coupling of the B2 -Adrenergic Receptor to Gs and Gi Proteins.” *Science Signalingnce Signaling* 104 (15): 1–11.

Yan, Kang, Vani Kalyanaraman, and Narasimhan Gautam. 1996. “Differential Ability to Form the G Protein Bγ Complex among Members of the β and γ Subunit Families.” *The Journal of Biological Chemistry* 271 (12): 7141–46.

Yao, X. J., G. Velez Ruiz, M. R. Whorton, S. G. F. Rasmussen, B. T. DeVree, X. Deupi, R. K. Sunahara, and B. Kobilka. 2009. “The Effect of Ligand Efficacy on the Formation and Stability of a GPCR-G Protein Complex.” *Proceedings of the National Academy of Sciences* 106 (23): 9501–6.

Youvan, Douglas C, Christopher M Silva, Edward J Bylina, William J Coleman, Michael R Dilworth, and Mary M Yang. 1997. “Calibration of Fluorescence Resonance Energy Transfer in Microscopy Using Genetically Engineered GFP Derivatives on Nickel Chelating Beads.” *Biotechnology* 3 (1): 1–18.

Zhang, Jin, Robert E. Campbell, Alice Y. Ting, and Roger Y. Tsien. 2002. “Creating New Fluorescent Probes for Cell Biology.” *Nature Reviews Molecular Cell Biology* 3 (12): 906–18.

Zhang, L., L. F. Brass, and D. R. Manning. 2009. “The Gq and G12 Families of Heterotrimeric G Proteins Report Functional Selectivity.” *Molecular Pharmacology* 75 (1): 235–41.

Zhang, Xin, and Ulrike S. Eggert. 2013. “Non-Traditional Roles of G Protein-Coupled Receptors in Basic Cell Biology.” *Mol Biosyst.* 9 (4): 586–95.

Zhang, Y., L. Zhang, F. Wang, Y. Zhang, J. Wang, Z. Qin, X. Jiang, and J. Tao. 2011. “Activation of M3 Muscarinic Receptors Inhibits T-Type Ca2+ Channel Currents via Pertussis Toxin-Sensitive Novel Protein Kinase C Pathway in Small Dorsal Root Ganglion Neurons.” *Cellular Signalling* 23 (6): 1057–67.

Zhao, Li-Hua, Shanshan Ma, Ieva Sutkeviciute, Dan-Dan Shen, X Edward Zhou, Parker W de Waal, Chen-Yao Li, et al. 2019. “Structure and Dynamics of the Active Human Parathyroid Hormone Receptor-1.” *Science (New York, N.Y.)* 364 (6436): 148–53.